Investigating the Role of Buried Valley Aquifer Systems in the Regional Hydrogeology of the Central Peace Region in Northeast British Columbia

by

Samantha E. Morgan

B.Sc., University of Calgary, 2014

Thesis Submitted in Partial Fulfillment of the
Requirements for the Degree of
Master of Science

in the
Department of Earth Sciences
Faculty of Science

SIMON FRASER UNIVERSITY
Spring 2018

Approval

Name:	**Samantha E. Morgan**
Degree:	**Master of Science (Earth Sciences)**
Title:	**Investigating the Role of Buried Valley Aquifer Systems in the Regional Hydrogeology of the Central Peace Region in Northeast British Columbia**
Examining Committee:	**Chair: Dr. Dan Gibson** Professor
	Dr. Diana Allen Senior Supervisor Professor
	Dr. Dirk Kirste Supervisor Associate Professor
	Mr. Carlos Salas Supervisor Geoscience BC
	Mr. Mike Wei External Examiner Head, Groundwater and Aquifer Science Section BC Ministry of Environment
Date Defended/Approved:	January 31, 2018

Abstract

Geological and numerical flow models were developed to explore the hydraulic role of buried valley aquifers in regional groundwater flow and assess the potential groundwater resource. The study area was the central Peace Region in Northeast British Columbia. The reservoir software Petrel was used to construct the geological model of a buried valley network by integrating interpretations from an airborne electromagnetic survey (SkyTEM) and borehole gamma-ray and lithology logs. This detailed geological model and a simplified geological model were used to develop two numerical flow models in MODFLOW. The modelling results suggest that permeable deposits exist within the buried valleys, but are not regionally connected throughout the whole network, and thus do not play a significant role in the regional groundwater flow regime. However, extensive permeable deposits within the buried valleys appear to exist at smaller scales, and may offer a viable water source in the area.

Keywords: buried valley aquifers; SkyTEM; Petrel; MODFLOW; regional groundwater flow model; Peace Region

Acknowledgements

I would first like to thank my senior supervisor, Dr. Diana Allen, for her continual support and guidance, and for providing me with the opportunity to work on this project. Her help and encouragement were invaluable, especially during the difficult parts of the thesis development. I also wish to thank my committee members, Dr. Dirk Kirste and Mr. Carlos Salas, as well as my external examiner Mr. Mike Wei. Their critiques and helpful insights provided me with direction throughout this process.

A well-deserved thank you goes out to my office mates, fellow Hydro Discussion Group members, and others in the SFU Earth Sciences Department, who were always ready to provide feedback on writing and conference presentations, or lend an ear when I needed to think out loud. They provided the ideal work environment in which to grow and learn. Much appreciation also goes out to Dr. Vic Levson who shared his valuable experience during the Peace Project drilling campaign, and supported me by providing insight and feedback on my research. I would also like to acknowledge all of the assistance I received from Schlumberger Support on using Petrel, and the generous help from Polina Abdrakhimova on the export from Petrel to MODFLOW.

This project was supported by a grant from the Pacific Institute for Climate Solutions (PICS) to Diana Allen, a Graduate Fellowship from Simon Fraser University through, and a scholarship from Geoscience BC. I would also like to thank Geoscience BC for all of the data for this research.

And finally, this thesis would not have been possible without the unwavering support of my family and friends. Your encouragement and motivation were vital throughout this whole journey and truly kept me going – thank you for believing in me!

Table of Contents

List of Tables

List of Figures

Chapter 1.

Introduction

Globally, groundwater resources are increasingly being considered for water supply (Green et al., 2011). With shallow groundwater resources often being more at risk of contamination, exploration for fresh groundwater at depth is becoming increasingly important. Buried valley aquifers are a viable option as potential fresh groundwater sources (Shaver and Pusc, 1992; Springer and Bair, 1992; Andriashek, 2000; Cummings et al., 2012). Buried valleys are channel-form depressions, or paleovalleys, that have been infilled by sediment and buried following their formation (Cummings et al., 2012). Within these buried valleys, permeable material can form thick units that have the potential to store and transmit significant amounts of water; hence the term 'buried valley aquifers' (Figure 1.1). Buried valleys have been identified below glaciated terrains in North America and northern Europe (e.g. Sandersen and Jørgensen, 2003; Sharpe and Russell, 2004; Steuer et al., 2009; Oldenborger et al., 2013; Seyoum and Eckstein, 2014; Hickin et al., 2016), and where permeable sediments are present within their fill, they can represent attractive targets for groundwater exploitation (Oldenborger et al., 2013). Studying buried valleys and gaining an understanding of their architecture (shape and fill), extent, and the continuity of the permeable units is crucial to managing groundwater resources (Hickin et al., 2016; Korus et al., 2017).

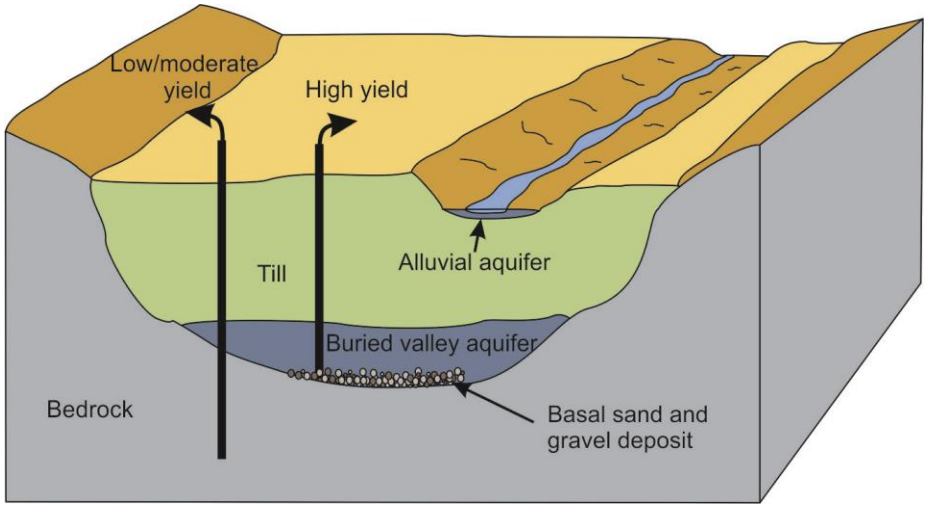

Figure 1.1. Conceptual model of a buried valley aquifer.

Several studies have explored the hydraulic role of buried valley aquifers through both field techniques (Troost and Curry, 1991; Shaver and Pusc, 1992; van der Kamp and Maathuis, 2012) and numerical modelling (Shaver and Pusc, 1992; Springer and Bair, 1992; Weissman et al., 2004; Seifert et al., 2008; Seyoum and Eckstein, 2014). Investigations into buried valley aquifers using numerical modelling have incorporated their geological architecture and have explored the continuity of the permeable units within their fill, which are among the key factors that control the effect that buried valleys have on groundwater flow (Russell et al., 2004). These studies, however, tend to be localized (e.g. one buried valley). There has been very limited investigation into the hydraulic role of buried valley aquifers at the regional scale (Russell et al., 2004). To examine the resource potential of buried valley aquifers as a water source, the impact that buried valleys have on the regional groundwater flow regime must be investigated.

When undertaking regional groundwater investigations, regional-scale numerical groundwater flow models are powerful tools, and can accommodate and address several needs (Ross et al., 2005). However, regional scale models require significantly more data, and the process of developing them tends to be much more intensive. On a regional scale, utilizing multiple geological and geophysical datasets becomes imperative, especially when characterizing complex buried valleys (Sharpe and Russell, 2004; Oldenborger et al., 2014). Using complementary high-resolution geological and geophysical datasets to construct a geological model and identify hydrostratigraphic units within the valley-fill helps to further refine the hydrogeological model of a buried valley network (Pugin et al., 2014).

The purpose of this research is to contribute to the knowledge of buried valley aquifer hydrogeology, and explore the influence that buried valley aquifers have on groundwater flow at a regional scale. The study area is within the Peace Region of Northeast British Columbia (BC) (Figure 1.2). Assessing the potential of buried valley aquifers is of critical importance in this region, given the high demand for water for industry. In the last 15 years, Northeast BC has seen a large increase in shale gas development. Hydraulic fracturing requires large volumes of water, with a single well requiring potentially more than 20,000 m^3 of water. Currently, most of the water used for hydraulic fracturing in the region is surface water (e.g. rivers or lakes), water source dugouts, or private acquisition and produced water (British Columbia Oil and Gas Commission (BCOGC), 2015); however, increased development may increase the

demand for groundwater stored in aquifers. Aquifers that are potential targets for groundwater development, both for industry and other uses (e.g. domestic and municipal drinking water supply and agriculture) may be associated with buried valleys.

The approximate extent of a large network of buried valleys had been delineated in the region prior to this thesis (Levson in Petrel Robertson Consulting Ltd., 2015); however, the hydrogeological characteristics of these buried valleys, in particular the continuity of high permeability materials, was largely unknown. Moreover, the broader role that these buried valleys play in the regional groundwater flow regime had yet to be explored. In this study, the buried valley aquifer system in the central Peace Region is investigated by developing a robust geological model using high-resolution geophysical and geological datasets (see study area in Figure 1.2). This geological model is then used to develop regional-scale numerical groundwater flow models to explore the hydraulic connectivity within the buried valley aquifer system.

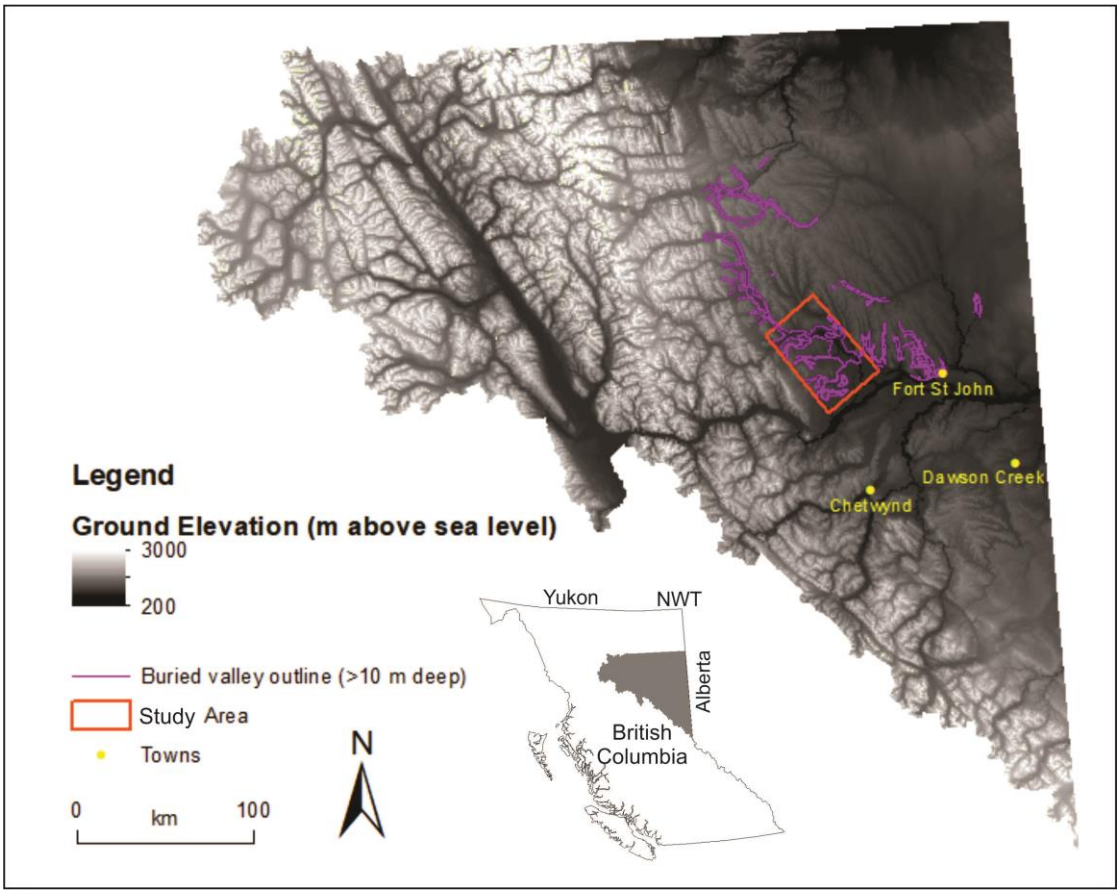

Figure 1.2. The Peace Region of Northeast British Columbia, Canada. Study area outline is shown in red rectangle. The outlines of buried valleys delineated by Levson in Petrel Robertson Consulting Ltd. (2015) are shown in purple.

1.1. Background and Literature Review

Buried valleys are channel-form depressions, or paleovalleys, that have been infilled by sediment and buried following their formation (Cummings et al., 2012). The term 'buried valley' is not exclusive to any type of genesis, and thus buried valleys can form via glacial, tectonic, fluvial, or other processes (Cummings et al., 2012).

There are two main conceptual models for buried valley formation in glaciated terrain (i.e. mid latitudes of North America and Europe, such as the Canadian Prairies): pre-glacial incision by large, Tertiary rivers (Figure 1.3a), and glacial incision by either proglacial or subglacial meltwater channels (Figure 1.3b and c) (Ahmad et al., 2009; Cummings et al., 2012; Pugin et al., 2014) (Figure 1.3). Across the western and central

plains of North America, well-developed drainage networks cut down into the bedrock prior to Pleistocene glaciation, forming valleys (Ritzi et al., 1994). Following the onset of glaciation, glacial and glaciofluvial processes further incised the bedrock, creating new valleys, or cutting further down into Tertiary valleys. The valleys were then subsequently filled and buried during periods of aggradation (Ritzi et al., 2000; Andriashek and Atkinson, 2007), making them difficult to identify and map on the modern landscape. In Denmark and Northern Europe, buried valleys are commonly of glacial origin; glacial processes during the Pleistocene carved out valleys that were subsequently filled with permeable outwash and then buried (Huuse and Lykke-Andersen, 2000; Jørgensen et al., 2003; Sandersen and Jørgensen, 2003).

The incision of the bedrock by pre-glacial rivers (Figure 1.3a), proglacial streams (Figure 1.3b) and subglacial streams (Figure 1.3c) resulted in highly permeable outwash deposits, low-permeability fine-grained material, and diamicton being left behind (Ritzi et al., 1994; Cummings et al., 2012). These sediments constitute the majority of the valley-fill, and some valleys may have been filled by multiple depositional events (Cummings et al., 2012). Therefore, valley-fill deposits can be highly heterogeneous.

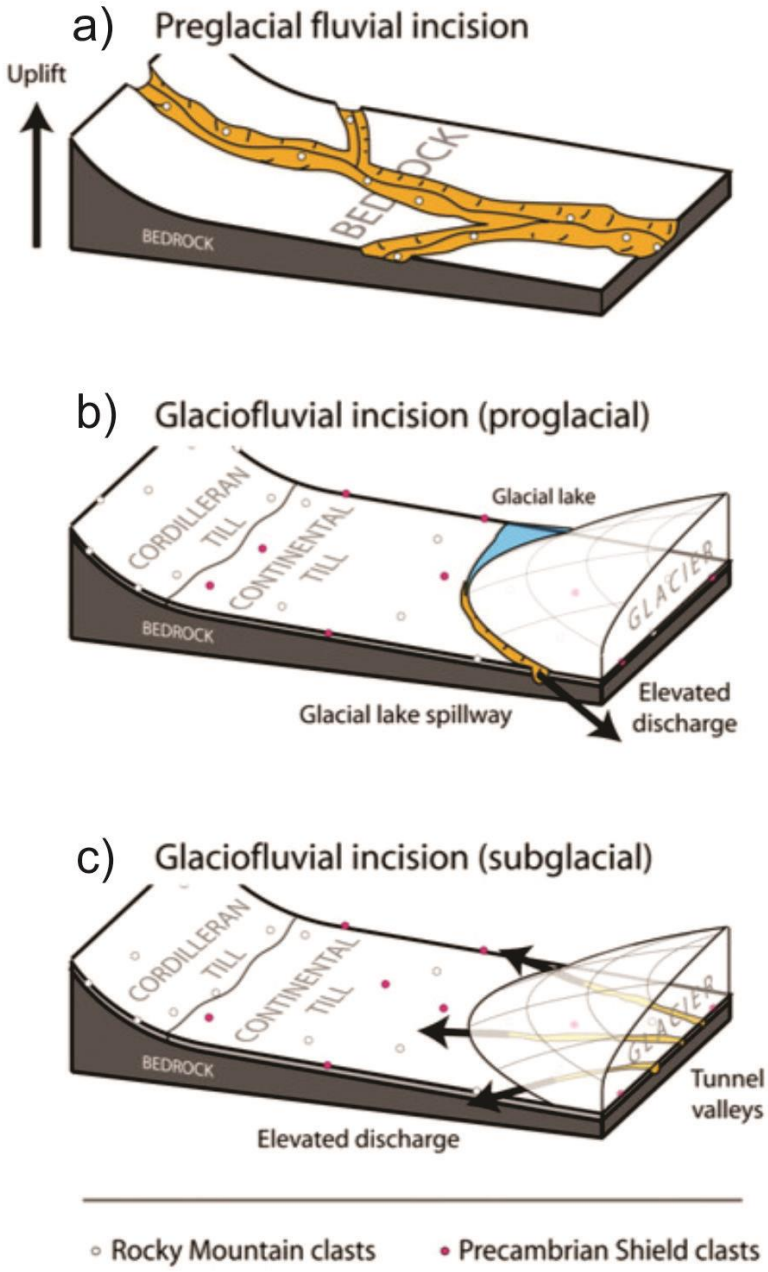

Figure 1.3. Conceptual models for Canadian Prairie buried valley incision. From Cummings et al. (2012) with permission.

The shape of a buried valley is a function of the processes that formed it. Buried valleys formed by pre-glacial fluvial incision are thought to be very wide and have shallow valley walls. Conversely, buried valleys formed by glaciofluvial processes (proglacial and subglacial) are believed to be narrow and deep (Cummings et al., 2012). However, these relationships are not always observed; buried valleys in Northeast British Columbia, Saskatchewan, and Manitoba, which are much wider compared to

modern river valleys, are interpreted to be formed by glaciofluvial processes (Mathews, 1978; Hartman and Clague, 2008; Hickin et al., 2008; Cummings et al., 2012). Combining shape with valley-fill provenance and stratigraphic position to infer origin is considered the appropriate method in most terrains (Cummings et al., 2012).

Due to their shape and heterogeneous fill, the hydrogeology of buried valleys can be quite complex. The sand and gravel bodies within the buried valleys can host significant aquifers (Jørgensen et al., 2003), both confined and unconfined, depending on the nature of the overlying drift and geology of the area (Di Salvo et al., 2012; Hickin et al., 2016). While these coarse-grained units can be thick, the architecture of the buried valley exhibits a primary control on the extent and continuity of the aquifers, directly impacting its role in flow and productivity as a groundwater resource (Russell et al., 2004).

Whether the buried valley formed as a result of pre-glacial Tertiary river incision or proglacial/subglacial meltwater channels affects the extent of the buried valley itself, and the continuity of its fill. Proglacial or subglacial buried valleys formed by rapid meltwater incision may terminate abruptly, and not demonstrate regional connections with other units (Gibling, 2006; Andriashek and Atkinson, 2007; Pugin et al., 2014). Hydraulic barriers, such as those formed by glacial processes, within the buried valley aquifers can also impede interconnections, and the heterogeneous nature of glacial sediments can cause segregation of permeable units, creating more localized flow systems (Shaver and Pusc, 1992). Pre-glacial buried valleys tend to form more regionally connected networks, and authors have described a hierarchical organization of “stacked” buried valleys in which smaller, glacially-formed buried valleys are inset in regional, pre-glacial buried valleys (Sharpe and Russell, 2004; Pugin et al., 2014). Sharpe and Russell (2004) note that the “nested” structure of some buried valleys can have a substantial impact on horizontal and vertical aquifer continuity and connectivity. Russell et al. (2004) suggest that the hydrogeological function of buried valley aquifers is dependent upon the extent and continuity of the aquifers, and may be variable at different scales (i.e. local, intermediate and regional).

Buried valleys may provide preferential pathways from near-surface to the deep subsurface, and can act as the connection between shallow and deep groundwater (Sandersen and Jørgensen, 2003; Seifert et al., 2008). Buried valley aquifers may also

act as an inter-aquifer recharge source for bedrock aquifers if the valleys are hosted in or adjacent to bedrock (Seyoum and Eckstein, 2014). Conversely, the buried valleys themselves can rely on this relationship for recharge. Andriashek and Atkinson (2007) describe different situations for buried valley aquifers to interact with surface water bodies or deep bedrock aquifers, some of which pertain to the Peace Region: (1) interactions with other buried valley aquifers (within a single buried valley, or other buried valleys); (2) interactions with bedrock aquifers; or (3) interactions with surface or near-surface water. It is important to consider all possible interactions of the buried valley aquifers within the hydrogeological regime to characterize their role in groundwater flow.

Several studies (described below) illustrate the effects that buried valley aquifers have on groundwater flow. These studies stem from concerns for both water availability, and possible contamination problems, due to the potential for rapid transport within the permeable sediments.

Russell et al. (2004) and van der Kamp and Maathuis (2012) discuss the large drawdown response from pumping tests in buried valley aquifers using the Estevan buried valley aquifer in Saskatchewan as a case study. Significant drawdowns were recorded at great distances from the pumping well, indicating a continuous permeable unit that is laterally and vertically confined.

Seifert et al. (2008) investigated the impact of a buried valley on groundwater vulnerability in two different conceptual hydrogeological models. From the conceptual hydrogeological models, two numerical models were created, one with the buried valley containing a high proportion of Quaternary sand, and the other without. The presence of the buried valley resulted in more rapid simulated particle transport, different recharge areas, and younger groundwater ages.

Weissman et al. (2004) explored the role of a coarse-grained valley-fill deposit incised into an alluvial fan. Results from a groundwater flow and solute transport model revealed that the valley-fill significantly affected the hydrogeological regime. The coarse-grained sediments (sands and gravels) had a high degree of connectivity, which resulted in rapid flow within the valley-fill compared to the surrounding fine-grained material.

Enhanced recharge and vertical transport occurred within the valley due to the high hydraulic conductivity of the sediments resulting from their coarse-grained texture.

Finally, Troost and Curry (1991) examined two bedrock buried valleys underlying a site that was proposed for a low-level radioactive waste disposal facility. The authors undertook an extensive investigation to evaluate the interconnections of the basal sand and gravel units within the buried valleys, as these would be the most problematic in terms of isolation of waste. Using borehole cores for lab testing and depositional modelling, in combination with aquifer pumping tests, the interconnections of the permeable sediments were found to be weak. This was attributed to the high proportion of silt and clay in the valley-fill.

Walton (1970) suggests that buried valley aquifers could have a significant impact on the groundwater flow regime at the regional scale. Andriashek and Atkinson (2007) conducted a fairly extensive investigation of the buried valley aquifers in the Fort McMurray region in Alberta, and while a regional geological model was constructed, no hydrogeological characterization of the buried valleys was performed. Russell et al. (2004) describe that there has been limited hydrogeological investigation into buried valley systems at a regional scale; specifically, the extent and continuity of aquifers within buried valley systems, their role in regional flow, and their potential as groundwater resources.

1.2. Purpose and Objectives of Research

The purpose of this research is to contribute to the knowledge of buried valley aquifer hydrogeology, and explore the influence that buried valley aquifers have on groundwater flow at a regional scale. It is hypothesized that if the permeable units of a buried valley network are continuous, have an adequate source of recharge, and a specific discharge area(s), then the buried valley aquifers will play a significant role in regional groundwater flow.

To test this hypothesis, the fundamental mechanics of groundwater flow need to be considered. Groundwater moving through a system is governed by Darcy's Law and is dependent upon the hydraulic gradient and the hydraulic conductivity of the substrate. While the sand and gravel bodies within buried valley aquifers tend to have high

permeability, if there is no gradient present, there will be no driving force to move the water. This requires recharge to the buried valley aquifers and a discharge location(s). The extent of this recharge area and the amount of recharge available will affect the amount of water that moves through the aquifers. Likewise, where the water discharges will influence the flow system. It also must be kept in mind that the permeable units must be spatially continuous and form a lithologically connected “network” to play an integral role in conveying groundwater at a regional scale.

The specific objectives of this thesis are:

1. Determine the nature of the continuity of the permeable units within the buried valley network in the central Peace Region.
2. Characterize the regional groundwater flow system for the buried valley aquifer network.
3. Analyze the impact of buried valley aquifers on the regional water budget and assess the potential of the buried valley network as a groundwater source.

This thesis also aims to extend the research conducted for Geoscience BC’s Peace Project to contribute new information about groundwater and shallow aquifers towards the management of Northeast BC’s water resources.

1.3. Scope of Work

This study focuses on the large network of buried valleys in the central Peace Region of Northeast BC (Figure 1.4). This network was delineated using bedrock mapping, mapped surficial geology, and borehole logs (Levson in Petrel Robertson Consulting Ltd., 2015). Levson in Petrel Robertson Consulting Ltd. (2015) classified the buried valleys as generally having >10 m of Quaternary fill. Therefore, various generations of buried valleys at different scales may exist within this network, including those incised into bedrock or those incised into Quaternary material; however, buried valley genesis was not investigated in this thesis. Moreover, permeable deposits within the buried valleys may be present in both confined and unconfined conditions.

More recently, a number of high quality geological and geophysical datasets were produced as part of Geoscience BC’s Peace Project (e.g. Petrel Robertson

Consulting Ltd., 2015; Aarhus Geophysics ApS, 2016a-e; Bemex Consulting International and Quaternary Geosciences Inc., 2016; Levson and Best, 2017a and b; Mykula, 2017; Best and Levson, 2017 unpublished report). These datasets include: 1) airborne time domain electromagnetic (TEM) interpretations for approximately 8000 km^2 of the Peace Region including horizontal resistivity depth slices and vertical resistivity cross-sections, 2) corrected gamma-ray logs for approximately 1400 wells, 3) borehole data including detailed lithologic logs and downhole geophysical logs for ten locations throughout the Peace Project area, 4) surficial and bedrock geology maps, and 5) tabulated databases from water and petroleum wells in the area.

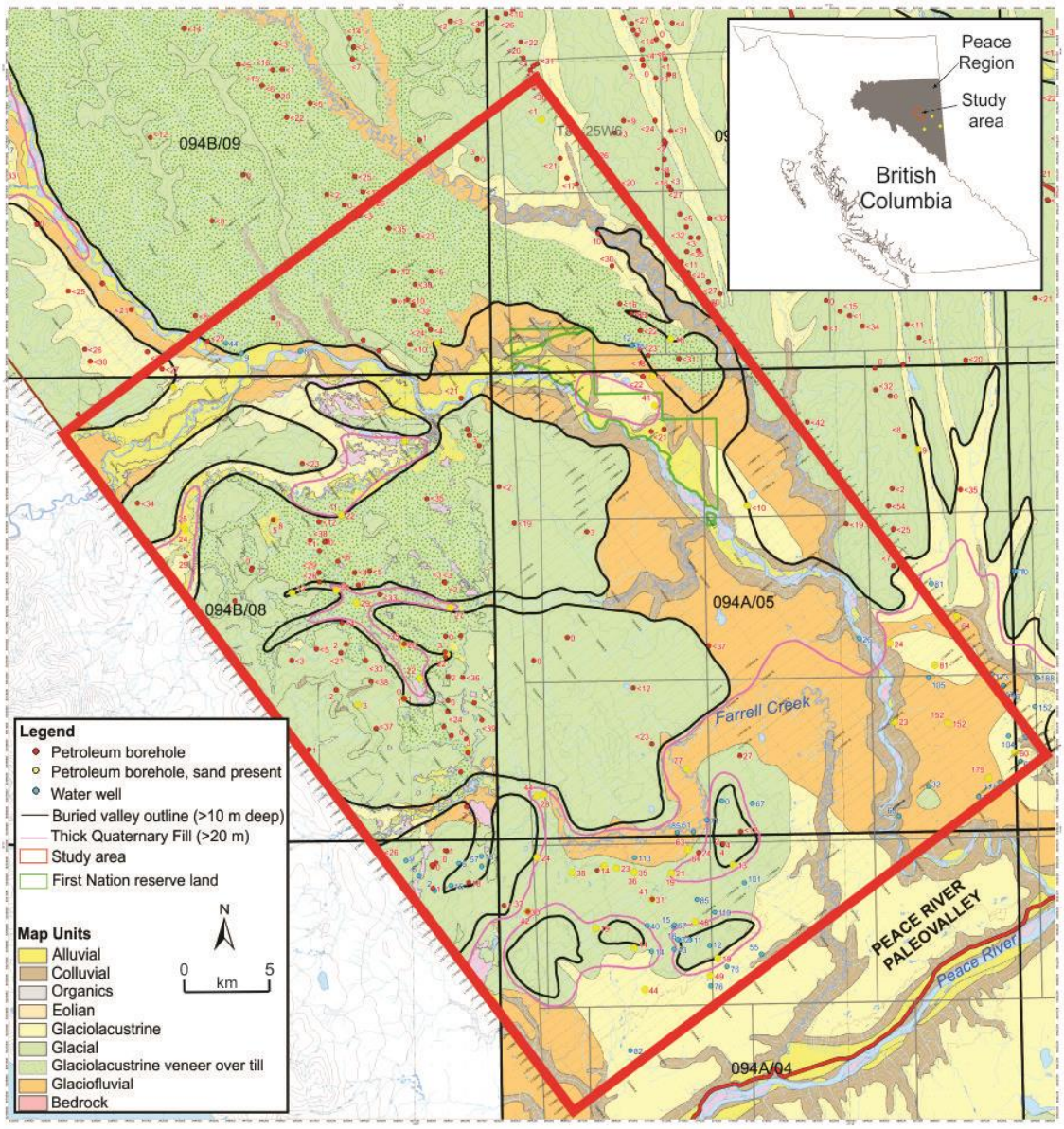

Figure 1.4. Surficial geology of the Peace Region of Northeast British Columbia. The study area is outlined in red and the thick black lines represent outlines of buried valleys (generally >10 m deep). Numbers next to well locations indicate depth to bedrock picks. Modified from Petrel Robertson Consulting Ltd. (2015) with permission.

The following three subsections describe the specific scope of work to be completed in order to accomplish each objective.

1.3.1. Objective 1: Determine the nature of the continuity of the permeable units within the buried valley network

In order to assess the continuity of the permeable sand and gravel units within the buried valley network, a geological model of the buried valley network was developed.

The geophysical and geological datasets produced from the Peace Project were imported into the reservoir software, Petrel (Schlumberger, 2016), and used to design a 3-D geological model of the buried valley network. The interpreted geology from the TEM resistivity data were used to differentiate fine- and coarse-grained material within the valley-fill. The corrected gamma-ray logs were used to delineate the outline of the buried valleys, identify top of bedrock contacts (Petrel Robertson Consulting Ltd., 2015), and contacts between bedrock formations. Additionally, in combination with the surficial geology map and lithology logs reported by well drillers (WELLS database; BC Ministry of Environment, 2017), they were used to supplement the TEM data to verify the geological interpretation of the valley-fill. Seven boreholes within the study area were also drilled to confirm the geological interpretation of the geophysical data. Different algorithms within Petrel were evaluated to model the geology based on the interpretation of the geophysical datasets.

1.3.2. Objective 2: Characterize the regional groundwater flow system for the buried valley aquifer network

Using the 3-D geological model developed in Objective 1, two interpretive, steady-state, 3-D numerical flow models were created in MODFLOW (Harbaugh, 2005) for the central Peace Region study area to characterize the regional groundwater flow system of the buried valley network. The first model incorporated the detailed geological complexity derived from the Petrel model, and the second was a simplified model based on the original conceptualization of the buried valley network (i.e. large bedrock valleys filled with thick packages of till overlying regionally connective basal sands and gravels; see Figure 1.1). The two models had the same parameterization and boundary conditions.

The hydraulic properties of the geological units were estimated primarily from consulting reports and from grain size analyses on samples collected from the boreholes

drilled within the study area to confirm the geological interpretation of the geophysical data. These were supplemented by estimates obtained from the literature based on the texture of the Quaternary deposits in the central Peace Region. The model boundary conditions were approximated based on existing information including surface topography, geology, and major water bodies. Spatial recharge has been estimated for the Peace Region by Holding and Allen (2015), who provide a range of average mean annual recharge between 0 and 128 mm/year based on the mean annual precipitation of the area. Recharge rates within this range were tested and applied to the uppermost active layer of the numerical models. Other boundary conditions thought to control the flow within the buried valley aquifer system were incorporated. These included major rivers such as the Peace River, Halfway River, Graham River, and other tributary creeks. Available hydrometric data were used to obtain estimates of baseflow.

Uncertainty analyses were performed to determine the model sensitivity to the hydraulic conductivity distribution, recharge, and other boundary conditions. The Particle Tracking tool within MODFLOW was used to identify and delineate likely recharge and discharge areas of the buried valley aquifer network. The groundwater travel paths were also observed to explore the regional groundwater flow system.

1.3.3. Objective 3: Analyze the impact of buried valley aquifers on the regional water budget and assess the potential of the buried valley network as a groundwater source

Within MODFLOW, the Zone Budget analysis tool was used to estimate the amount of water moving through the buried valley aquifer network. Zone Budget was also used to estimate the amount of water moving outside the buried valleys, within the bedrock. These two amounts were compared to address the question of the impact of the buried valley aquifers on regional groundwater flow.

Additionally, within the numerical model containing geological complexity, simulations were carried out to assess the potential of these buried valley aquifers as a groundwater resource. This was achieved through adding pumping wells to the steady-state model that were completed in the buried valley aquifers. Abstraction was simulated, and the Particle Tracking tool was used to identify capture zones in the steady-state flow field.

1.4. Thesis Organisation

This thesis is organized into six chapters that are described as follows:

- Chapter 1 provides an introduction to the thesis, and gives an overview of buried valley formation, general architecture, and the concepts related to their role in groundwater flow. The specific purpose and objectives of the thesis are defined and the scope of work is outlined.
- Chapter 2 is split into two sections; the first section describes the study area, the Peace Region of Northeast British Columbia, provides an overview of the region, and discusses the climate, hydrology, bedrock geology, glacial history and hydrogeology of the area. The second section outlines the geophysical and geological datasets that were used to develop the geological model, and provides some background information on the geophysical surveys conducted by Geoscience BC prior to this study to produce said datasets.
- Chapter 3 describes the construction of the geological model of the buried valley network using the reservoir software Petrel. The incorporation of the geological and geophysical datasets within Petrel is explained, and a new workflow for incorporating these data in Petrel is presented.
- Chapter 4 presents the results of the geological modelling in Petrel. The results are analyzed and limitations of the datasets and the modelling are discussed. The final geological model that was imported to MODFLOW is presented and discussed.
- Chapter 5 describes the development and results of the numerical models of the buried valley network in MODFLOW. The impact that the buried valley network has on regional groundwater flow is explored, and the buried valley aquifers are assessed as a groundwater resource for the region. This chapter forms the basis for a manuscript for a peer-reviewed journal paper provisionally titled: “Investigating the Hydraulic Role of a Large Buried Valley Network on Regional Groundwater Flow”.
- Chapter 6 outlines the conclusions of the thesis and provides recommendations for future research.

Chapter 2.

Study Area and Data Sources

This chapter is divided into two sections. The first section presents an overview of the physiography of the Peace Region in Northeast BC, describes the climate and hydrology, the glacial history and surficial sediments, the Cretaceous bedrock, and the hydrogeology. The second section introduces the data sources used in this research and provides background and supplementary information on how the data were processed and used.

2.1. Study Area: The Peace Region

2.1.1. Physiography

The Peace Region is situated in Northeast BC, east of the Rocky Mountains and along the western edge of the Alberta Plateau (Holland, 1964) (Figure 2.1). With the exception of the mountainous region to the west, Northeast BC has a generally low-relief terrain with thick deposits of glacial drift and extensive forest cover (Levson, 2008). The average elevation of the Peace Region is approximately 600 masl (metres above sea level) (Holland, 1964), with an average relief of 300 m (Catto, 1991). Mathews (1978) described three distinct classes of topography in the Peace Region: uplands with steep to gently rolling ridges; incised river valleys; and, flat benches adjacent to river valleys (Figure 2.1).

In the uplands, bedrock is typically found within 15 m of the surface, and depth to bedrock beneath the terraces adjacent to river valleys ranges from 15 to 180 m (Mathews, 1978; Hartman and Clague, 2008). Within the study area in the central part of the region (see study area outline in Figure 2.1), the bedrock elevation ranges from 460 to 975 masl.

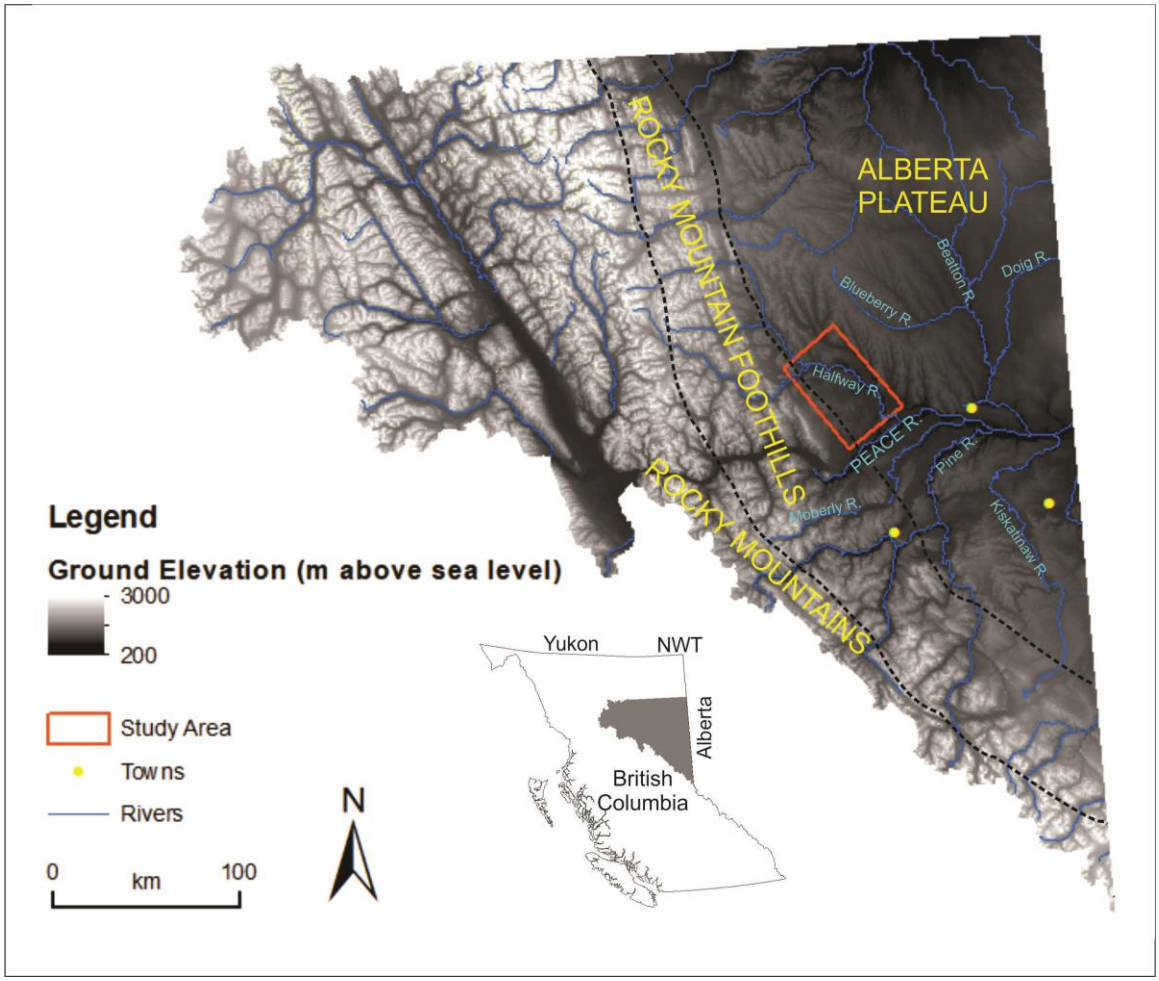

Figure 2.1. The Peace Region of Northeast British Columbia, Canada. The red rectangle shows the study area outline.

2.1.2. Climate and Hydrology

The climate of the Peace Region is continental boreal and consists of long cold winters, and short warm summers. Throughout the year, average daily temperatures at Fort St. John (Climate Station ID: 1183000) range from 16 to -13°C, mean monthly precipitation ranges from 19 to 75 mm, and mean annual precipitation is 445 mm/year (Environment Canada, 2017a: Climate Normals 1981-2010). Mean monthly precipitation and daily temperature for Fort St. John are shown in Figure 2.2. The location of the Fort St. John climate station is shown in Figure 2.3.

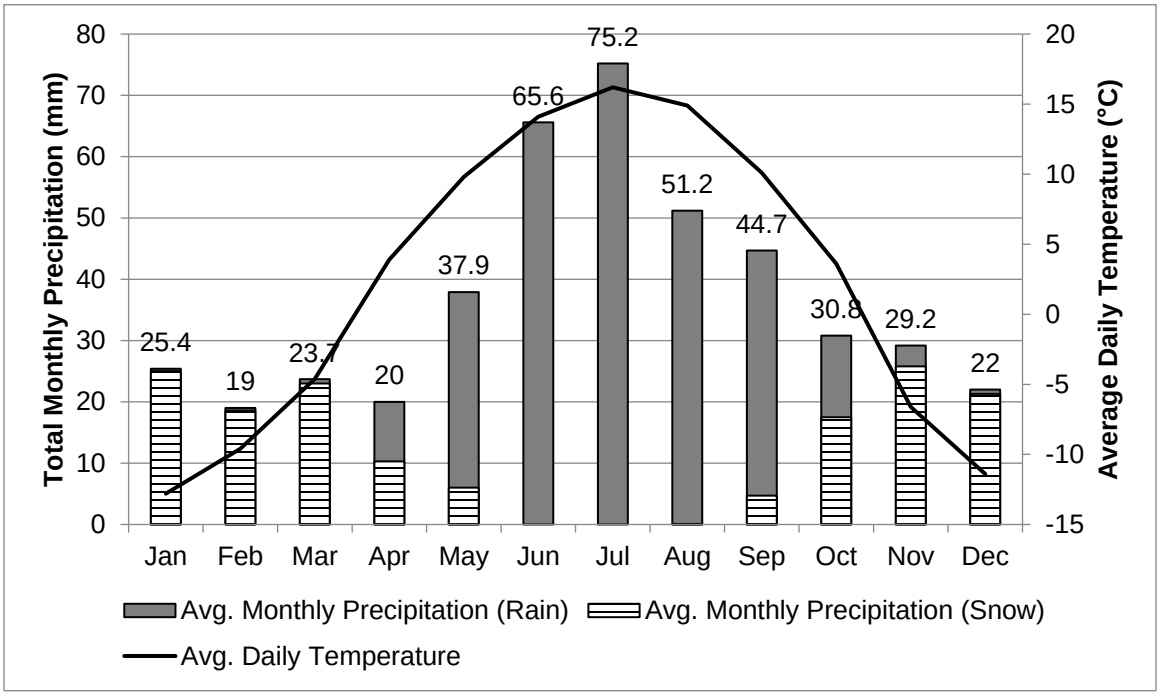

Figure 2.2. Average monthly precipitation (rain and snow) and daily temperature at Fort St. John (Climate Station ID: 1183000). Climate Normals (1981 to 2010) were obtained from Environment Canada (2017a).

The Peace Region has a mixed pluvial and nival regime, with rainfall typically occurring in the summer months (May-September) and snowfall occurring in the winter months (November-March). Due to the topographic transition from mountains to plains, higher elevation areas in the region receive significant snowfall and are subject to rain on snow melting and melting of snowpack which contribute to the spring freshet (peak in June).

The Peace River is the major river in the Peace Region and drains an area of approximately 122,000 km^2 within BC. Its headwaters are located in the Rocky Mountains, and it flows east into Alberta (Figure 2.1). There are several major river systems tributary to the Peace River including the Halfway, Pine, Beatton and Kiskatinaw Rivers (see Figure 2.1). Along the banks of these rivers, mass movements such as landslides are a common occurrence (Catto, 1991).

There are several rivers within the study area including the Halfway River, Cameron River, and Graham River, which together drain approximately 9,260 km^2.

There are also smaller creeks that are tributaries to these rivers including Farrell Creek, Groundbirch Creek, and Kobes Creek (see Figure 2.3 for locations).

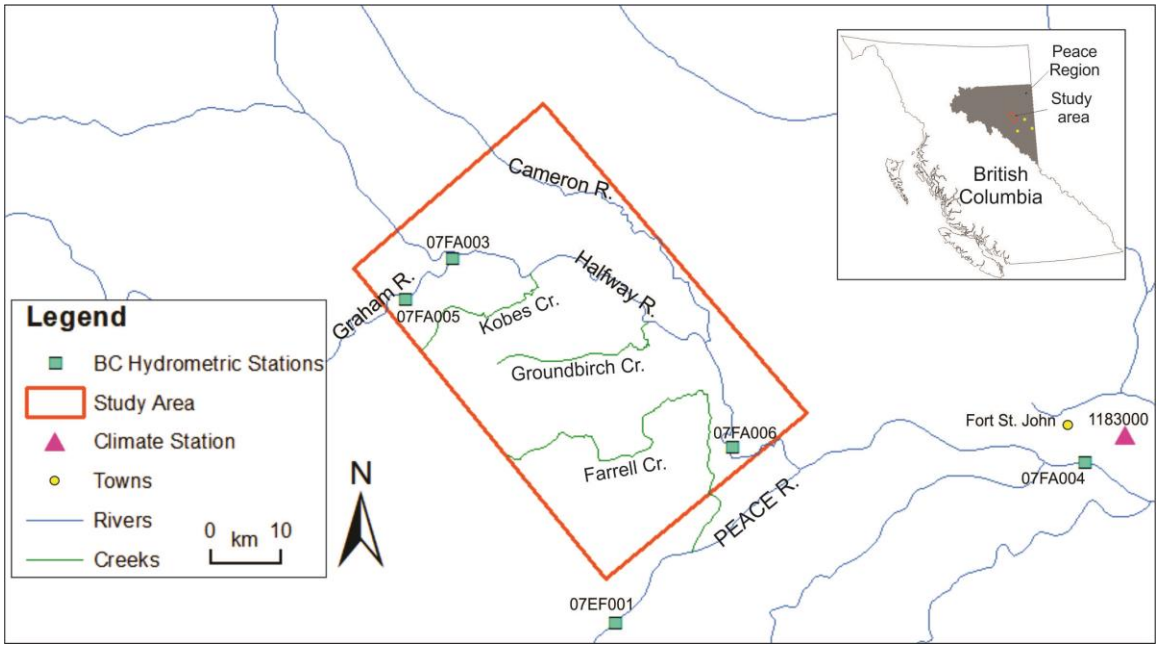

Figure 2.3. Locations of BC hydrometric stations within study area. Major rivers and creeks within the study area are also shown.

There are three hydrometric stations in the study area (07FA003 and 07FA006 along the Halfway River and 07FA005 along the Graham River), and two along the Peace River south of the study area (07EF001 and 07FA004) (Figure 2.3). Figure 2.4 shows the average monthly discharge at each hydrometric station, along with mean monthly precipitation at Fort St. John. The highest streamflows occur from May to July, with peak flows in June and July, which correspond to snowmelt during the spring freshet. These two months also correspond to high mean monthly precipitation; however, the evapotranspiration (ET) in the summer months is so high that much of the precipitation is lost to ET.

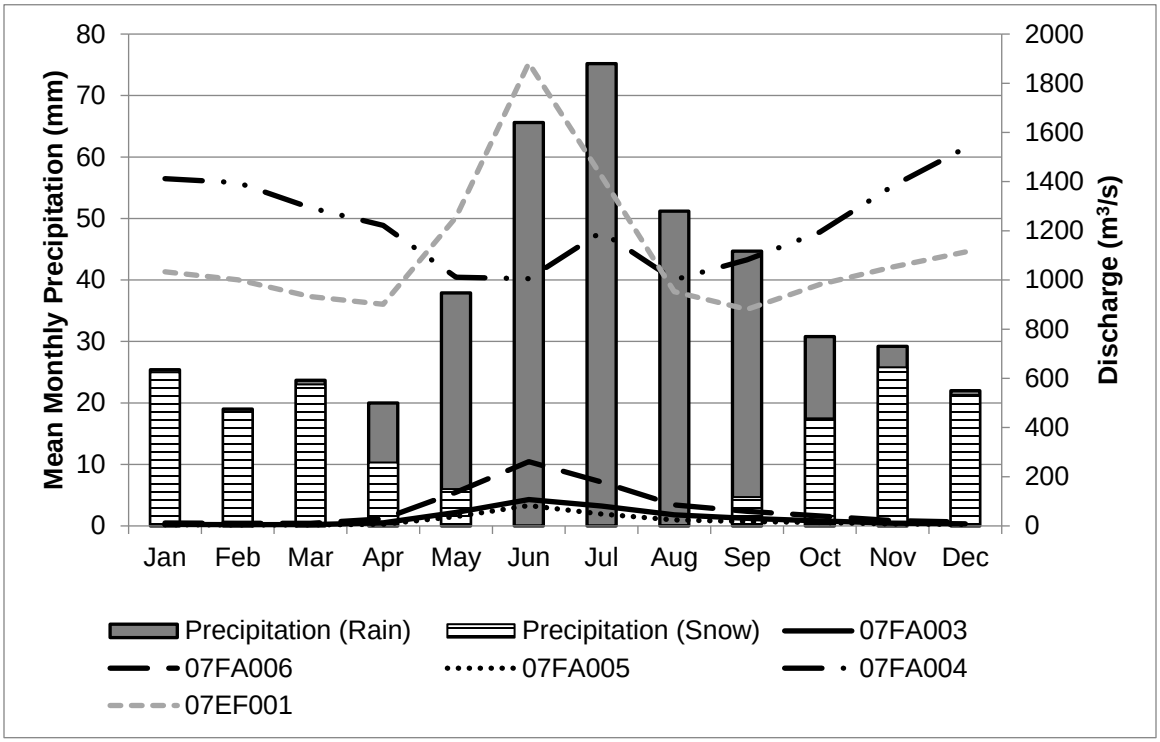

Figure 2.4. Mean monthly streamflow data for hydrometric stations 07FA003 (1977-2014), 07FA004 (1979-2011), 07FA005 (1981-2014), 07FA006 (1984-2014), and 07EF001 (1950-2012). Also shown is the average monthly precipitation (rain and snow) at Fort St. John (Climate Station ID: 1183000) for the 1981 to 2010 Climate Normal Period. Data were obtained from Environment Canada (2017a-f).

Figure 2.5 shows the 2013 monthly river stages for stations 07FA003 and 07FA006 along the Halfway River and 07FA005 along the Graham River plotted with average monthly precipitation at Fort St. John. Figure 2.6 shows the 2011 monthly river stages for stations 07FA004 and 07EF001 along the Peace River, also plotted with average monthly precipitation. These figures allow investigation of the response of river levels to precipitation and snowmelt at a monthly scale.

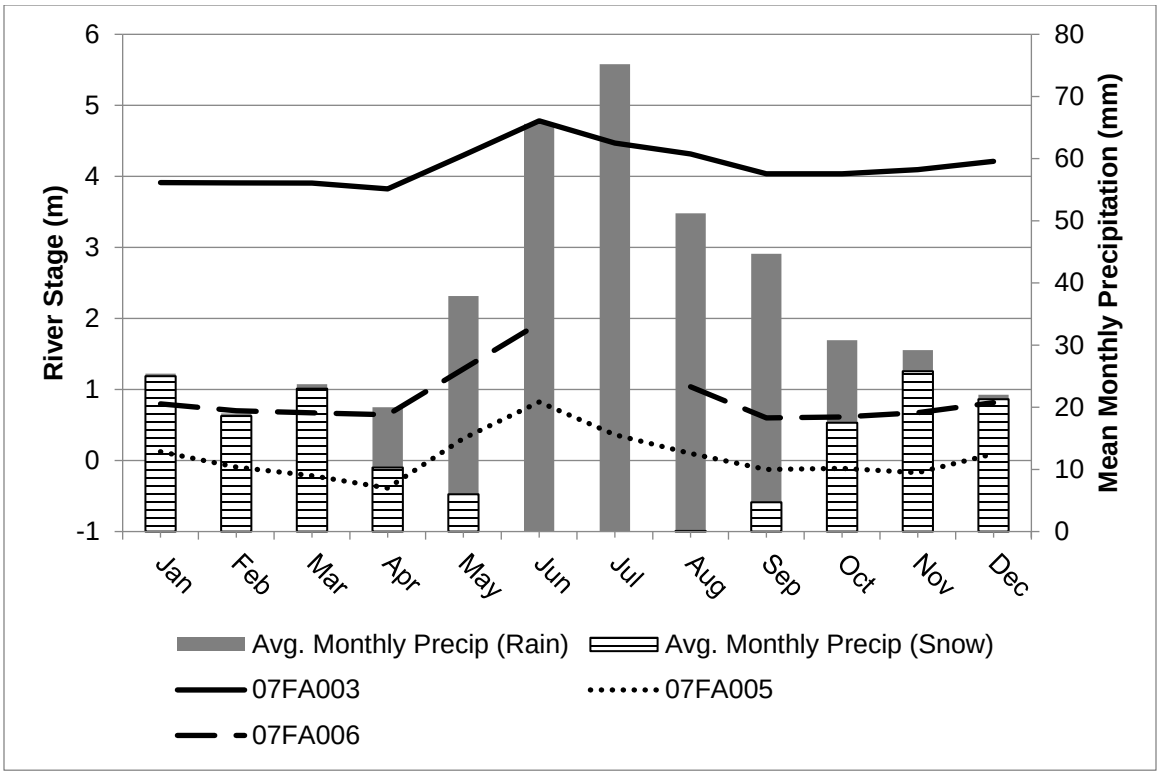

Figure 2.5. **2013 monthly river stages for the Halfway River above the confluence with the Graham River (station 07FA003), the Halfway River near Farrell Creek (station 07FA006) and the Graham River (station 07FA005). Hydrometric data were obtained from Environment Canada (2017b,d,e) Also shown is the average monthly precipitation (rain and snow) at Fort St. John (Climate Station ID: 1183000) for the 1981 to 2010 Climate Normal Period (Environment Canada, 2017a).**

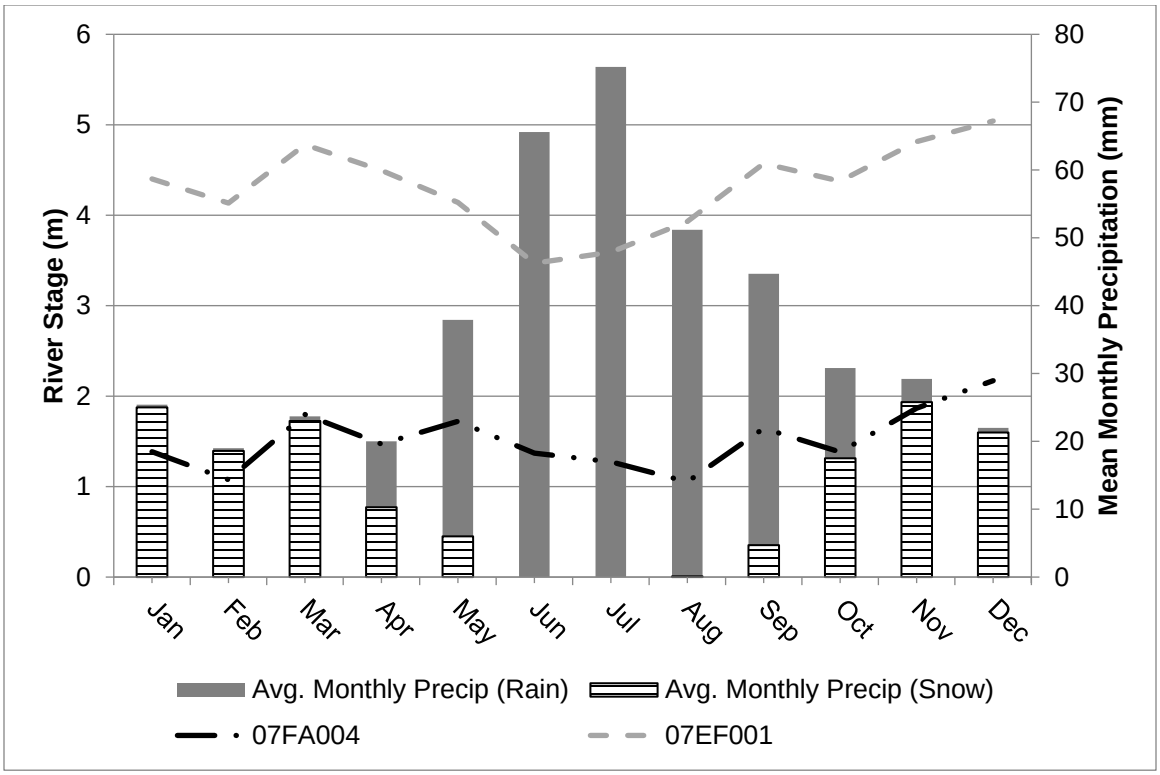

Figure 2.6. 2011 monthly river stages for the Peace River at Hudson's Hope (station 07EF001) and above the confluence with the Pine River (station 07FA004). Hydrometric data were obtained from Environment Canada (2017c and f). Also shown is the average monthly precipitation (rain and snow) at Fort St. John (Climate Station ID: 1183000) for the 1981 to 2010 Climate Normal Period (Environment Canada, 2017a).

Stations 07FA003, 07FA005, and 07FA006 all show a similar river stage profile of peak levels in June (Figure 2.5), whereas stations 07FA004 and 07EF001 have peak levels in March and September, with low river levels in July and June (Figure 2.6). While it should be kept in mind these two figures show river stage data from two different years, general trends can still be deduced. As the river flows can largely be attributed to spring freshet, the stations further upstream (07FA003, 07FA005 and 07FA006) will have peak river levels earlier than those further downstream (07FA004 and 07EF001).The lower river stages of stations 07FA004 and 07EF001 at times of high precipitation (June and July) highlight the effect of precipitation being lost to high ET. It should also be noted that the WAC Bennett hydroelectric dam is upstream of stations 07FA004 and 07EF001, which likely has an impact on river stage throughout the year.

2.1.3. Bedrock Geology

The bedrock strata underlying the Peace Region comprise Paleozoic to Tertiary age sedimentary rock overlying Precambrian basement (BC Ministry of Natural Gas Development, 2011). The sedimentary bedrock can reach thicknesses of up to 6 km in the Cordilleran foreland, but thins towards the northeast (BC Ministry of Energy and Mines, 2011). Cretaceous sedimentary rocks outcrop at surface or directly underlie surficial sediments in the study area. They represent several marine transgression-regression-transgression cycles and are, for the most part, gently dipping towards the southwest (BC Ministry of Energy and Mines, 2011). The Cretaceous units in the study area are further underlain by Jurassic strata (Stott, 1982). It is these Cretaceous units that are of interest to this research. A generalized stratigraphic column is shown in Figure 2.7, and a stratigraphic column highlighting the Cretaceous formations and their lithology is shown in Figure 2.8.

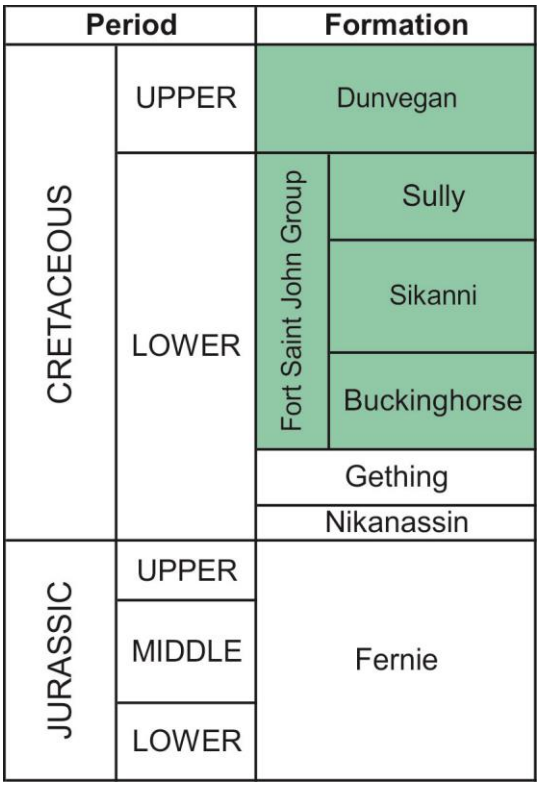

Figure 2.7. Generalized bedrock stratigraphic column of the Peace Region of Northeast British Columbia (after Stott, 1982). The Cretaceous bedrock units of interest to this research are highlighted in green.

The marine shale and minor sandstone of the Fort Saint John Group, composed of the Lower Cretaceous Buckinghorse Formation, Lower Cretaceous Sikanni Formation, and Upper Cretaceous Sully Formation, are overlain by the Upper Cretaceous Dunvegan Formation (BC Ministry of Natural Gas Development, 2011) (Figure 2.8).

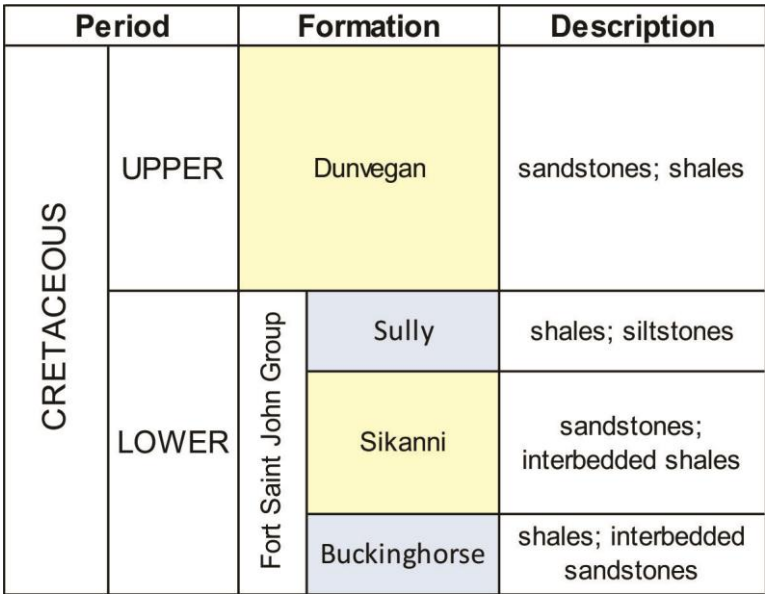

Figure 2.8. Simplified stratigraphy of the Cretaceous bedrock formations in the Peace Region of Northeast British Columbia. Predominantly sandstone units are shown in yellow and predominantly shale units are shown in grey.

The Lower Cretaceous (Albian) Buckinghorse Formation is composed of a thick marine package of predominantly shales with interbedded fine-grained sandstones. This formation was deposited in an offshore/shelf setting of the Albian foreland basin and can reach thicknesses exceeding 1000 m (Schroeder-Adams and Pedersen, 2003). The Buckinghorse Formation is underlain by the Gething Formation, and overlain by the Lower Cretaceous Sikanni Formation. The Sikanni Formation was deposited in a shoreface environment, and is composed of alternating sandstone and shale beds that range in thickness from 100 to 400 m (Schroeder-Adams and Pedersen, 2003; Jowett et al., 2007). Overlying the Sikanni Formation is the Sully Formation, comprised predominantly of shales and siltstones.

The Upper Cretaceous Dunvegan Formation conformably overlies the marine units of the Fort Saint John Group and is composed of sandstone, shale, and minor

conglomerate. These sediments were deposited in a deltaic and pro-deltaic environment and typically form cliffs, which are seen on the modern landscape (Hickin et al., 2008).

2.1.4. Glacial History and Surficial Deposits

The Quaternary geology of the Peace Region has been the subject of numerous studies over the past few decades. Both the Cordilleran and the Laurentide ice sheets traversed the landscape during Pleistocene glacial periods (Hartman, 2005; Hartman and Clague, 2008). However, the timing, extent, and possible coalescence of these two glacial systems have been a subject of debate among various researchers (Hartman, 2005). While the objectives of this thesis are not to determine the glacial history of the Peace Region, processes that occurred during the Pleistocene glacial and interglacial periods have a profound impact on the formation and subsequent architecture of the paleovalleys (buried valleys) in the region.

Seminal work conducted by Mathews (1978) suggested that there were at least three Laurentide advances in the Peace Region during the Quaternary, with three or possibly four Cordilleran advances. However, recent work has reduced this number, and has also reduced the number of Cordilleran advances (Hartman, 2005). While it is possible this area was subject to several glacial-interglacial cycles throughout the Quaternary, the most recent cycle during the Late Wisconsinan (ca. 25-10 ka) had the most pronounced effect on the landscape and topographic features of the region (Hickin et al., 2008). Both advancing and retreating ice sheets impounded large proglacial lakes by blocking drainages (Mathews, 1980). This resulted in the deposition of thick sequences of glaciolacustrine sediments, which are variably preserved in the region (Hickin et al., 2008). Each time an ice sheet traversed the landscape, the soft Cretaceous bedrock was eroded. Glaciofluvial activity from proglacial and subglacial meltwater channels also contributed to this erosion. During interglacial periods, fluvial systems further incised the bedrock, and deposited coarse-grained material. These combined processes created and shaped buried valleys found throughout the region.

The surficial deposits left behind during these glacial periods are glaciolacustrine silts and clays, glaciofluvial sands and gravels, and till in which the provenance is distinguished by the presence or absence of clasts from the Canadian Shield, indicating Laurentide or Cordilleran origin, respectively. Paleovalleys formed during both pre-

glacial and glacial times were subsequently filled with this material. As this fill is more easily erodible than bedrock, the valley-fill deposits may have also been further eroded. Finally, these valleys were further filled and then buried during the Late Quaternary by processes such as aggradation. As a result, in many areas, these valleys have little to no surface expression due to thick accumulations of Quaternary sediments (Levson et al., 2006; Hickin et al., 2016). This makes the process of identifying and mapping these buried valley aquifers challenging.

2.1.5. Aquifers in the Peace Region

The Peace Region is comprised of unconfined, confined, and bedrock aquifers. Lowen (2011) identified, classified, and delineated developed aquifers in the area, mapping a total of 55 aquifers; 23 are bedrock and 32 are comprised of unconsolidated sediments. The highest yielding bedrock wells are those completed in the Dunvegan Formation. Unconsolidated aquifers are primarily located along modern river valleys, and the most productive water wells drilled into the surficial sediments are those completed in glaciofluvial deposits (Lowen, 2011). Unconsolidated aquifers are also associated with glaciofluvial sand and gravel deposits within buried valleys (Levson et al., 2006). In some areas, these valley-fills may constitute productive aquifers (Lowen, 2011), so there is an interest in identifying the location of buried valleys in the Peace Region and characterizing their fill materials.

Several studies have documented the existence of buried paleovalleys in the Peace Region, and their importance as groundwater sources (e.g. Mathews, 1978; Levson et al., 2006; Hartman and Clague, 2008; Hickin et al., 2016). Hickin (2011) identified nine paleovalleys in the South Peace Region through bedrock mapping, which was further modified by Hickin et al. (2016) to include four additional paleovalleys. Hickin et al. (2016) also provide an extensive overview of the Groundbirch paleovalley, describing its architecture and valley-fill stratigraphy. Hartman and Clague (2008) identified two buried paleovalleys, both with a basal fluvial gravel unit, along the modern Peace River valley. Figure 2.9 shows the outlines of these paleovalleys that have been mapped in the Peace Region.

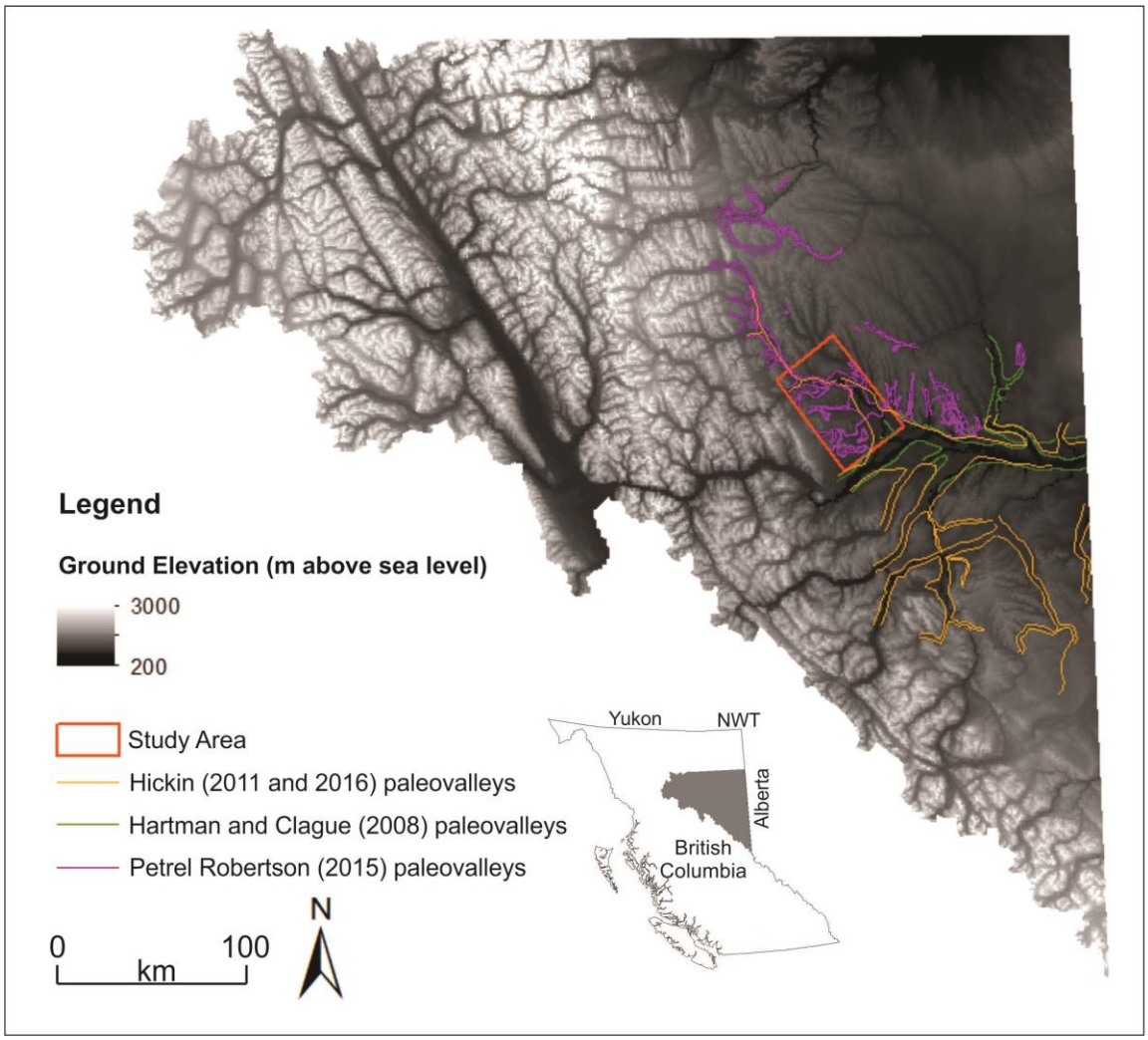

Figure 2.9. Mapped paleovalleys of the Peace Region. Paleovalley outlines obtained from Hartman and Clague (2008), Hickin (2011), Hickin et al. (2016), and Levson in Petrel Robertson Consulting Ltd. (2015).

While these localized investigations characterize single buried valleys, or a small network, there has not been a regional study conducted in Northeast BC that has attempted to characterize a large network of multiple buried valleys in the Peace Region, such as the one considered in this study (Levson in Petrel Robertson Consulting Ltd. (2015) outline shown in Figure 2.9). Similarly, no studies have attempted to model the geological architecture of a buried valley network and assess what impact the network would have on the regional groundwater flow regime. Being able to assess the potential of buried valley aquifers is of critical importance in the Peace Region, given the high demand for water resources.

2.2. Data Sources for the Geological and Numerical Models

The first phase of this study involved developing a conceptual geological model of the buried valley network of the central Peace Region (Figure 2.9). A conceptual model brings together all of the available data that impact the hydrogeology of the study area, and provides a framework for creating the numerical model (Anderson et al., 2015). A conceptual model should draw from various data sources such as: geology, geophysics, hydrology, climate and geomorphology (Kolm, 1996). The design of a conceptual geological model or geological framework helps to identify possible hydrostratigraphic units, and units that may have similar hydrogeological characteristics such as hydraulic conductivity. Facilitating the estimation or inference of properties, such as hydraulic conductivity, is necessary, as numerical models are highly parameterized. Due to the size of regional hydrogeological investigations, it becomes essential to combine multiple geological and geophysical datasets to ensure an accurate and well-constrained model.

A variety of data sources were used in this study to develop the conceptual geological model:

- Airborne transient electromagnetic (TEM) survey data
- Corrected gamma-ray logs from oil and gas wells
- Lithology logs from water wells
- Lithology and borehole geophysical logs from boreholes drilled for field verification of the geophysical data for the Peace Project

Each of these data sources is discussed in detail in the following four sections.

2.2.1. Airborne Transient Electromagnetic (TEM) Survey Data

Transient electromagnetic (TEM) surveying is a common geophysical investigation technique used in groundwater studies (Danielsen et al., 2003; Jørgensen et al., 2003; Aucken et al., 2008; Sapia et al., 2014). Over the last decade, airborne TEM systems have been developed and proven successful for hydrogeophysical studies of buried valleys (e.g. Steur et al., 2009; Aucken et al., 2008; Høyer et al., 2011; Oldenborger et al., 2013; Høyer et al., 2015; Oldenborger et al., 2016; Korus et al.,

2017). The airborne systems are flown with a helicopter, suitable for data acquisition over larger study areas. The transmitter and receiver coils, power supplies, GPS, etc. are all carried as a sling load from the helicopter (Sørensen and Auken, 2004), which is flown along pre-determined survey lines in the study area. The SkyTEM system developed by Sørensen and Aucken (2004) was specifically designed for groundwater and environmental investigations.

In TEM surveying, a transmitter loop induces an electric current into the ground, producing a primary magnetic field (Fitterman and Stewart, 1986). When a steady current has been built up in the loop, the current is quickly turned off, interrupting the primary magnetic field. Satisfying Faraday's law, new currents are induced into the ground. The decaying magnetic field from these new currents induces a voltage to the receiver coil. This voltage gives information about the resistivity of the subsurface, as the magnitude and distribution of the current intensity being recorded depends upon the resistivity of the substrate (Fitterman and Stewart, 1986; Aucken et al., 2008). Generally, low resistivity is interpreted to represent fine-grained material such as clay, or saltwater, and high resistivity is interpreted to represent coarse-grained material such as sand and gravel. However, it must be kept in mind that electrical conductivity (and resistivity) is a function of multiple variables such as composition, porosity, water content, salinity of pore waters, and texture, and thus specific lithologies do not necessarily have a unique conductivity (Oldenborger et al., 2014).

The raw data acquired from SkyTEM surveys are then subject to geophysical inversion, which models the raw data to determine the distribution of the physical properties of the subsurface that likely produced said data. In the case of EM surveys, using the measured data and other prior knowledge (i.e. borehole logs), inversion schemes can be carried out to produce resistivity models of the subsurface.

During Geoscience BC's Peace Project, approximately 21,000 line kilometres were flown with the SkyTEM system to collect airborne TEM data. Figure 2.10 shows a map of the Peace Project study area, and Figure 2.11 shows the flight lines for the SkyTEM survey. Data were acquired for four main areas: Peace Project Main, Sikanni Chief, Doig River, and Charlie Lake.

SkyTEM Surveys ApS (**ST**) performed one-dimensional (1-D) inversions of the airborne TEM data for all four areas, and produced 10 m horizontal depth slices of resistivity distribution (SkyTEM Surveys ApS, 2015; 1-D inversions are not shown in this thesis).

Based on the raw SkyTEM data and 1-D inversions from **ST**, Aarhus Geophysics ApS (**AG**) performed three-dimensional (3-D) inversions on the data in five areas (Aarhus Geophysics ApS, 2016a-e); two sub-areas are within the Peace Project Main area: Main (Phase 1) and Conoco (Figure 2.10). The Sikanni Chief, Doig River, and Charlie Lake areas are located outside the Peace Project Main area (Figure 2.10). This thesis focuses on the Peace Main (Phase 1) sub-area.

AG produced 5 and 10 m horizontal depth slices of resistivity distribution (Figure 2.12), and vertical resistivity cross-sections along survey lines (Figure 2.13). Appendix 2 in Aarhus Geophysics ApS (2016d) lists the depth intervals for the horizontal resistivity slices available for the Peace Main (Phase 1) sub-area. The specific slices used in this thesis are the slices corresponding to 0 to 40 metres below ground surface, and those corresponding to 670 to 460 metres above sea level.

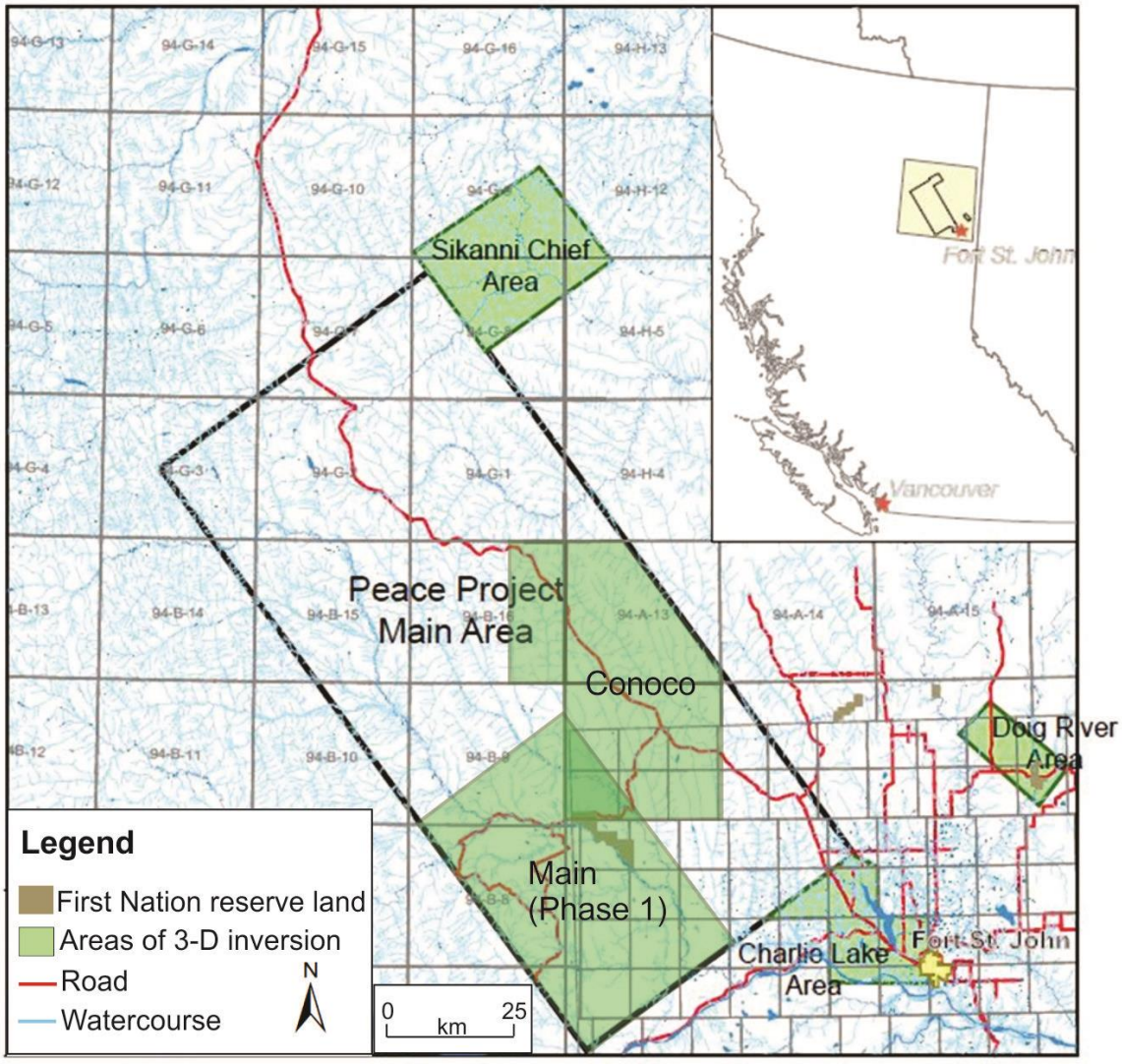

Figure 2.10. Geoscience BC Peace Project area outline. The areas where Aarhus Geophysics ApS (2016a-e) performed 3-D inversions on the SkyTEM data are shown in green. Modified from Petrel Robertson Consulting Ltd. (2015) with permission.

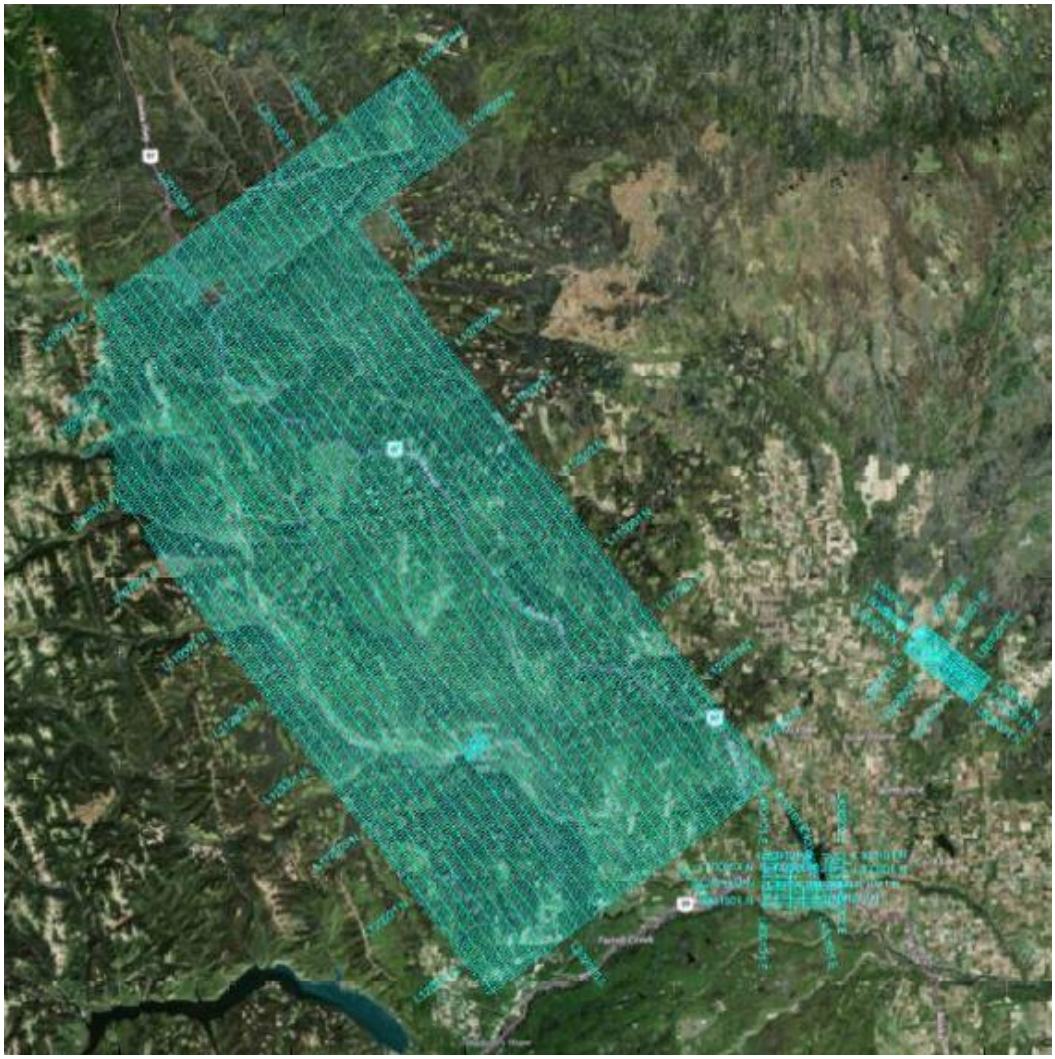

Figure 2.11. Flight lines for Geoscience BC Peace Project SkyTEM survey. From SkyTEM Surveys ApS (2015) with permission.

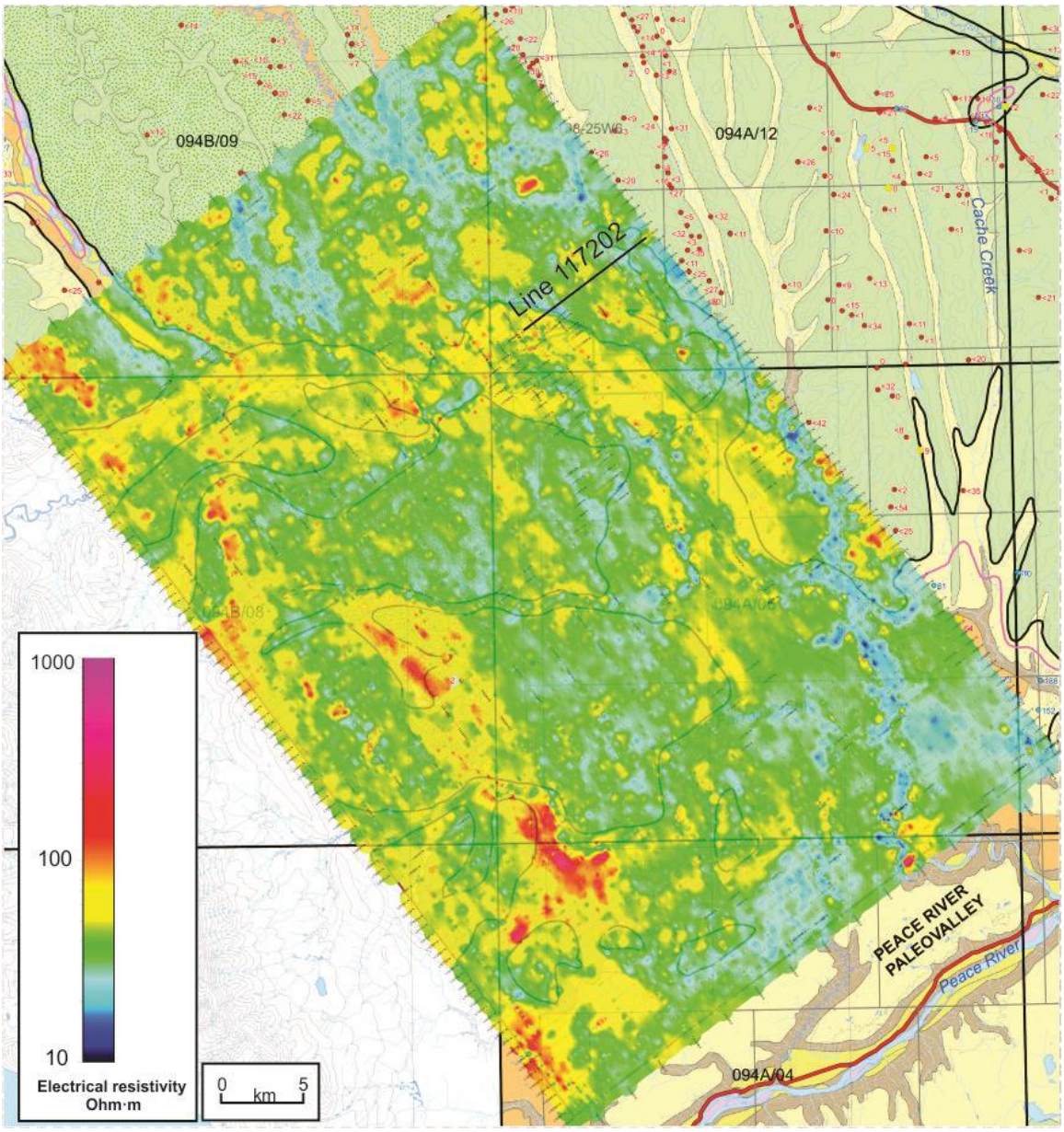

Figure 2.12. **Example of a horizontal subsurface resistivity slice showing the resistivity distribution interpreted from 3-D inversion for the Peace Main Phase 1 sub-area (coinciding with the study area for this thesis). The slice is from 5 to 10 m below ground surface. The resistivity distribution was derived from spatially constrained inversion (SCI). The location of the resistivity section line (Line 117202) for Figure 2.13 is shown. Modified from Aarhus Geophysics ApS (2016d) with permission.**

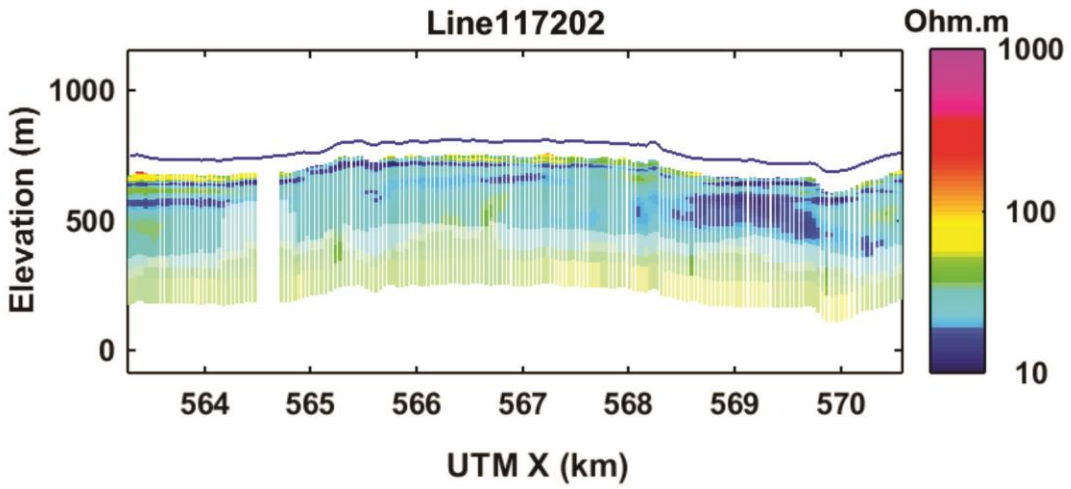

Figure 2.13. Example of a vertical resistivity section showing resistivity distribution along flight line 117202 interpreted from 3-D inversion. The resistivity section line is shown in Figure 2.10. The resistivity distribution was derived from spatially constrained inversion (SCI). From Aarhus Geophysics ApS (2016d) with permission.

2.2.2. Corrected Gamma-ray Logs

Gamma-ray logs are commonly used to determine subsurface lithology and stratigraphy and they record the natural radioactivity of the sediments. High gamma-ray values generally imply clays, and result from higher concentrations of radioactive elements found in clay minerals, such as uranium, potassium and thorium (Quartero et al., 2014). Low gamma-ray values generally imply sands and other coarse-grained materials.

Logging is best done in open boreholes. When present, the steel surface casing in a well mutes the gamma-ray response from the formation, reducing the amplitude and variance of the data, which is problematic for geologic interpretation (Quartero et al., 2014). To enable the use of gamma-ray logs from cased oil and gas wells, Quartero et al. (2014) developed a gamma-ray normalization procedure that corrects for the casing attenuation by adjusting the statistical distribution of the cased gamma-ray values so that the high and low percentiles are equal to those of the non-cased gamma-ray values. This normalization method allows the cased and non-cased log intervals to be merged into one continuous gamma-ray curve for stratigraphic correlation (Quartero et al., 2014).

In accordance with the British Columbia Oil and Gas Activities Act (BCOGC, 2010), gamma-ray logs are required to be run from ground surface to the bottom of an oil and gas well upon completion. The resulting data, therefore, are valuable for the investigation of near-surface Quaternary sediments, and possible identification of the Quaternary-bedrock contact. Within the study area, the gamma-ray logs from 199 wells were corrected using the Quartero et al. (2014) technique (Petrel Robertson Consulting Ltd., 2015). An example of a corrected gamma-ray log is shown in Figure 2.14. The corrected gamma-ray logs were used to identify the Quaternary-bedrock contact and interpret the buried valley network outline (Petrel Robertson Consulting Ltd., 2015), and identify contacts between the Cretaceous formations in the study area. They were also used to supplement the airborne TEM data in differentiating fine- and coarse-grained Quaternary sediments. Table A1 in Appendix A lists the Unique Well Identifiers (UWI) and easting and northing coordinates for all wells with corrected gamma-ray logs used in the geological modelling.

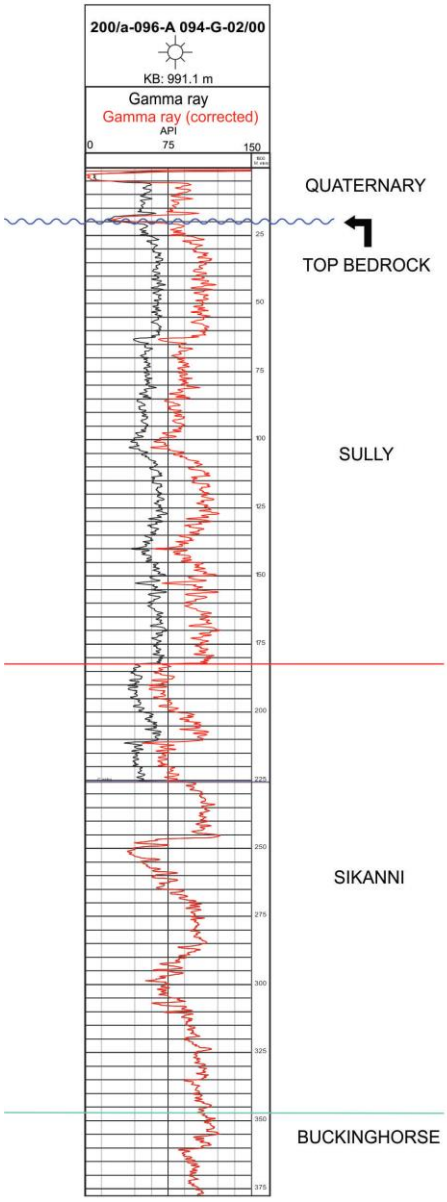

Figure 2.14. Example of a gamma-ray log from the Peace Project area corrected using the Quartero et al. (2014) method. The gamma-ray curve from the cased-hole interval is shown in black and the corrected gamma-ray curve is shown in red. Stratigraphic picks for the Quaternary-bedrock contact and other bedrock contacts are also shown. Modified from Petrel Robertson Consulting Ltd. (2015) with permission.

2.2.3. WELLS Database: Drillers Logs

Within the study area, there are 35 water wells with usable lithologic logs available from the WELLS database (BC Ministry of Environment, 2017). As these logs

were recorded by drillers who may or may not have formal training, the quality and reliability of the data are highly variable. However, due to the regional-scale nature of this investigation, incorporation of all available data was necessary.

The lithologic logs were used to determine depth to bedrock contacts and interpret the outline of the buried valleys (Petrel Robertson Consulting Ltd., 2015), and were also used to supplement the airborne TEM data in interpreting the Quaternary sediments. For the interpretation of the Quaternary sediments, the Standardised BC WELLS database (Toews and Allen, 2007 unpublished report) was used, which provides a standardised description of lithology from the driller's logs. Five additional well logs, which were not included in this Standardised BC WELLS database, were standardised and used in classifying the recorded lithology. Table A2 in Appendix A provides the Well Tag Numbers (WTN's), easting and northing coordinates, driller's description of lithology, and the subsequent modelled geology for all 35 wells.

2.2.4. Field Verification Data

To verify the results of the geophysical data, eight locations throughout Geoscience BC's Peace Project area were selected for drilling ten boreholes for verification, seven of which are within the study area for this thesis (Figure 2.15). The wells were drilled with a sonic rig, in which the drill bit vibrates up and down in addition to being pushed downwards. This allows for excellent core recovery compared to conventional rotary drilling. Core was collected and logged along the entire length of the hole. The holes were completed with solid PVC pipe and backfilled with cement grout to enable geophysical logging. At two drilling locations (6a and 10x), a water-bearing unit, with high enough permeability to warrant the installation of a monitoring well, was intersected. The drill rig was moved less than 5 m away, and a new borehole was drilled to that particular depth. The borehole was then screened using slotted PVC pipe over the defined interval of the aquifer.

Sediment samples were collected from the cores of holes 10b and 10x from the depth interval corresponding to the screened interval, and from other locations of coarse-grained units (i.e. sand), for grain size analysis (described in section four of Appendix A).

Finally, various geophysical logging tools including resistivity, neutron-porosity, density-porosity, gamma-ray and dipole sonic were run down each of the geophysical holes.

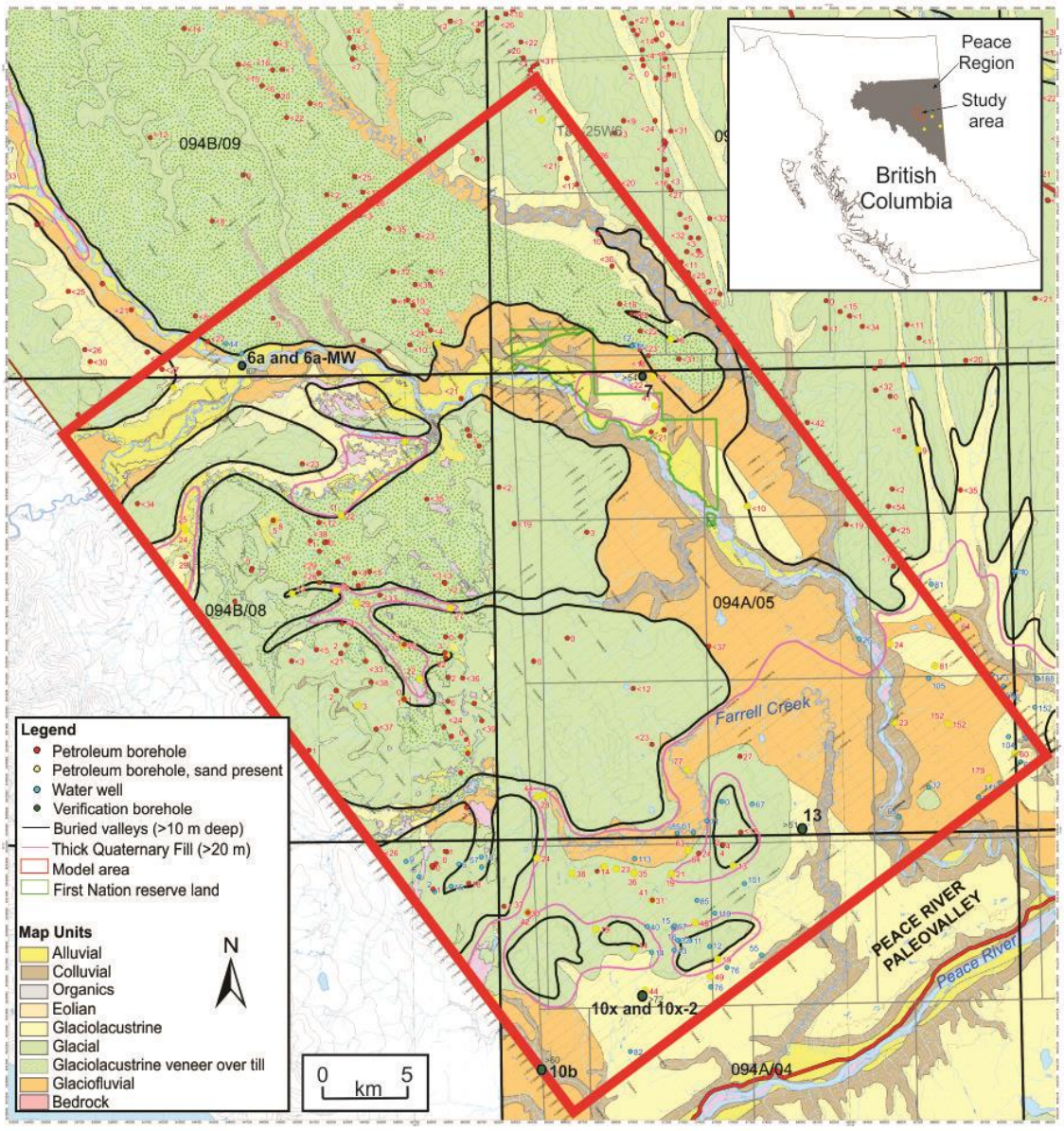

Figure 2.15. Study area map showing locations of Peace Project boreholes drilled for verification of the geophysical data. Modified from Petrel Robertson Consulting Ltd. (2015) with permission.

The detailed lithologic logs from the boreholes were used as input in the geological model to supplement the interpretation of the geology from the airborne TEM data. However, of all seven holes drilled within the model area, the Quaternary-bedrock contact was only encountered at holes 6a and 6a-MW. Tables A3-A9 in Appendix A

provide the detailed lithologic logs for each borehole drilled. The accompanying Figures A1-A6 provide the downhole gamma-ray and resistivity logs with geological interpretations.

Chapter 3.

Methodology for Building the Geological Model

Characterizing a groundwater flow system requires a geological model. It is within the geological modelling stage that distinct hydrostratigraphic units are defined on the basis of similar hydraulic properties such as hydraulic conductivity, porosity, and specific storage. A robust geological model is needed to simulate a realistic groundwater flow system and thus it becomes critical to incorporate data in the geological model as accurately as possible.

Utilizing multiple geological and geophysical datasets is important in regional-scale modelling; especially in complex flow systems like buried valleys (Sharpe and Russell, 2004; Oldenborger et al., 2014). Modelling Quaternary buried valleys is complicated by the discontinuous nature, variable thickness, and heterogeneity of Quaternary sediments. Therefore, obtaining information on the architecture of the Quaternary deposits and identifying ways to distinguish permeable from less permeable material is very important. It is here that high-resolution geophysical datasets can assist in identifying different units and their distribution within the valley-fill. This allows for the refinement of conceptual models of the architecture and sedimentary heterogeneity of buried valley networks (Pugin et al., 2014). Incorporating these datasets into computer-based modelling software allows the visualization and assessment of a geological model for further hydrogeological investigations.

In this thesis, the software platform Petrel (Schlumberger, 2016) was used to design a 3-D geological model of the central Peace Region study area. Petrel is subsurface modelling software that allows for easy integration of geophysical and drill log data and is normally used in the energy sector to conduct engineering and production modelling of deep hydrocarbon reservoirs. The software is not typically used to model discontinuous and heterogeneous Quaternary sediments in the shallow subsurface. Recent studies (e.g. Hartz et al., 2016; Lau et al., 2016; Peterson and Malone, 2016), however, have demonstrated that Petrel can also effectively be used to model Quaternary deposits. Although, the main datasets used in those studies to construct geological models are numerous borehole lithology logs and, in one example

(Hartz et al., 2016), seismic refraction data, which are both easily imported into Petrel. The main dataset used in this research, however, is spatial resistivity data, for which there is no standard workflow for import. Thus, a new approach for importing and integrating these data in Petrel was necessary.

The geological model of the study area was constructed in two separate phases: a bedrock model and a Quaternary model. The vertical extent of the model is from ground surface down to approximately 200 metres below the top of bedrock, below which there is likely limited groundwater flow. Prior to creating these models, the datasets had to first be imported into Petrel. The first section of this chapter outlines the methodologies used to import the various datasets into Petrel, and the proceeding two sections describe how these datasets were used to construct the bedrock and Quaternary models, respectively. Figure 3.1 shows the workflow used to develop the geological model, and Chapter 4 discusses the results of the geological modelling.

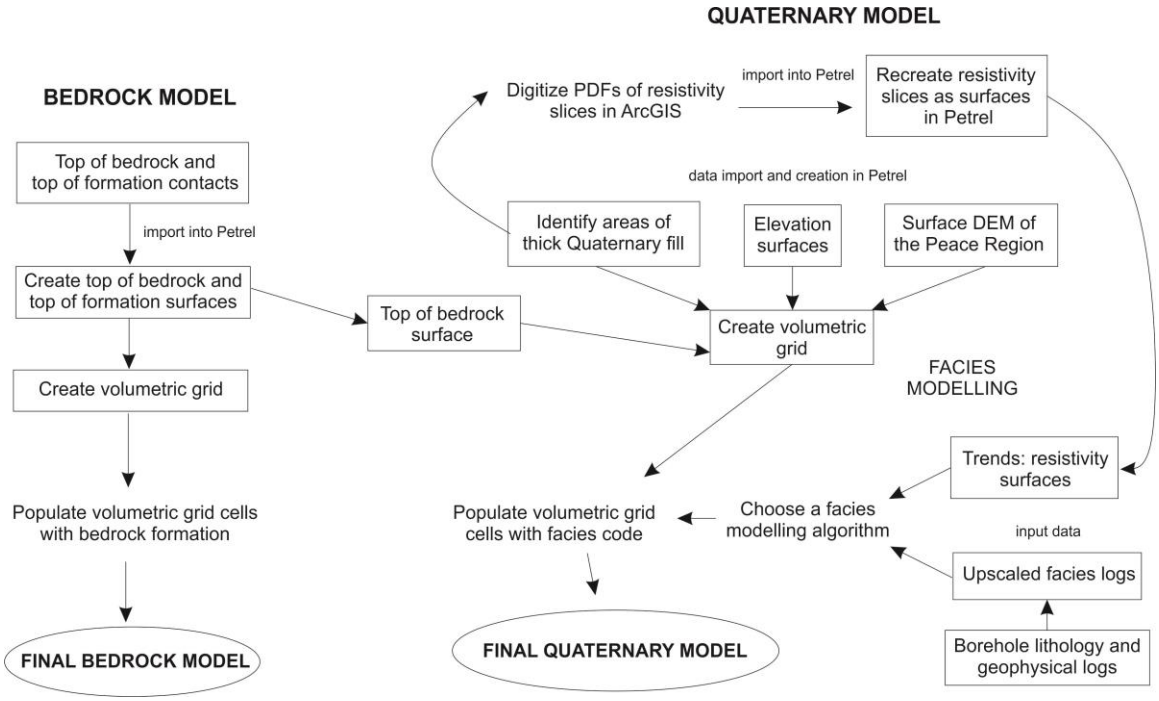

Figure 3.1. Petrel workflow for creating the geological model of the central Peace Region.

3.1. Import of Data into Petrel

3.1.1. Borehole Geophysical Logs

The import of well logs into Petrel is straightforward as this software is specifically designed for the energy industry. The workflow for importing well logs into Petrel is summarized as follows: (1) import well head file; (2) import well path/deviation; and (3) import well logs. The wells did not have deviation (i.e. deviation from vertical) in the subsurface region that was modelled, as this research is only concerned with Quaternary sediments and the shallow bedrock formations, which are not targets for hydrocarbon exploration.

A well head file includes the names, coordinates, and Kelly Bushing elevation (KB) of each well to be imported. The necessary components of a well head file are the well name, the X and Y coordinates, the total depth (TD) of the well, and the KB elevation. An arbitrary TD of 500 metres below ground surface (mbgs) was set for each well as this research is only concerned with the shallow subsurface. The KB value is the elevation of the well in metres above sea level (masl) plus the height of the KB from ground surface (usually about 5 metres; however, this depends on the drill rig. Appendix 1 from Petrel Robertson Consulting Ltd. (2015) provides the height of the KB from ground surface for each well). To determine the surface elevations, the X and Y coordinates for each well were plotted in ArcGIS. The surface elevations at each well location were then obtained using a digital elevation model (DEM) of the ground surface of the Peace Region (United States Geological Survey (USGS), 2014) and the Spatial Analyst tool ‘Extract raster values to points’. These surface elevations were added to the height of the KB provided by Petrel Robertson Consulting Ltd. (2015) and included in the well head file as the KB elevation.

Once the well head file was imported, the final step was to import the well logs. The corrected gamma-ray logs from Petrel Robertson Consulting Ltd. (2015) and the borehole geophysical logs from the Peace Project field campaign were imported in LAS (Log ASCII Standard) format and were matched to each well name imported in the well head file. Figure 3.2 shows the well head locations of all wells that were imported into Petrel that have associated borehole geophysical logs.

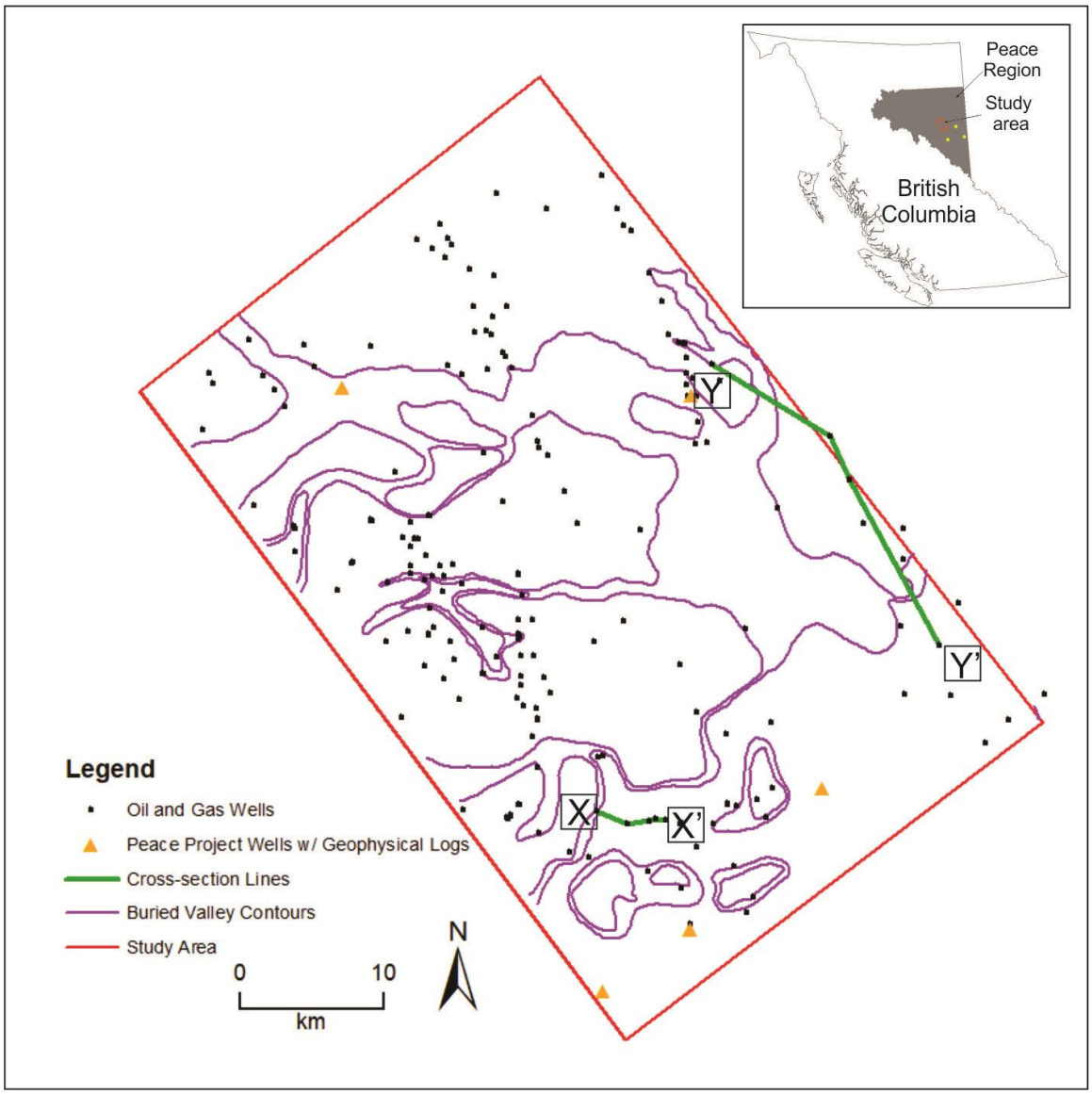

Figure 3.2. Well head locations of oil and gas wells and Peace Project drilling wells that were imported into Petrel with associated borehole geophysical logs. Buried valley contours are shown in purple (Levson in Petrel Robertson Consulting Ltd., 2015). Locations of cross-section lines for Figure 3.5 and 3.6 are shown in green.

3.1.2. Resistivity Data

The results from the SkyTEM survey were presented as 5 and 10 m horizontal depth slices of resistivity distribution from ground surface down to 40 mbgs, horizontal slices of resistivity distribution in units of absolute elevation (masl), and vertical resistivity cross-sections, as described in Chapter 2 (Aarhus Geophysics ApS, 2016a-e). The horizontal resistivity depth slices were the main dataset used to model the Quaternary

sediments; however, these data were presented as PDF maps of resistivity distribution. These could not be imported directly into Petrel and have resistivity information associated with them in a way that geological interpretation could be performed. Therefore, a methodology was developed to recreate the resistivity slices in Petrel, by converting the PDF maps of resistivity distribution into a file format that could be imported into Petrel.

Digitizing the Resistivity Slices in ArcGIS

The resistivity slices in PDF format were first converted to TIFF (Tag Image File Format) format, and then imported into ArcGIS. The slices were georeferenced within ArcGIS using the polygon shapefile of the buried valley outlines (Petrel Robertson Consulting Ltd., 2015). Each resistivity slice was then digitized by tracing distinct geological units based on their resistivity values (Table 3.1). A shapefile for each geological material type (Table 3.1) was created for each resistivity slice (i.e. four shapefiles for each slice). Tools within the ArcToolbox were then utilized to convert the traces to a format which could be imported into Petrel (as described below).

Table 3.1. Resistivity values for different geological materials. Modified from Bemex Consulting International and Quaternary Geosciences Inc. (2016).

Geologic Material	Resistivity (ohm·m)
Clay/clay-till	<15
Till/silt/fine sand	15-50
Sand	50-100
Coarse sand and gravel	>100

The shapefiles were first created as polylines in the tracing process. The Editing Tool ‘Densify’ was used to place more vertices along the lines at a spacing of 10 m. The vertices of the polylines were then converted to points using the Data Management Tool ‘Feature Vertices to Points’. X and Y coordinates were added to the points using the Data Management Tool ‘Add XY Coordinates’. Surface elevations for each point were then obtained using the Spatial Analyst Tool ‘Extract Values to Points’ and the DEM of the Peace Region.

The database file (.dbf) of the shapefile that included traces of the geological unit as points with surface elevation values was opened in Microsoft Excel. A thickness was subtracted from each surface elevation value based on the specific depth interval of the

resistivity slice that was being digitized. As the slices are in 5 and 10 mbgs increments, the middle values of 2.5 m and 5 m increments, respectively, were subtracted from the surface elevations. This ensured that the points corresponding to the trace of the geological unit also corresponded to the specific depth interval. For example, when digitizing the 10-15 mbgs resistivity slice, 12.5 m was subtracted from each point's surface elevation value. The Microsoft Excel files of the traces were then converted to ASCII text files for subsequent import into Petrel.

The outline of the Peace Main (Phase 1) sub-area (see Chapter 2) in which 3-D inversions of the resistivity data were performed was traced out in ArcGIS in a similar fashion as described above. The ASCII text file of this trace was imported into Petrel and converted to a model area boundary polygon.

Recreating the Resistivity Slices in Petrel

Each ASCII text file was imported into Petrel under the format 'Petrel points with Attributes (ASCII)'. The files were then edited in Petrel to add a resistivity value as an attribute to each point. Resistivity values were selected within the ranges shown in Table 3.1; specifically, clay/clay-till: 10 ohm·m; till/silt/fine sand: 40 ohm·m; sand: 70 ohm·m; sand and gravel: 100 ohm·m. The four point files corresponding to the four geological material types for each depth interval were appended to each other to make one file for each interval.

Each resistivity slice was recreated in Petrel by gridding and interpolation. This was done using the 'Make/edit surface' process in Petrel. The attribute upon which the gridded surface was based was the resistivity value. The point file containing the now appended traces was used as the main input, the grid increment was left at the default of 50 x 50 m, and the model area polygon was set as the surface boundary. Within Petrel there are several algorithms for creating surfaces. The Convergent Interpolation algorithm was selected for this study. It is a control point oriented algorithm in which the convergence process retains general trends in areas with few data while honouring detail in areas where data exist. A comparison of an original resistivity slice to a recreated resistivity slice is shown in Figure 3.3. Figures B1-B4 in Appendix B show all comparisons of the original PDF resistivity depth slices from Aarhus Geophysics ApS (2016d) to the Petrel recreated resistivity slices. Overall, there is very good visual agreement between the two resistivity maps for each depth slice. It should be noted,

however, that the resistivity colour bar scales differ because a more extensive resistivity scale was used by Aarhus Geophysics ApS (2016d). The actual ranges in the original dataset and the recreated datasets are the same.

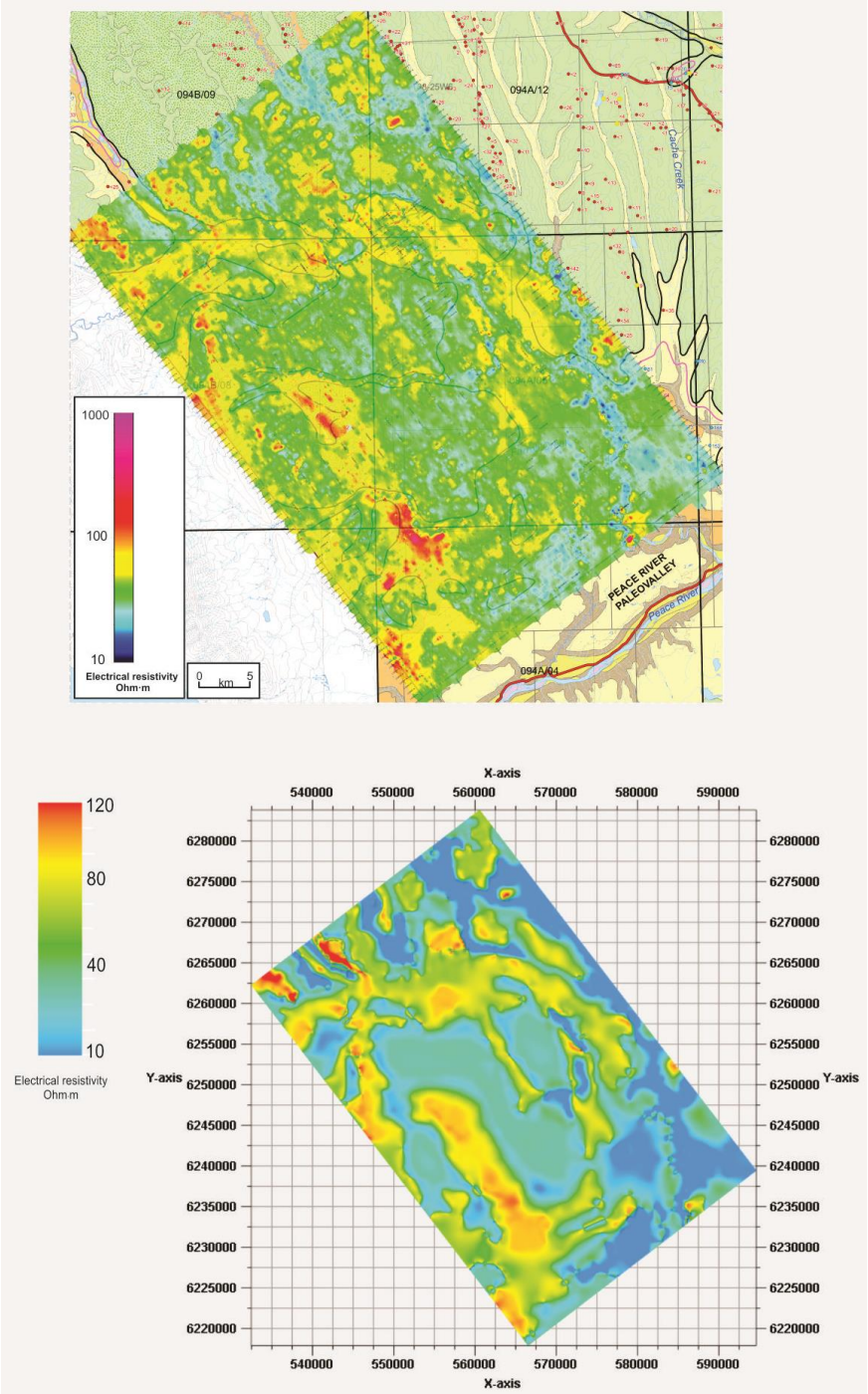

Figure 3.3. **Comparison of horizontal resistivity depth slices. The figure on the top shows the original interpreted resistivity distribution from 5 to 10 m below ground surface in the Peace Main (Phase 1) sub area (modified from Aarhus Geophysics ApS (2016d) with permission). The figure on the bottom shows the resistivity distribution from 5 to 10 m below ground surface recreated from the original figure using Petrel (Schlumberger, 2016). Note the different colour scales. However, the actual ranges in the original dataset and the recreated datasets are the same.**

3.1.3. Surface Digital Elevation Model

The DEM used to determine the well elevations is a raster file which can be easily imported into ArcGIS, but cannot be imported into Petrel. Therefore, the raster file was converted to a format that is supported by Petrel using the Data Assistant tool from Exprodat (Exprodat Consulting Limited, 2017; an extension for ArcGIS which allows the transfer of data between ArcGIS and Energy and Petroleum software systems, including Petrel).

Within ArcGIS, the DEM raster file was clipped to the boundary of the model area and then converted to a GeoTIFF using the Data Management Tool ‘Copy Raster’. The GeoTIFF raster was then exported using the Data Assistant as a Zmap grid (.asc) file, a format that can be imported into Petrel. The DEM as a Zmap grid file was imported into Petrel under the format ‘Zmap + grid (ASCII)’ which automatically generates the surface of the DEM within Petrel (Figure 3.4).

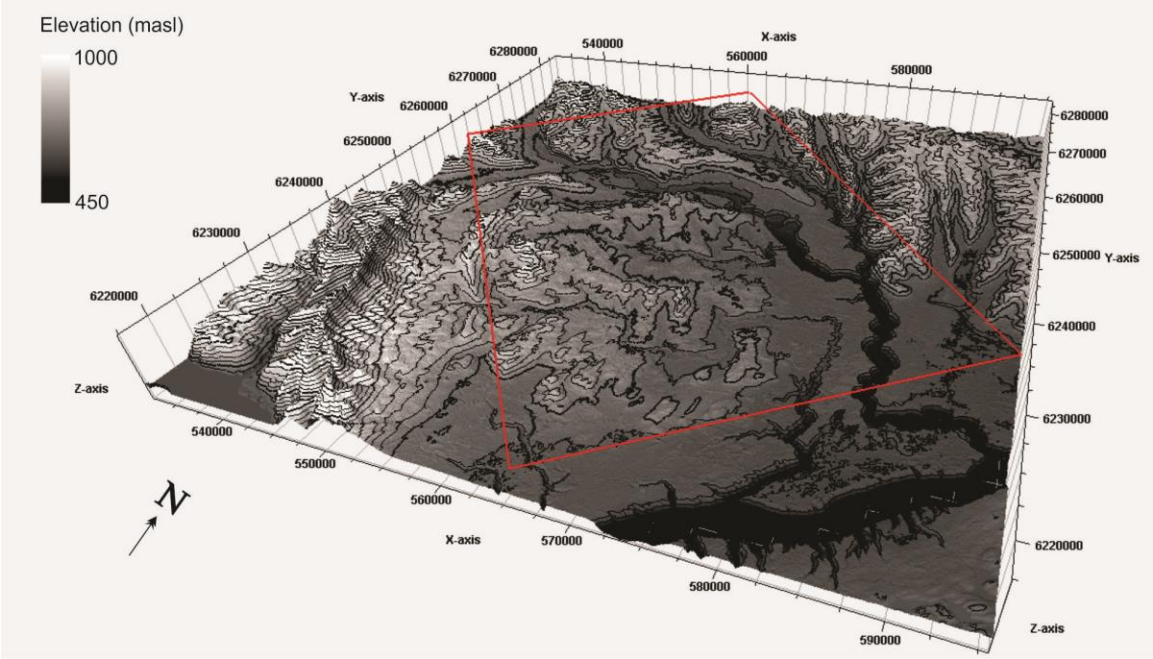

Figure 3.4. Surface DEM (USGS, 2014)of the model area in Petrel. The red rectangle shows the model area. 5x vertical exaggeration.

3.1.4. Bedrock Contacts

As described in Chapter 2, the corrected gamma-ray logs were used to interpret the Quaternary-bedrock contact (Petrel Robertson Consulting Ltd., 2015) and identify

contacts between the Cretaceous formations in the model area. Petrel Robertson Consulting Ltd. (2015) provide a database of the depth to bedrock values for the wells determined from the corrected gamma-ray logs within the Peace Project area. Those within the model area were extracted and imported into Petrel as an ASCII point file under the format 'Petrel points with Attributes (ASCII)'. This file contained the top of bedrock elevation for all wells, along with their X and Y coordinates. Top of bedrock contacts identified from the Peace Project drilling and those from water well lithology logs were also included in this file (see Chapter 2 and Appendix A). Thus, all available data were imported so that a top of bedrock surface could be created which contained the maximum number of data points. This surface, however, does not differentiate between the four Cretaceous bedrock formations that were modelled. A separate process was needed to determine bedrock formations.

The corrected gamma-ray logs were used to identify possible contacts between the bedrock formations, as the different units are expected to have different hydraulic properties. Described in Chapter 2, the four bedrock formations represent several marine transgression-regression-transgression cycles and are broadly the Dunvegan sandstones, Sully shales, Sikanni sandstones, and Buckinghorse shales. In the database (i.e. top of bedrock picks from Petrel Robertson Consulting Ltd., 2015), the bedrock formation at the Quaternary-bedrock contact was identified. Using this information, each corrected gamma-ray log was investigated to 200 m below the top of bedrock, and additional possible bedrock contacts were determined using the following identifying characteristics provided by John Carrey (personal communication, April 2017):

1. The Dunvegan sandstones can have a much more "irregular" gamma-ray response compared to the Sikanni sandstones as more shale beds are present in some locations.

2. The Sully formation typically has a fairly consistent shale response (i.e. high gamma). Therefore, the top of Sully was identified where Dunvegan was determined as the Quaternary-bedrock contact (Petrel Robertson Consulting Ltd., 2015), and an irregular sandstone-shale gamma response transitioned to a consistent shale response.

3. The Sikanni formation typically has 4-5 coarsening upwards sequences. While not all of these sequences are always present in the log, some usually are. The top of Sikanni was determined as the

point at which the shale response from the Sully changed to a sandstone response at the top of a coarsening-upwards sequence.

4. The Buckinghorse generally shows a sweeping transition from sandstone to shale after the last coarsening upwards sequence of the Sikanni. The top of the Buckinghorse was chosen as the base of the last sequence in the Sikanni in which sandstone transitions to shale.

Figure 3.5 and Figure 3.6 show cross-sections of corrected gamma-ray logs with bedrock formation contacts identified. The locations of the cross-section lines are shown in Figure 3.2 and were drawn in these areas to show both the western and eastern portions of the model with as many formation contacts as possible. The top of the Sikanni Formation was set as the datum, following a similar approach as Petrel Robertson Consulting Ltd. (2015). Similar to the ASCII point file for the top of bedrock, point files were created and imported into Petrel for each bedrock formation that contained the X and Y coordinates of the wells and the contact elevations (in masl) for the top of each respective formation. It should be noted that identifying bedrock formation contacts from a single gamma-ray log can be very uncertain. However, there are no other available data as both the lithology logs and resistivity data cannot differentiate between the formations by themselves. It was necessary to differentiate the formations because they have different hydraulic properties which will result in different groundwater flow rates.

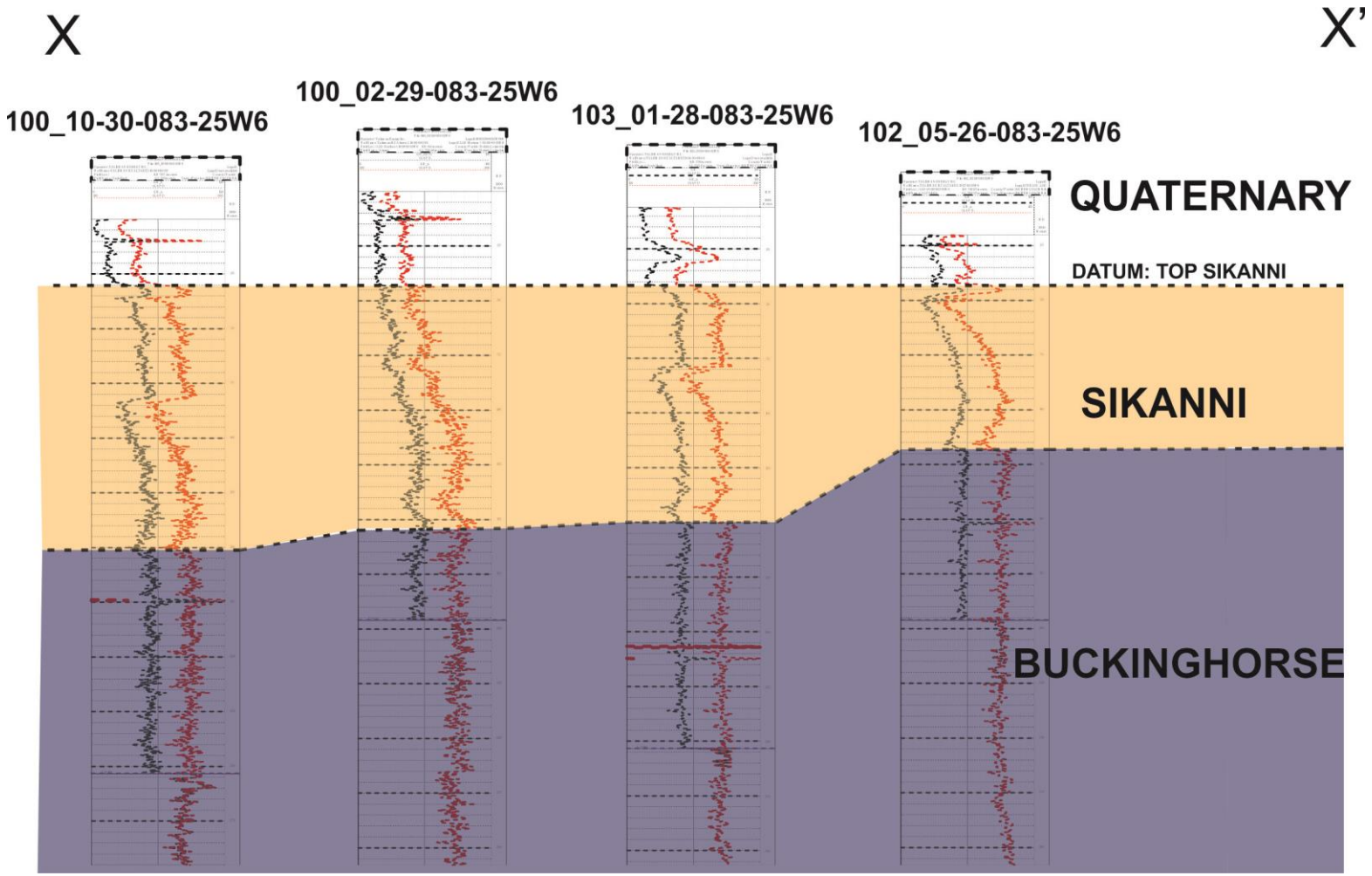

Figure 3.5. **Cross-section of corrected gamma-ray logs showing Sikanni Formation and Buckinghorse Formation contact. The top of bedrock contacts were provided by Petrel Robertson Consulting Ltd. (2015). The top of Sikanni was chosen as the datum. Horizontal distance between wells is not to scale. Vertical depth interval on well logs is 5 metres. See Figure 3.1 for cross-section location.**

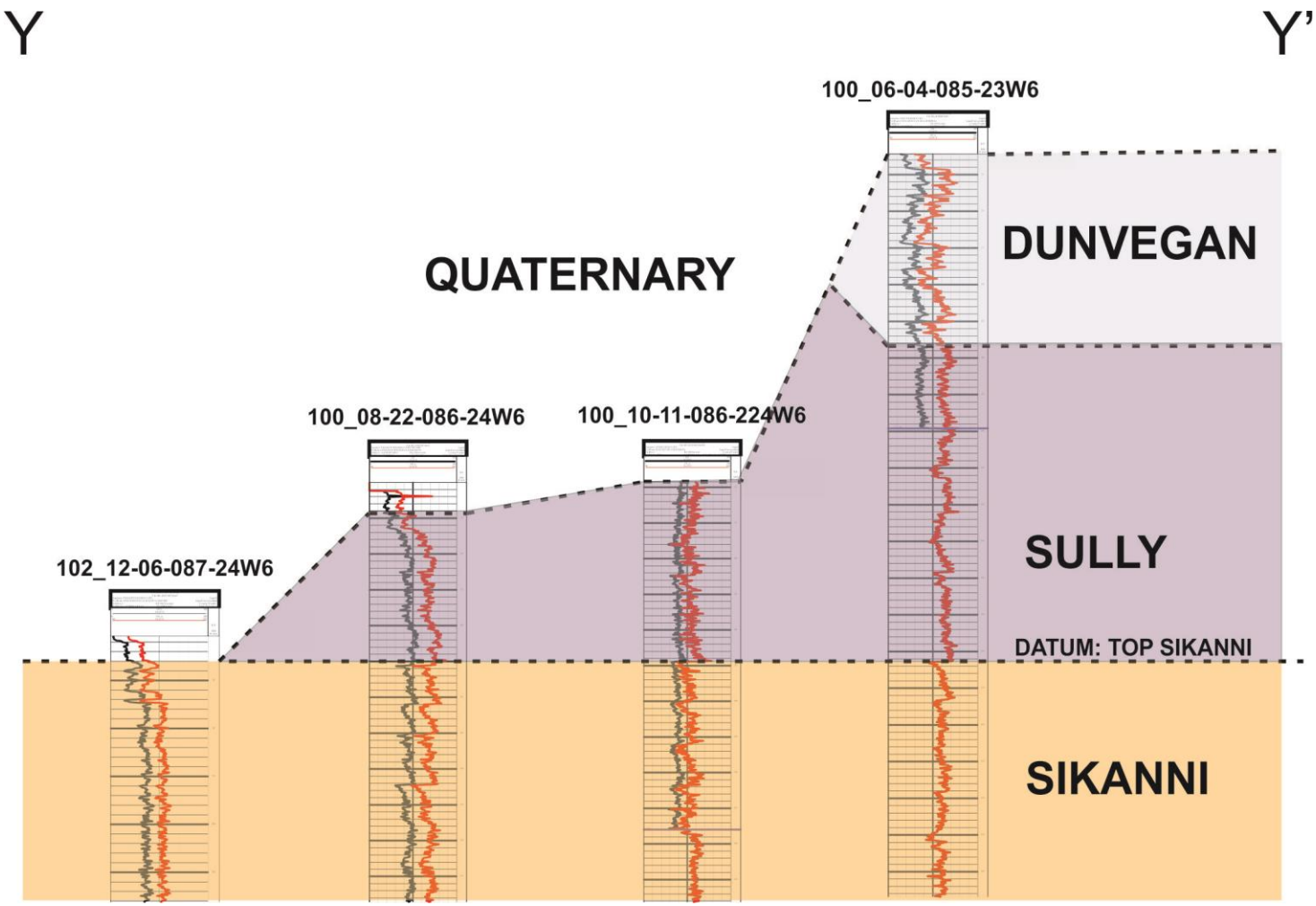

Figure 3.6. **Cross-section of corrected gamma-ray logs showing Dunvegan Formation, Sully Formation, and Sikanni Formation contacts. The top of bedrock contacts were provided by Petrel Robertson Consulting Ltd. (2015). The top of Sikanni was chosen as the datum. Horizontal distance between wells is not to scale. Vertical depth interval on well logs is 5 metres. See Figure 3.1 for cross-section location.**

The five point files relating to bedrock elevations (top of bedrock, top of Dunvegan, top of Sully, top of Sikanni, and top of Buckinghorse) were then used to create five surfaces corresponding to each of the “tops” using the ‘Make/edit surface’ process as described above in Section 3.1.2. However in this case, the attribute upon which these surfaces were gridded was the elevation of the “tops”. The grid increment was left at the default of 50 x 50 m, and the model area polygon was set as the boundary for each surface.

Within the ‘Make/edit surface’ process it is also possible to include a ‘trend surface’ which is used if the expected surface to be generated is governed by another surface trend. The original input data is honoured, but in areas of sparse data the algorithm will use both the interpolations from the input data and the trend surface. Accordingly, the DEM surface was used as a trend surface for each of the five generated bedrock surfaces, as there are areas within the region where bedrock outcrops at, or is near to, surface. This also ensured the algorithm did not produce erroneous bedrock surfaces that were largely above the DEM stratigraphically. The Convergent Interpolation algorithm was again used to generate all five bedrock surfaces as it is suited for a variety of data types of various densities, including sparse point data.

3.2. Bedrock Model

The ‘Make simple grid’ process was used to create the bedrock model in Petrel. Similar to the ‘Make/edit surface’ process, this process requires main inputs, a specified grid increment, and a model boundary. The polygon of the model area was set as the boundary, and the grid increment was set at 200 x 200 m as this was the expected grid size for the numerical models in MODFLOW. The five bedrock surfaces created (described in Section 3.1.4) were the main inputs for the bedrock model.

Surfaces in Petrel can be specified as Erosional, Conformable, Discontinuous or Base. Since the top of the bedrock surface was created to show the Quaternary-bedrock contact and does not relate to a specific bedrock formation, it was set as Discontinuous. This means the surface is erosional, such that surfaces below will be truncated; however, surfaces above will lap onto it. The formation surfaces were set as Conformable, and a Base surface representing 200 m below the top of Buckinghorse was generated. A 3-D grid of the bedrock was then generated.

To populate the cells of the 3-D grid with a bedrock formation, geometrical property modelling within Petrel was used. The ‘Zone index’ method was chosen as it creates a discrete index property for each zone of the model. The zones of the model represent the areas in between the “top” surfaces; therefore, the generated properties of the cells were the four bedrock formations (for example, the zone between the top of Dunvegan and top of Sully was the Dunvegan Formation zone).

3.3. Quaternary Model

Undertaking hydrogeological modelling with complex and heterogeneous glacial sediments can benefit by taking into account lithofacies associations (Sharpe et al., 2003). Therefore, for this study, Facies Modelling was carried out in Petrel to create the Quaternary model of the central Peace Region.

The main inputs used for Facies Modelling in this research were facies logs derived from the corrected gamma-ray and lithology logs, and surface “trends” derived from the resistivity slices. The four facies types modelled correspond to the four geological material types listed in Table 3.1. Several stochastic and deterministic algorithms are available for Facies Modelling in Petrel; the particular algorithm chosen should be based on the type of input data available. Of the various algorithms available in Petrel, Sequential Indicator Simulation (SIS) was chosen as the stochastic method, and Assign Values (AV) as the deterministic algorithm, to create two different Quaternary models. The two models were compared to assess differences in how the modelling algorithms honour input data and how the resultant facies models differ.

These two algorithms require slightly different methodologies for generating the facies model; however, some of the model set-up is similar. The following five subsections (Sections 3.3.1 to 3.3.5) describe components of the model set-up that are the same for both the SIS and AV algorithms. Sections 3.3.6 and 3.3.7 differentiate the SIS and AV modelling, respectively.

3.3.1. Elevation Surfaces

Similar to creating the bedrock model, the ‘Make simple grid’ process was the first step in creating the Quaternary model in Petrel. This process requires the input of

surfaces that govern the structure of the grid. The top surface of the grid was the DEM of the Peace Region and the bottom surface was the top of bedrock. However, intermediate surfaces, corresponding to the elevation of the resistivity slices (in masl) were also needed.

To generate these intermediate elevation surfaces, the Data Management tool 'Create random points' in ArcGIS was used to populate random points within the model area polygon in ArcGIS. The points were generated at a maximum horizontal separation of 200 m, and the Spatial Analyst tool 'Extract raster values to points' was used to add ground surface elevation values to the points. This generated a database file (.dbf) of the random points shapefile. Several ASCII files were then created in Excel that contained the X, Y, and elevation (in masl) of the random points for each resistivity slice.

Following a similar methodology to that described in Section 3.1.2, a thickness corresponding to the end values of the resistivity depth slices (i.e. 5 m, 10 m, etc.) was subtracted from each ground surface elevation value. This ensured the resistivity slices were situated in the middle of the elevation surfaces. The generated elevation ASCII files were imported into Petrel and used to create elevation surfaces using the 'Make/edit surface' process.

3.3.2. Identifying Areas of Thick Quaternary Fill

As discussed previously, the resistivity data were available in two formats; horizontal depth slices (from ground surface to a depth of 40 mbgs) and absolute elevation (AE) slices. The resistivity data imported thus far into Petrel extended to a maximum depth of 40 mbgs. Therefore, in some areas, there was a zone between the base of the resistivity data and the top of bedrock that contained no data to constrain the Facies Model. These areas were identified by overlaying the 40 mbgs elevation surface onto the top of bedrock surface (Figure 3.7). In some areas this fill is quite thick; the colored areas in Figure 3.8 represent the thickness of Quaternary fill that extends deeper than 40 mbgs to the top of bedrock. Therefore, several of the absolute elevation (AE) resistivity slices (Aarhus Geophysics ApS, 2016d) were also imported to serve as "trends" in areas of thick Quaternary fill. It should be noted that areas of thick fill outside of the buried valley network outline (Levson in Petrel Robertson Consulting Ltd., 2015) in Figures 3.7 and 3.8 may be anomalies that are a result of an uncertain top of bedrock

surface, or they may in fact be present. This uncertainty is discussed further in Chapter 4.

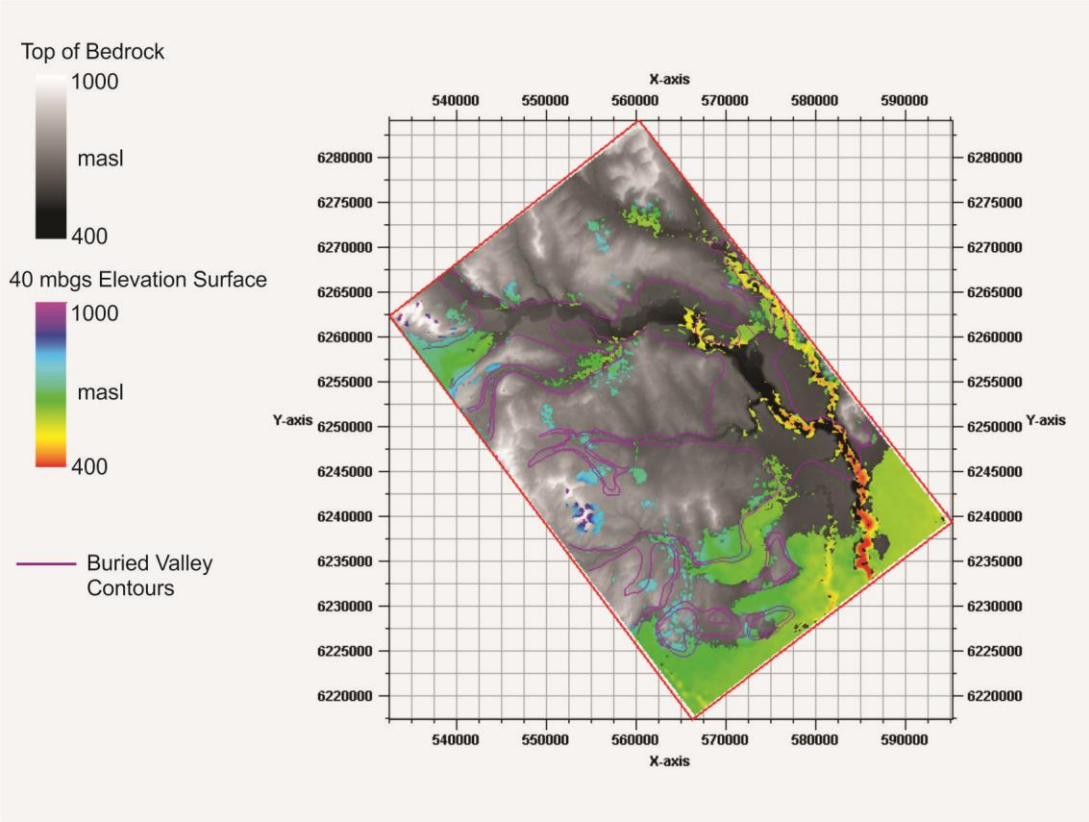

Figure 3.7. Regions within the model area with thick (>40 m) Quaternary fill are shown in colour. The map was generated by overlaying the 40 mbgs (metres below ground surface) elevation surface on to the top of bedrock surface. In some locations, there is additional Quaternary fill present below the 40 mbgs surface but above the top of bedrock. The buried valley contours (Levson in Petrel Robertson Consulting Ltd., 2015) are shown in purple.

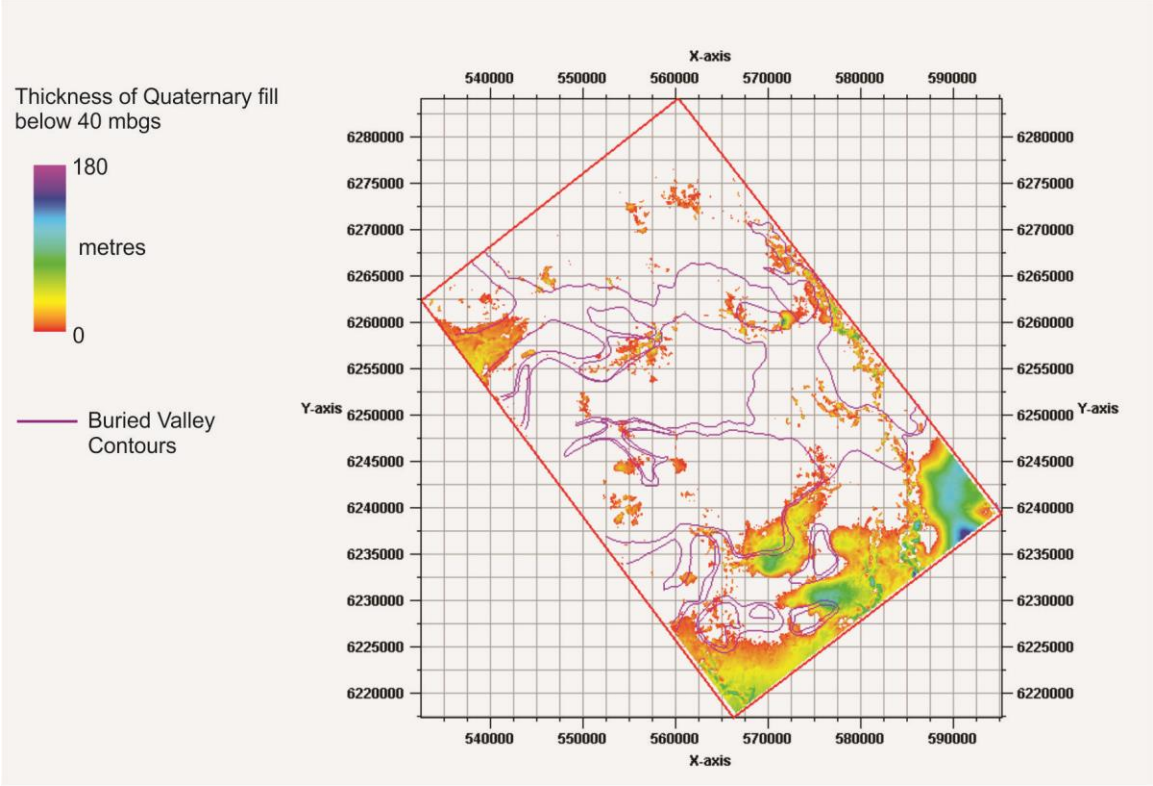

Figure 3.8. Thickness of Quaternary fill that extends below the 40 mbgs (metres below ground surface) elevation surface but above the top of bedrock surface. The buried valley contours (Levson in Petrel Robertson Consulting Ltd., 2015) are shown in purple.

The AE resistivity slices from Aarhus Geophysics ApS (2016d) were in 10 m increments and range from 800 to 350 masl. Clearly importing all of these slices would be impractical and time consuming, as only a certain range of the slices was actually needed to infill areas with thick Quaternary fill. To determine the range of AE resistivity slices needed, the 40 mbgs elevation surface and top of bedrock surface were displayed in a 2D window in Petrel (see Figure 3.7) and the maximum and minimum AE values were determined from all areas of thick Quaternary fill; a range of 670-460 masl.

All AE resistivity slices within this range were examined. Some of the deeper slices likely show mostly bedrock, with few areas where Quaternary fill is present. These deeper slices show very similar trends of resistivity distribution for subsequent elevation increments, so some of the slices were grouped together on the basis of having similar resistivity distributions. Similarly, some of the shallower AE resistivity slices also show patterns of similar resistivity distributions and were also grouped. This grouping reduced the number of additional slices that needed to be imported into Petrel. The groupings of

AE resistivity slices are shown in Table 3.2, and the elevation slice that was chosen as a representative distribution for each group is identified. These five representative slices were digitized in ArcGIS and imported into Petrel using the same methodology described in Section 3.1.2. Elevation surfaces were also created for the representative slices using the same methodology described in Section 3.3.1. The elevation values included in all imported ASCII files were the mean elevation values of each grouping in Table 3.2.

Table 3.2. Elevation values of absolute elevation (AE) resistivity slices and representative elevations chosen to recreate in Petrel.

Absolute Elevation Resistivity Slice Value (masl)	Representative Slice (masl)
670-660	660-650
660-650	
650-640	
640-630	630-620
630-620	
620-610	
610-600	590-580
600-590	
590-580	
580-570	550-540
570-560	
560-550	
550-540	
540-530	
530-520	
520-510	500-490
510-500	
500-490	
490-480	
480-470	
470-460	

3.3.3. Volumetric Grid

The polygon of the model area was set as the boundary of the grid, and the grid cell increment was set at 200 x 200 m, similar to the bedrock model. The DEM of the Peace Region was inserted as the top surface and was set as Erosional. The elevation

surfaces from the resistivity depth slices (i.e. 5 mbgs, 10 mbgs, etc.) were sequentially inserted and were all set as Conformable. The elevation surfaces from the AE resistivity slices (i.e. 655 masl, 625 masl, etc.) were then sequentially inserted and also set as Conformable. Conformable surfaces are truncated by all other surfaces, and lower conformable surfaces are truncated by upper conformable surfaces. Inserting the elevation surfaces from the resistivity depth slices first ensured that they would truncate the elevation surfaces from the AE resistivity surfaces at any intersection. This resulted in the AE resistivity surfaces only being used for areas of thick Quaternary fill. Finally, the top of bedrock surface was inserted as the bottom surface and was set as Base. A 3-D volumetric grid of the model area was then created. The skeleton of this grid showing the individual cells is shown in Figure 3.9.

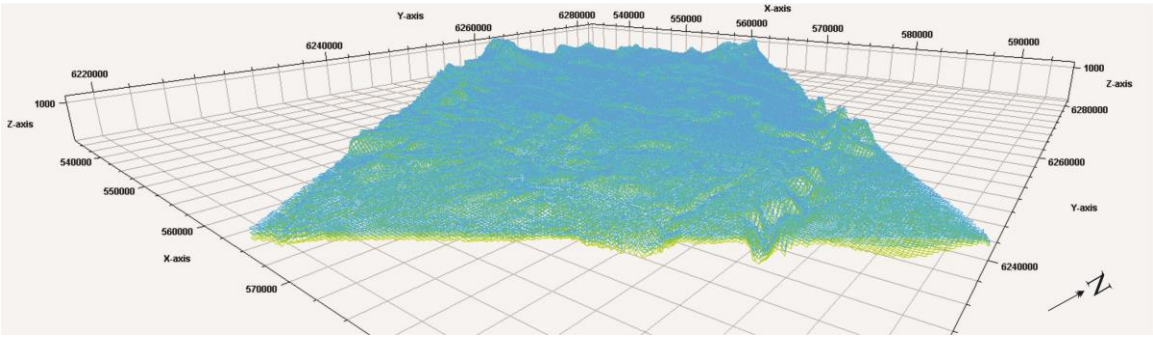

Figure 3.9. Skeleton of volumetric grid created for Quaternary model in Petrel. 5x vertical exaggeration.

3.3.4. Facies Logs

Facies logs are one of the main inputs used in most Facies Modelling algorithms in Petrel. Although no actual facies logs are available for the Peace Region, the borehole geophysical and lithology logs (from water wells in the WELLS database and from the Peace Project drilling) were used to manually create facies logs for the modelling.

Table A2 and Tables A4-A10 in Appendix A list the lithology and corresponding depth below ground surface for wells from the WELLS database and the Peace Project drilling, respectively. The column ‘Modelled Geology’ describes the facies type assigned to the depth interval.

The facies logs for these wells had to be drawn manually in Petrel. To do this, the wells were displayed in various “well section windows” in Petrel. The well section

windows display the track of each well and all associated well logs, along with the vertical depth along the well. A new discrete log, specified as a facies log, was added to each well track. The four facies types to be modelled (see Table 3.1) were specified in the settings for the facies log; each was assigned a specific facies code: coarse sand and gravel: 0; sand: 1; till/silt/fine sand: 2; clay/clay-till: 3. The 'Paint discrete log' tool in the Tool Palette was then used to manually draw the information from Tables A2 and A4-A10 onto the facies log tracks.

Facies logs were also created from the corrected gamma-ray logs using the Well Log Calculator in Petrel. The Well Log Calculator is used to edit imported well logs, or to make new well logs based on existing ones. An equation uses a combination of "if" and "and" statements that take each corrected gamma-ray log and creates a facies log for that well based on different ranges of gamma-ray values (API); for example:

"New_facies=If(GR>75,3,If(GR≤75AndGR>60,2,If(GR≤60AndGR≥45,1,If(GR<45, 0))))"

(3.1)

This particular equation assigns a facies code 3 (clay/clay-till) if the gamma-ray value is >75 API; a facies code 2 (till/silt/fine sand) if the gamma-ray value is between 75 and 60; a facies code 1 (sand) if the gamma-ray value is between 60 and 45; and a facies code 0 (coarse sand and gravel) if the gamma-ray value is <45. The ranges of gamma-ray values correspond to the four geological material types listed in Table 3.1. Two different ranges were considered for each facies to test the model's sensitivity to the gamma-ray classification (Table 3.3). Equation 3.1 is shown for Gamma-ray range 1. A similar equation was used for Gamma-ray range 2 using the different values. Figure 3.10 shows an example of a facies log generated from a corrected gamma-ray log using the Gamma-ray range 2. Differences in the model results are discussed in Chapter 4.

Table 3.3. Ranges of gamma-ray values used in generating facies logs

Gamma-ray range 1 (API)	Gamma-ray range 2 (API)	Facies
>75	>90	clay/clay-till
75-60	90-65	till/silt/fine sand
60-45	65-30	sand
<45	<30	Coarse sand and gravel

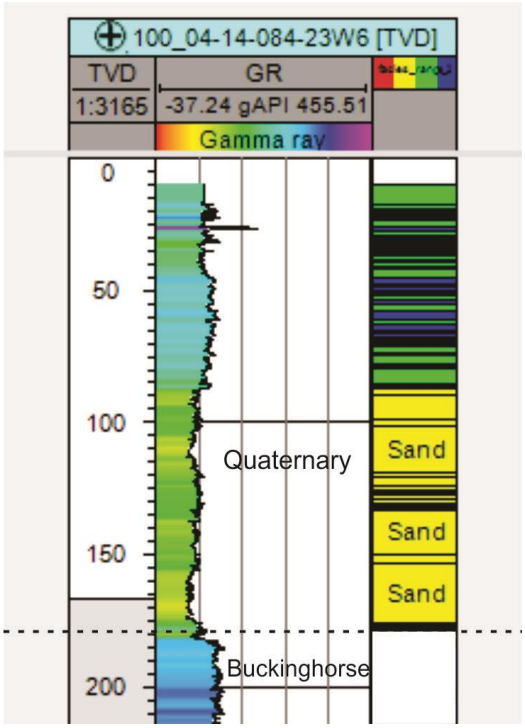

Figure 3.10. Generated facies log from corrected gamma-ray log for well 100_04-14-084-23W6 shown on the right track. Gamma-ray range 2 is shown (see Table 3.3) is shown on the left track. The facies log is coloured as follows: red: coarse sand and gravel; yellow: sand; green: till/silt/fine sand; blue: clay/clay-till. The top of bedrock is indicated by the dashed line.

3.3.5. Facies Log Upscaling

The first step in Facies Modelling is to “upscale” the facies logs. Upscaling involves applying the information (specifically the facies codes) for the discrete well to all of the cells of the volumetric grid that it penetrates (Section 3.3.3).

The next step in the Facies Modelling process is to populate the rest of the cells of the volumetric grid that do not have wells with a facies code. As stated previously, each of a stochastic and deterministic algorithm was used. These are described in Sections 3.3.6 and 3.3.7.

3.3.6. Stochastic Algorithm: Sequential Indicator Simulation

The stochastic algorithm 'Sequential Indicator Simulation' (SIS) was first used to create a Quaternary model. In this facies modelling algorithm, both the upscaled facies logs and trends (resistivity data) can be used as main inputs. SIS is most appropriate when the shape of facies bodies is uncertain, or when input trends may have an impact on the facies type. However, SIS always honours the well data over input trends, and attempts to interpolate between the wells where possible. For this study area, SIS may yield unrealistic results, because while there are some well data, they are fairly irregular and sparse. The main input governing the facies distribution is more likely to be the resistivity slices (as trends). Nevertheless, this stochastic approach was tested.

When using any Facies Modelling algorithm within Petrel, each zone in the volumetric grid (zones are based on the elevation surfaces input when creating the grid) requires an input describing facies distribution in that zone, whether it be upscaled well logs, trends, or both. In the case of SIS, each facies type present in each zone requires its own input. Based on the upscaled well logs, the algorithm determines what percentage of each facies is present in each zone; however, because the well log data are sparse, trends are also needed.

The trends used were the horizontal resistivity slices. However, the resistivity slices do not have information that relates a resistivity value to a particular facies type. Therefore, operations had to be performed on the resistivity slices to convert them to surfaces that correspond to facies type. The Surface Calculator in Petrel was used to perform the conversions. Similar to the Well Log Calculator, the Surface Calculator creates new surfaces based on existing ones. An equation relates each facies type to a resistivity range, and creates a new surface that shows only the areas where the specific facies exists; for example:

"New=If(Res_5_10≤100AndRes_5_10>50,Res_5_10,U)" (3.2)

This equation specifies that if the resistivity value in the 5-10 mbgs resistivity slice is between 100 and 50 ohm·m, keep the surface, otherwise, leave it undefined. This creates a new surface that shows only where sand is present in the zone of 5-10 mbgs (Figure 3.11). The resistivity classifications are provided in Table 3.1. Surfaces were created using similar equations for each facies type in each zone of the volumetric grid. These "facies surfaces" were then used as horizontal trends for their respective zones and facies types within the SIS algorithm.

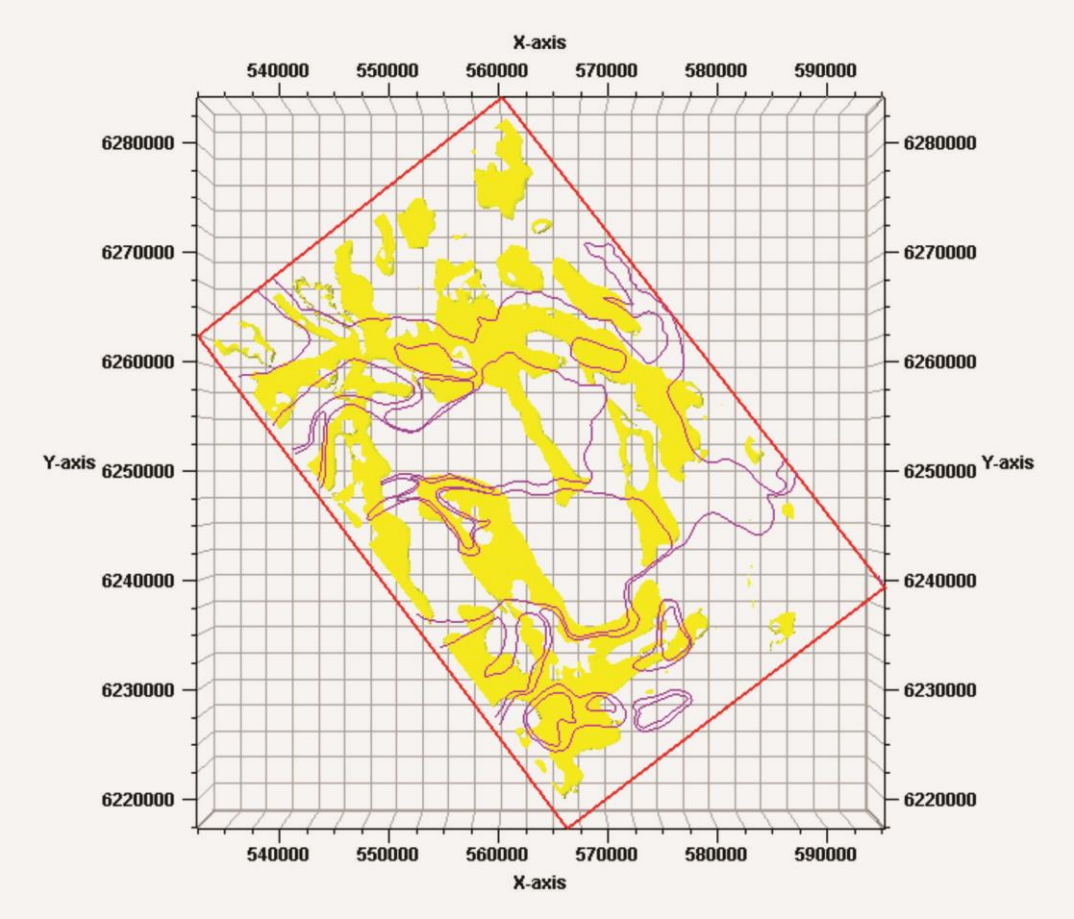

Figure 3.11. Distribution of sand facies from 5-10 mbgs (metres below ground surface) based on digitizing the horizontal resistivity slices from Aarhus Geophysics ApS (2016d). The model area outline is shown in red and buried valley contours (Levson in Petrel Robertson Consulting Ltd., 2015) are shown in purple.

3.3.7. Deterministic Algorithm: Assign Values

The deterministic algorithm 'Assign Values' (AV), specifically, the 'Surface' option within AV, was used to create a second Quaternary model for comparison with the SIS

model. In this facies modelling algorithm, the cells of the volumetric grid are assigned a property value (here the facies code) based on a surface (the resistivity slices). The upscaled facies log data are used in areas where they exist; however, interpolation between the wells is not performed. Where well data do not exist, the surfaces (resistivity slices) are used as the main input.

Similar to SIS, operations had to be performed on the resistivity slices to add information within the surface that relates resistivity values to facies types. However, AV is different from SIS in that each zone in the volumetric grid can only have one surface describing all facies distributions, as opposed to one surface for each facies type. The Surface Calculator was used to convert the resistivity slices. Instead of using an equation that creates a surface showing only one facies type, a new surface was created that contained a facies code in each cell of the surface based on the resistivity value from the original resistivity slice. Again the resistivity ranges used are those found in Table 3.1. For example,

"New=If(Res_5_10>100,0,If(Res_5_10≤100AndRes_5_10>50,1,If(Res_5_10≤50AndRes_5_10>15,2,If(Res_5_10≤15,3,U))))" (3.3)

Which, for the 5-10 mbgs resistivity slice, assigns a facies code 0 (coarse sand and gravel) if the resistivity is >100; a facies code 1 (sand) if the resistivity is between 100 and 50; a facies code 2 (till/silt/fine sand) if the resistivity value is between 50 and 15; and a facies code 3 (clay/clay-till) if the resistivity ≤15. The same formula was used to create facies-coded surfaces for each zone in the volumetric grid.

These surfaces were used as the surface inputs for the AV algorithm. Within the AV algorithm, the option to keep the upscaled log values unchanged was selected to incorporate the well data in the facies modelling. Facies Modelling was then run and a second Quaternary model was generated.

Chapter 4.

Results of the Geological Modelling

This chapter presents the results of the geological modelling in Petrel. The results of the bedrock model are presented first, followed by a comparison of the two Facies Modelling algorithms used in creating the Quaternary model. The justification for the selection of the final Quaternary model that was exported to MODFLOW is provided, followed by a discussion of uncertainty. Finally, the conceptual model of the buried valley network is presented.

4.1. Results of the Bedrock Model

As described in Chapter 2, the shallow Cretaceous bedrock formations that underlie the study area are the marine shales and sandstones of the Fort Saint John Group (Buckinghorse Formation, Sikanni Formation, and the Sully Formation.) and the Dunvegan Formation. These formations were modelled in Petrel using depth to bedrock picks and formation contacts from the corrected gamma-ray logs (see Chapter 3).

Figure 4.1 and Figures C1 to C4 in Appendix C show the results of the bedrock model created in Petrel. These figures show different viewpoints of the 3-D model, and highlight areas where formations are the top bedrock units (either outcropping at surface or underlying Quaternary sediments). The figures are displayed with 10x vertical exaggeration resulting in apparently steep bedrock surfaces; however, regionally, the bedrock gently dips to the southwest (BC Ministry of Energy and Mines, 2011). It should be noted that the accuracy of this bedrock model is uncertain primarily because the region is data-sparse. The only data sources used to construct the bedrock model were the 199 corrected gamma-ray logs from oil and gas wells, and top of bedrock picks from 23 water well lithology logs in the study area, so it is challenging to constrain the bedrock model. Petrel also has several different surface-generation algorithms. The Convergent Interpolation Algorithm was deemed the most suitable for this type of data as it is suited to fit a variety of data types of various densities, including sparse point data (Schlumberger, 2016). It should also be noted that in some of the figures throughout this

chapter displaying the results of the Petrel modelling, there appears to be some inconsistencies in the bedrock stratigraphy (i.e. formations appear to be missing. For example, Figure 4.1 shows that in the southeast part of the model area, the Dunvegan Formation is abutting up against the Sikanni Formation without any intervening Sully Formation). Even though it appears these formations are missing, they are actually present as very thin layers. As described in Chapter 3, the DEM was used as a trend surface to ensure that topographic features such as river valleys were retained, and the formation surfaces were all set as Conformable, meaning that the modelling algorithm will maintain stratigraphic hierarchy. However, due to the sparsity of formation tops, especially for the Dunvegan and Buckinghorse, the surfaces may converge very close to each other in areas of little or no data, and follow the designated DEM trend surface. This results in the appearance of a missing formation when in fact; the modelled bedrock formation is very thin because the surfaces are so close together. It is not possible to enforce a minimum thickness in the grid-building process in Petrel so that the formations are not so thin, and due to the similar resistivity values of sands and sandstones and clays and shales, the TEM data could not be used to supplement modelling the bedrock formations at this scale. In more localized investigations, the TEM data, particularly the TEM resistivity sections, may be able to be incorporated.

To evaluate the results of the modelling in Petrel, the bedrock model was compared to a compilation of bedrock geology maps for Northeast BC available through the British Columbia Ministry of Energy and Mines MapPlace website (MapPlace, 2017). This bedrock geology map is shown in Figure 4.2.

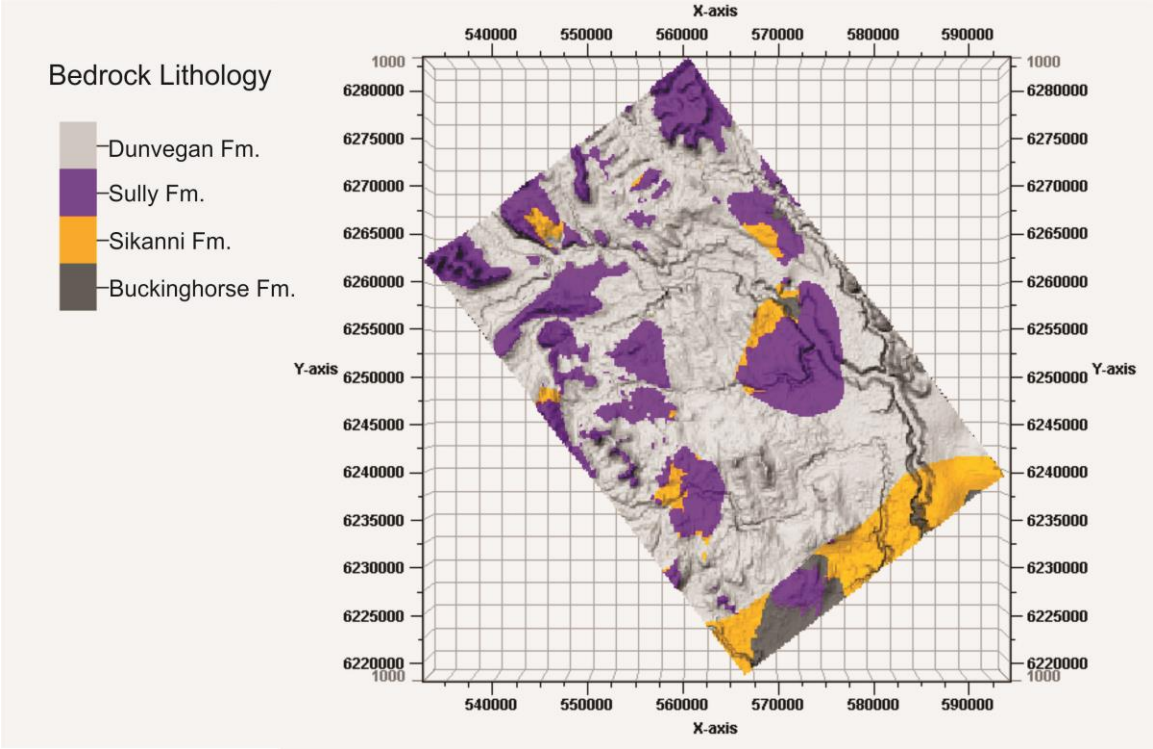

Figure 4.1. **Plan view map of bedrock lithology modelled in Petrel. As described in section 4.1 of Chapter 4, the inconsistencies in the bedrock stratigraphy are a result of the sparse formation tops, and while formations appear to be missing, they are actually present as very thin layers. See section 4.1 for a full explanation.**

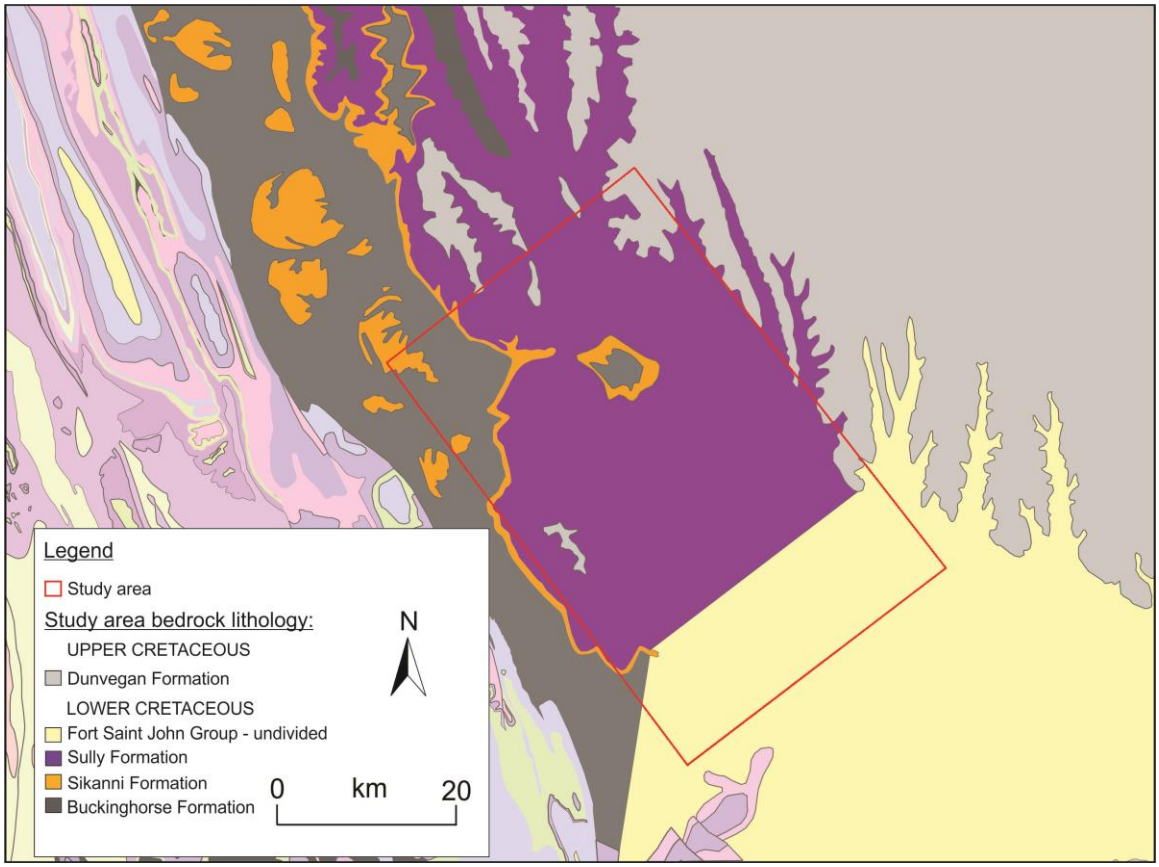

Figure 4.2. Plan view map of bedrock lithology within the study area. Data from the British Columbia Ministry of Energy and Mines MapPlace website (MapPlace, 2017).

4.1.1. Discussion on the Results of the Bedrock Model

When comparing the Petrel plan view results (Figure 4.1) and the mapped bedrock (Figure 4.2), there are some notable differences. Figure 4.1 shows the Dunvegan Formation (light grey unit) to be fairly extensive throughout the model area with the exception of the most southern part; whereas Figure 4.2 shows that the Dunvegan scarcely outcrops in the model area, but rather is dominant to the east of the model area. While this appears to be an inconsistency, Figures C1 to C4 show that the Dunvegan Formation is not as extensive as it appears in Figure 4.1. The Dunvegan Formation is quite thick at the eastern edge of the model (which is consistent with Figure 4.2); however, all other locations throughout the model show the Dunvegan surface to be very thin and in some areas non-existent. The reason for this is that the modelling algorithm (Convergent Interpolation) uses the whole study area polygon as a boundary. Due to the stratigraphic hierarchy, Petrel will model Dunvegan as overlying the Sully

Formation, but it will only be present as a very thin layer. It is also worth noting the Dunvegan “tops” had the fewest number of data points in the files used to generate bedrock surfaces.

The Sully Formation (purple) seems to be the most extensive bedrock unit in the study area (Figure 4.2). Figure 4.1 shows that there are areas where Sully is the top bedrock formation; however, these areas seem to be isolated due to the extensive top surface of the Dunvegan Formation. Figures C1 to C4 show that the Sully Formation is mostly present in the northern portion of the model as a thick unit overlying the Sikanni Formation.

The Sikanni Formation (orange) is sparse in Figure 4.2. This may be due to the fact that the Fort Saint John Group (Sully Formation through to Buckinghorse Formation) is commonly mapped as an undivided unit, except in areas where the sandy Sikanni Formation is distinguishable (Riddell, 2012). Figure 4.1 and Figures C1 to C4 show the Sikanni Formation to be quite extensive in the model area, with the exception of the southeast corner (due to the thick Dunvegan package) and the northwest corner (due to the thick Buckinghorse package). The Sikanni contacts were the most numerous contacts identified through the corrected gamma-ray logs, thus better constraining that surface. However, as these contacts were identified from only one type of geophysical log, the Sikanni may not be as extensive as it appears in the Petrel model.

There is consistency between Figure 4.1, Figures C1 to C4 and Figure 4.2 when comparing the extent of the Buckinghorse Formation (dark grey). Both the Petrel model and the bedrock map show that the Buckinghorse is extensive in the southwest portion of the model area, towards the Peace River, as well as in the northwest portion of the model area. Similar to the extent of the Dunvegan surface, Petrel generated the Sikanni surface to overlie these areas; however, it is very thin and discontinuous.

As mentioned earlier, the bedrock in this area is known to be gently dipping to the southwest (BC Ministry of Energy and Mines, 2011). It is hard to confirm this with the Petrel model, but some of the contacts do appear to be fairly flat for the most part, even with the 10x vertical exaggeration applied (Figures C1 to C4). The western portion of the study area comprises a portion of the Rocky Mountain Foothills, in which the bedrock has been subject to folding and faulting (Baye et al., 2016). Therefore, the bedrock

stratigraphy in that area is likely more complex. Additionally, this deformation and structural complexity of the bedrock units may have provided preferential areas for erosion from the processes that formed paleovalleys in the area (e.g. along faults).

Overall, neither the Petrel-generated bedrock model nor the mapped bedrock are certain due to the lack of lithology data in the area and subsequent issues with modelling surfaces with few data points in Petrel. For the purposes of this study, the bedrock model is considered a reasonable representation of the shallow Cretaceous Formations within the model area.

4.1.2. Relating the Bedrock Model to Regional Hydrogeology

In a regional hydrogeological context, the Dunvegan and Sikanni sandstone Formations can be considered aquifers, and the Sully and Buckinghorse shale Formations can be considered aquitards (Riddell, 2012). Therefore, for the purpose of this study, which is to model Quaternary fill within the buried valley aquifers, the bedrock formations were grouped into two main hydrostratigraphic units: 1) the Dunvegan and Sikanni Formations are considered aquifers and 2) the Sully and Buckinghorse Formations are considered aquitards. The Dunvegan Formation in particular is a widely-used aquifer for domestic and industrial use that directly underlies the populated Peace River valley (Riddell, 2012). Locally, however, both units can be lithologically heterogeneous given their depositional environments; the coarse-clastic formations have been described as containing shale beds, and the marine shale formations as containing continuous or lensoid coarse clastic units that may be potential aquifers (Riddell, 2012). Furthermore, fractures present throughout the bedrock formations may enhance secondary porosity, resulting in increased well yields. For example, Baye et al. (2016) report hydraulic conductivity values from pumping test analyses that are on the order of 10^{-5} m/s within the Kaskapau Formation, a shale formation south of the Peace River that is stratigraphically above the Dunvegan Formation. These values are much higher than the typical literature range for shale rocks (Freeze and Cherry, 1979: 10^{-9} – 10^{-13} m/s), suggesting that localized high permeability zones within shale units may be present. Therefore, Riddell (2012) recommends that local-scale groundwater exploration investigations into bedrock aquifers should refrain from generalizing aquifer properties based on formations. These heterogeneities within the bedrock formations may result in variable responses in both gamma-ray, and resistivity as well; however, with the regional

scale nature of this research, the effects that these heterogeneities may have on aquifer potential were not considered.

4.2. Results of the Quaternary (Facies) Models

The results of the two different Facies Modelling algorithms used in Petrel (Sequential Indicator Simulation and Assign Values; see Chapter 3) are presented in this section. The results are displayed using a combination of plan view maps, cross-sections, and statistics. When possible, well logs were projected onto the cross-sections from wells that a) were in the vicinity of the section lines and b) had a gamma-ray response for the Quaternary interval. For the locations of the cross-sections refer to Figure 4.3. Justification is provided for the selection of the final Quaternary model imported into MODFLOW.

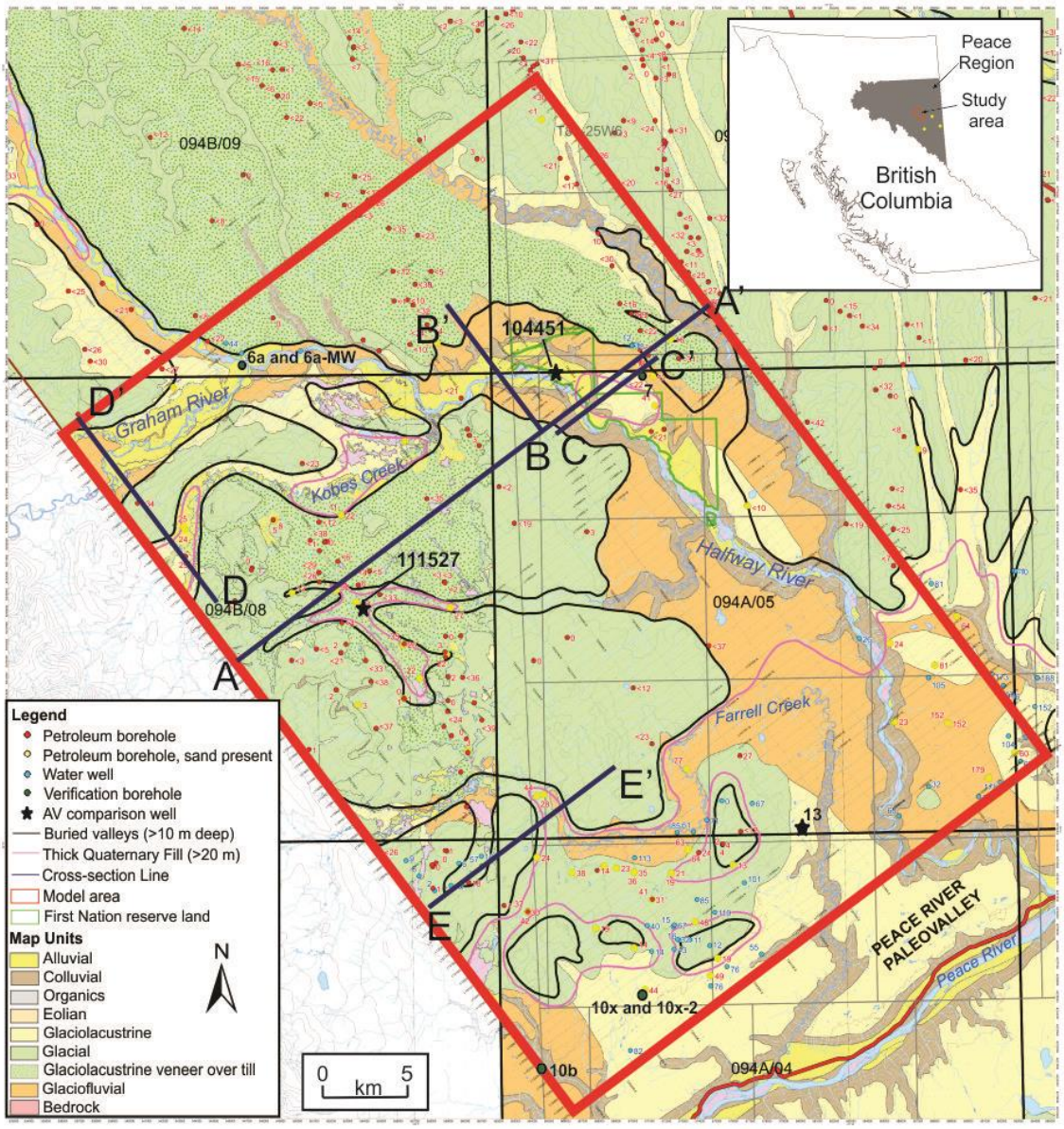

Figure 4.3. Locations of geological cross-sections for displaying the results of the different Facies Modelling algorithms in Petrel. Map modified from Petrel Robertson Consulting Ltd. (2015) with permission.

4.2.1. Comparison of SIS Results to AV Results

Sequential Indicator Simulation (SIS) Results

As described in Chapter 3, the Sequential Indicator Simulation (SIS) algorithm is a stochastic facies-modelling algorithm in Petrel. This algorithm was chosen as it is suited for when the shapes of the facies bodies are uncertain, and when input trends may have an impact on the facies distribution (Schlumberger, 2016). However, SIS

always honours the well data over the input trends (in this case the resistivity data) and attempts to interpolate between the wells where possible. This can be problematic for this study area as the well data are quite sparse.

Figure 4.4 and 4.5 show plan view maps of the facies distribution from SIS using the two different gamma-ray classification ranges (see Chapter 3), respectively, throughout three different elevation intervals of the model: shallow (Figure 4.4a and 4.5a: 5-10 mbgs); intermediate (Figure 4.4b and 4.5b: 20-30 mbgs); and deep (Figure 4.4c and 4.5c: 580-520 masl). Figures C5 (gamma-ray range 1) and C6 (gamma-ray range 2) in Appendix C are panel figures showing the full suite of plan view maps of facies distribution from SIS for all elevation intervals of the model. These elevations correspond to the intervals in which the resistivity depth slices were presented by Aarhus Geophysics ApS (2016d).

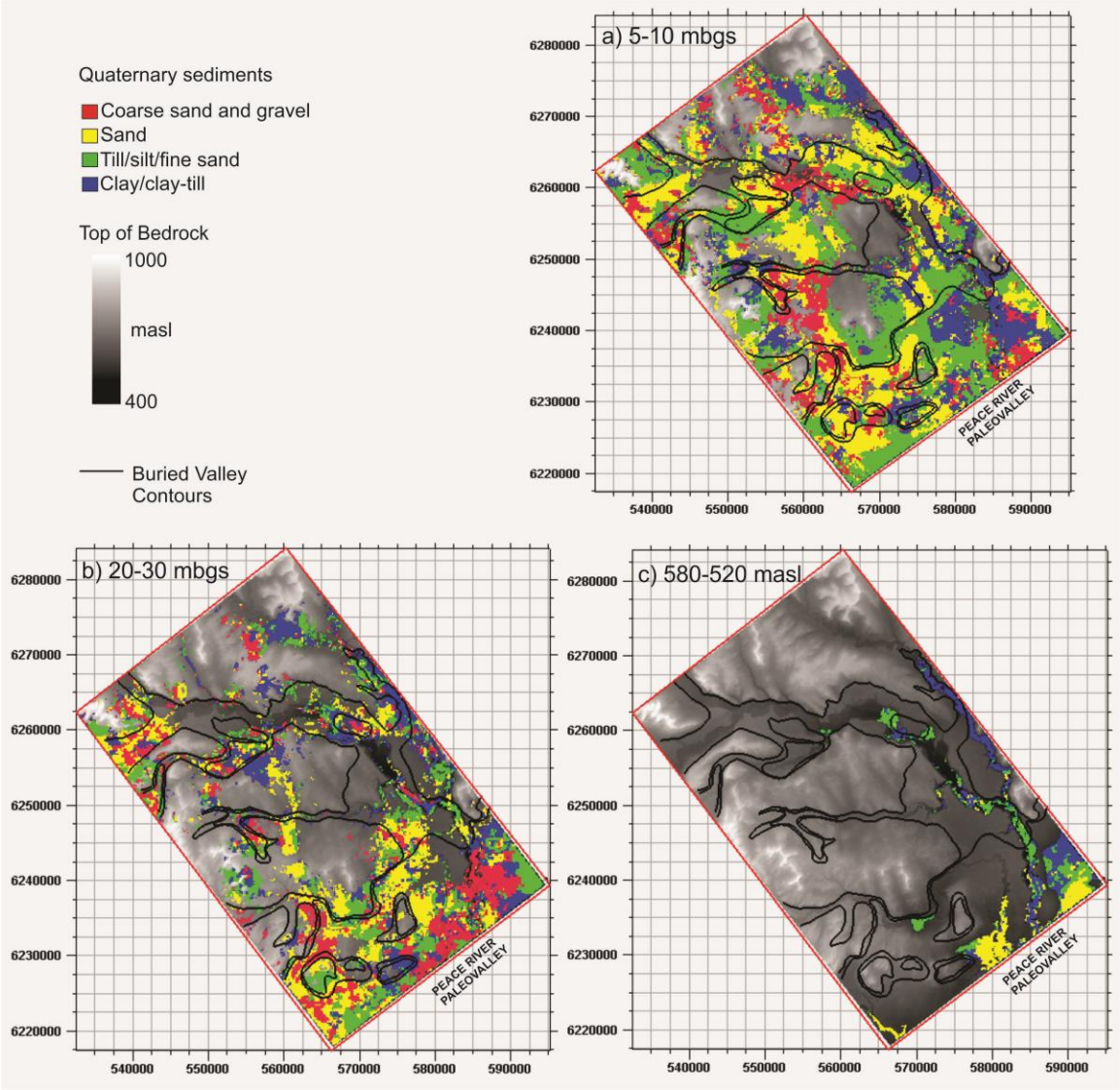

Figure 4.4. **Plan view maps of facies distribution using Sequential Indicator Simulation (SIS) and gamma-ray range 1 (>75 API: clay/clay-till; 75-60 API: till/silt/fine sand; 60-45 API: sand; <45 API: coarse sand and gravel). The outline of the buried valley network is shown in black (Levson in Petrel Robertson Consulting Ltd., 2015). Zones shown are the generated elevation surfaces in Petrel in metres below ground surface (mbgs) and absolute elevation in metres above sea level (masl).**

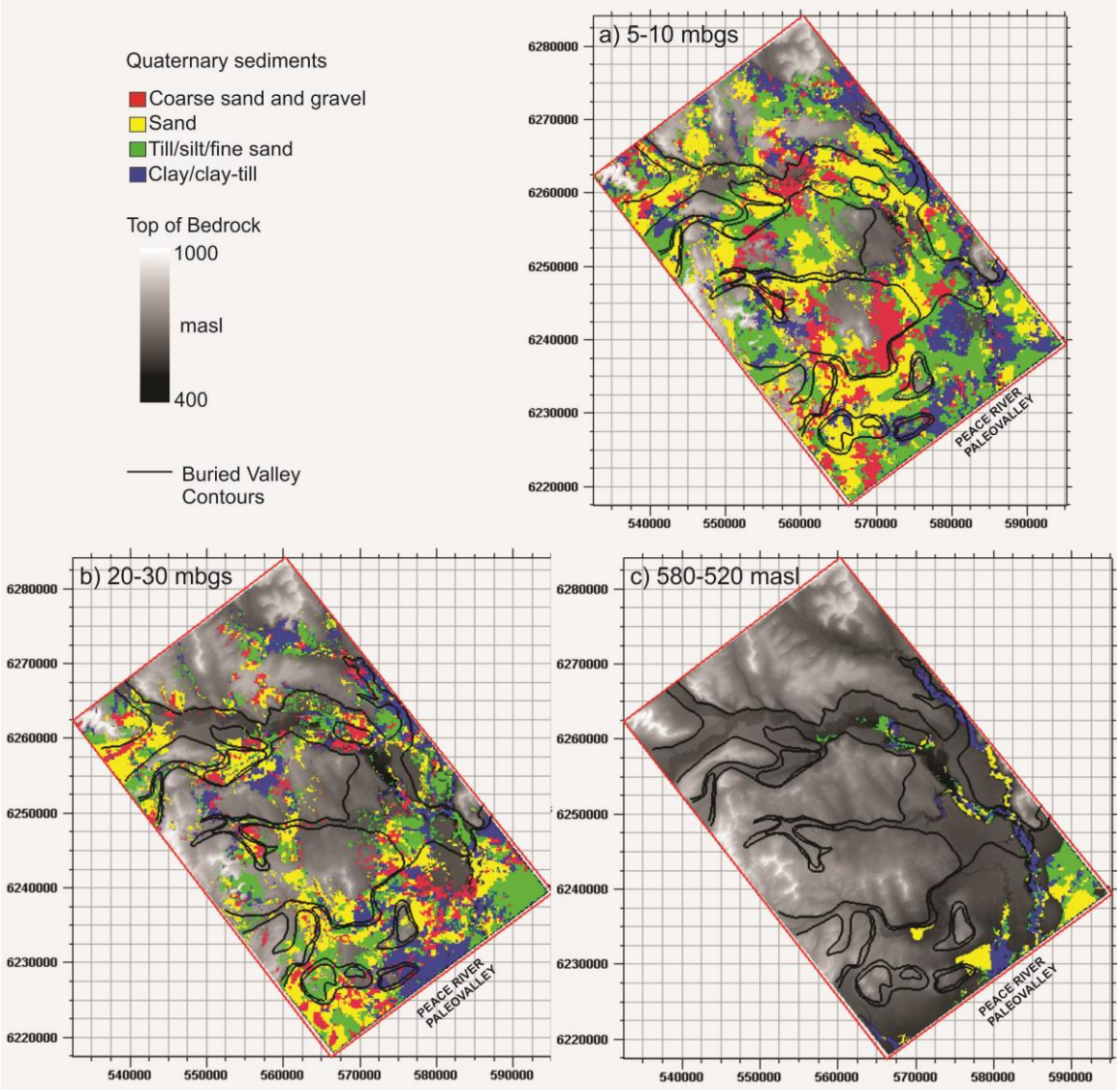

Figure 4.5. Plan view maps of facies distribution using Sequential Indicator Simulation (SIS) and gamma-ray range 2 (>90 API: clay/clay-till; 90-65 API: till/silt/fine sand; 65-30 API: sand; <30 API: coarse sand and gravel). The outline of the buried valley network is shown in black (Levson in Petrel Robertson Consulting Ltd., 2015). Zones shown are from the generated elevation surfaces in Petrel in metres below ground surface (mbgs) and absolute elevation in metres above sea level (masl).

As can be seen in Figure 4.4 and 4.5, and Figures C5 and C6 the SIS algorithm results in a very heterogeneous distribution of Quaternary sediments. This is a result of the stochastic nature of the facies modelling algorithm, and the emphasis SIS places on well data. Geological material types vary greatly over short distances, and it is very difficult to assess continuity within the buried valleys.

Figure 4.4 and 4.5, and Figures C5 and C6 all illustrate that Quaternary material is present throughout most of the study area; however, in some areas bedrock is at surface and there is no Quaternary cover (e.g. Figure C5a and Figure C6a). With increasing depth, the Quaternary material becomes mostly confined to the outlines of the buried valleys. In some areas, however, the Quaternary fill is not completely confined to the buried valley outlines, and in some locations within the buried valleys no Quaternary material is present. This is to be expected as the preliminary outline of the buried valleys in this model area (Levson in Petrel Robertson Consulting Ltd., 2015) was interpreted using limited borehole data and was done without the airborne TEM survey results. Additionally there are areas outside the buried valley outlines where thick Quaternary material is modelled at depth (up to 30-40 mbgs: in the central part of the study area at 560000, 6240000 m, and in the northern part of the study area at 560000, 6270000 m).

In the deeper layers (Figure C5g-k and Figure C6g-k), Quaternary material is still present within the buried valleys, particularly along the Halfway River and towards the southeast of the study area, approaching the large Peace River paleovalley. With increasing depth, the Quaternary material begins to disappear, although towards the southeast of the study area at 590000, 6240000 m the thickest Quaternary deposits are present.

In these panel figures, it is difficult to compare the effect of using different gamma-ray ranges for generating facies logs. Therefore, statistics of the facies distributions were produced to quantify the differences in ranges, and a cross-section was created for visual comparison.

Table 4.1 shows the percentages of each facies present throughout the SIS Quaternary models using the two different gamma-ray ranges. The percentage of both coarse sand and gravel, and clay and clay-rich till are higher in gamma-ray range 1 (GR 1). This is expected as gamma ray range 2 (GR 2) has a higher API cut-off for clay and a lower API cut-off for coarse sand and gravel, being more inclusive with respect to sand and till/silt/fine sand. This is shown in Figure 4.4 and C5 by the relatively higher proportion of red and blue compared to Figure 4.5 and C6.

Table 4.1. Statistics for Sequential Indicator Simulation (SIS) results in Petrel for the two different gamma-ray ranges.

SIS Gamma-ray range 1		SIS Gamma-ray range 2	
Facies	**%**	**Facies**	**%**
Entire Model		**Entire Model**	
Coarse sand and gravel	20.36	Coarse sand and gravel	18.96
Sand	28.61	Sand	31.39
Till/silt/fine sand	27.48	Till/silt/fine sand	28.95
Clay/clay-till	23.55	Clay/clay-till	20.69
Upscaled Cells		**Upscaled Cells**	
Coarse sand and gravel	26.48	Coarse sand and gravel	11.93
Sand	22.6	Sand	43.25
Till/silt/fine sand	29.16	Till/silt/fine sand	30.83
Clay/clay-till	21.75	Clay/clay-till	13.99

These statistics also highlight that the differences in percent of geological material type throughout the entire model are directly related to the percentage of upscaled cells with that particular facies code, from the upscaled well logs. For example, SIS GR1 has a much higher percentage of upscaled cells with the coarse sand and gravel code compared to SIS GR2, resulting in a higher percentage of coarse sand and gravel throughout the entire model. This same correlation is seen in the remaining three facies codes as well.

Figure 4.6 compares the cross-sections (A-A'; see Figure 4.3 for location) generated using the two different gamma-ray ranges. In the vicinity of the wells projected onto the section, Figure 4.6a shows more of a variation in sediment type (i.e. clays, gravels, and sand), whereas Figure 4.6b shows a higher propensity for sands and/or tills/silts/fine sands. Again, this is due to GR 2 being more inclusive of the middle-range (i.e. sand and till/silt/fine sand) API classifications. The cross-sections also highlight the variations in Quaternary material type from the stochastic algorithm: in areas along the cross-section where wells are not present, the two different gamma-ray ranges result in very different Quaternary models. If additional SIS runs were generated, those subsequent models would likely vary from GR 1 and GR 2 as well.

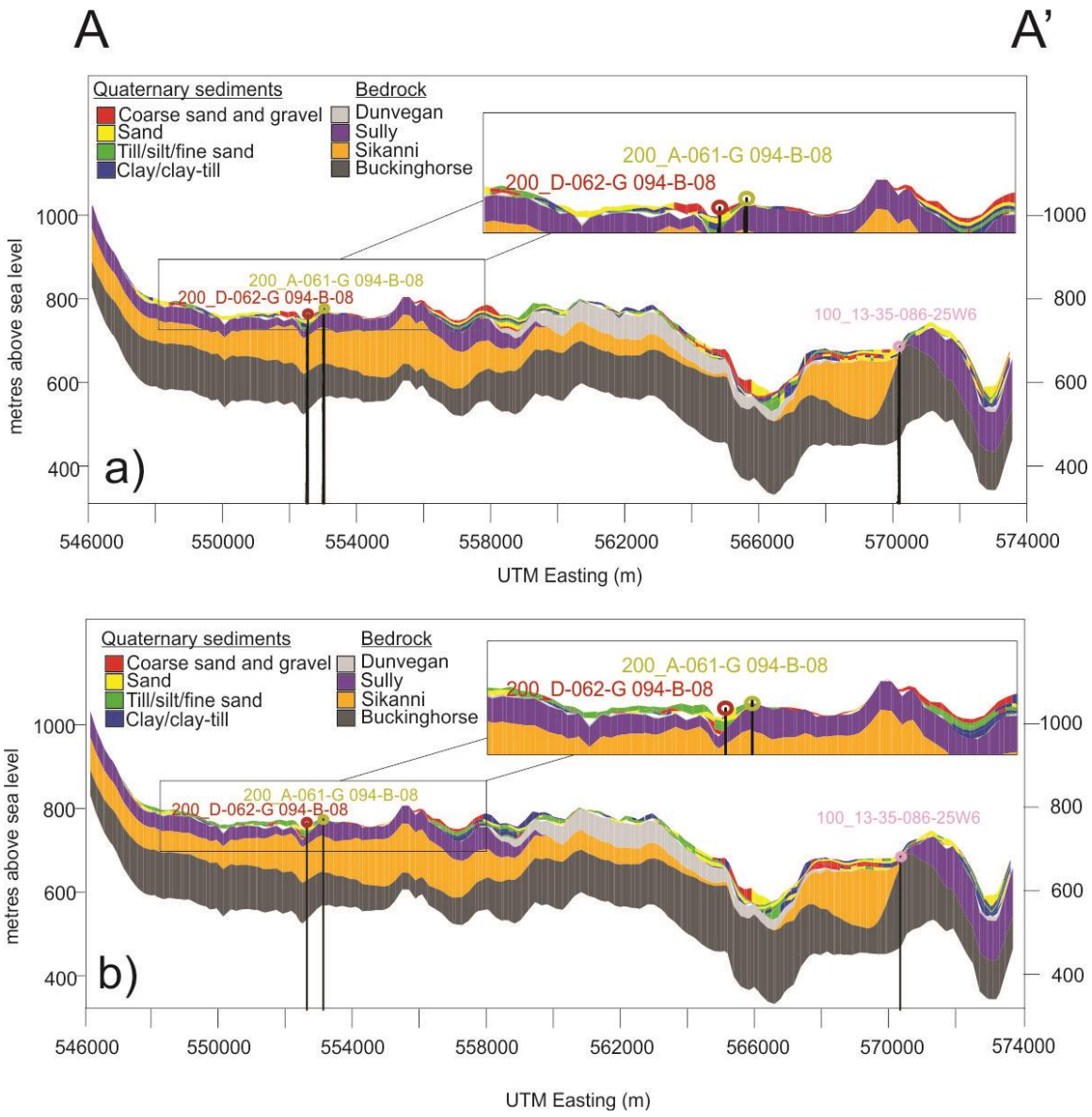

Figure 4.6. Geological cross-sections comparing the differences in the Sequential Indicator Simulation (SIS) model results using gamma-ray ranges 1 (a) and 2 (b). See Chapter 3 for Gamma-ray range classifications, and Figures 4.3 for cross-section location.

The following figures (Figure 4.7 and 4.8) compare the cross-sections B-B' and C-C', respectively, to the vertical resistivity sections from the TEM data. Both of these figures were created using the GR 1 range. Figure 4.7 is aligned roughly NW-SE in the northern, more confined, portion of the buried valley network, and Figure 4.8 is aligned roughly ENE-WSW across the central portion of the buried valley network (see Figure 4.3 for locations).

Figure 4.7b shows the B-B' cross-section through the SIS GR 1 geological model. The cross-section was drawn through the geological model in a similar location and orientation as the resistivity section shown in Figure 4.7a (Line 201804). The resistivity section shows isolated, highly resistive units close to surface; therefore, sand and gravel units appear to be present in the shallow subsurface in the geological cross-section (Figure 4.7b and c). These may be fluvial deposits associated with the modern Halfway River. The Quaternary material throughout the section is also quite heterogeneous.

The deeper Quaternary fill within the Halfway River valley appears to be of low resistivity. On the geological section these deeper deposits are till/silt/fine sands. The predominance of sands to the south of the Halfway River (south of the river in Figure 4.7c) can be attributed to the higher resistivity units shown in Figure 4.7a, and also possibly from interpolation of lithology from nearby wells.

Within the outline of the buried valley network and the vicinity of B-B', there are two wells with corrected gamma-ray logs; however, only one logged Quaternary: 200/D-015-A 094-B09. This well was projected onto the cross-section from a distance of 1.7 km to the west. As this well is a significant distance away from the cross-section, it is not surprising the interpretations are dissimilar. Figure 4.7c shows the gamma log for this well. The top of bedrock contact was determined to be Buckinghorse; however, Petrel generated a thick overlying Dunvegan with no Sully or Sikanni present. While this well is located a far distance from the section line, this inconsistency in bedrock unit is likely a result of the algorithm used in generating the bedrock surfaces in Petrel, as discussed in section 4.1.

Some discrepancy exists between the interpreted top of bedrock in the resistivity section compared to the bedrock surface modelled in Petrel, especially on the uplands of the valley near 6264000-6265000 m; however, a main finding from the Peace Project drilling program (Chapter 2) was that the depth to bedrock in this area is uncertain, and it is challenging differentiating clay-rich Quaternary material from shale bedrock, or permeable Quaternary material from sandstone based on the airborne resistivity data. So along the resistivity section lines, the thickness of Quaternary deposits is uncertain.

Figure 4.7 highlights that the Quaternary material in the region is heterogeneous, and that depth to bedrock is difficult to predict. Permeable deposits within the valley do not appear to persist with depth, and are likely either sands and gravels associated with the modern Halfway River, or exposed meltwater sands. The high-resistivity and subsequently modelled sand deposit to the south of the river valley may be an older/upper paleovalley deposit, or clastic bedrock exposed at surface.

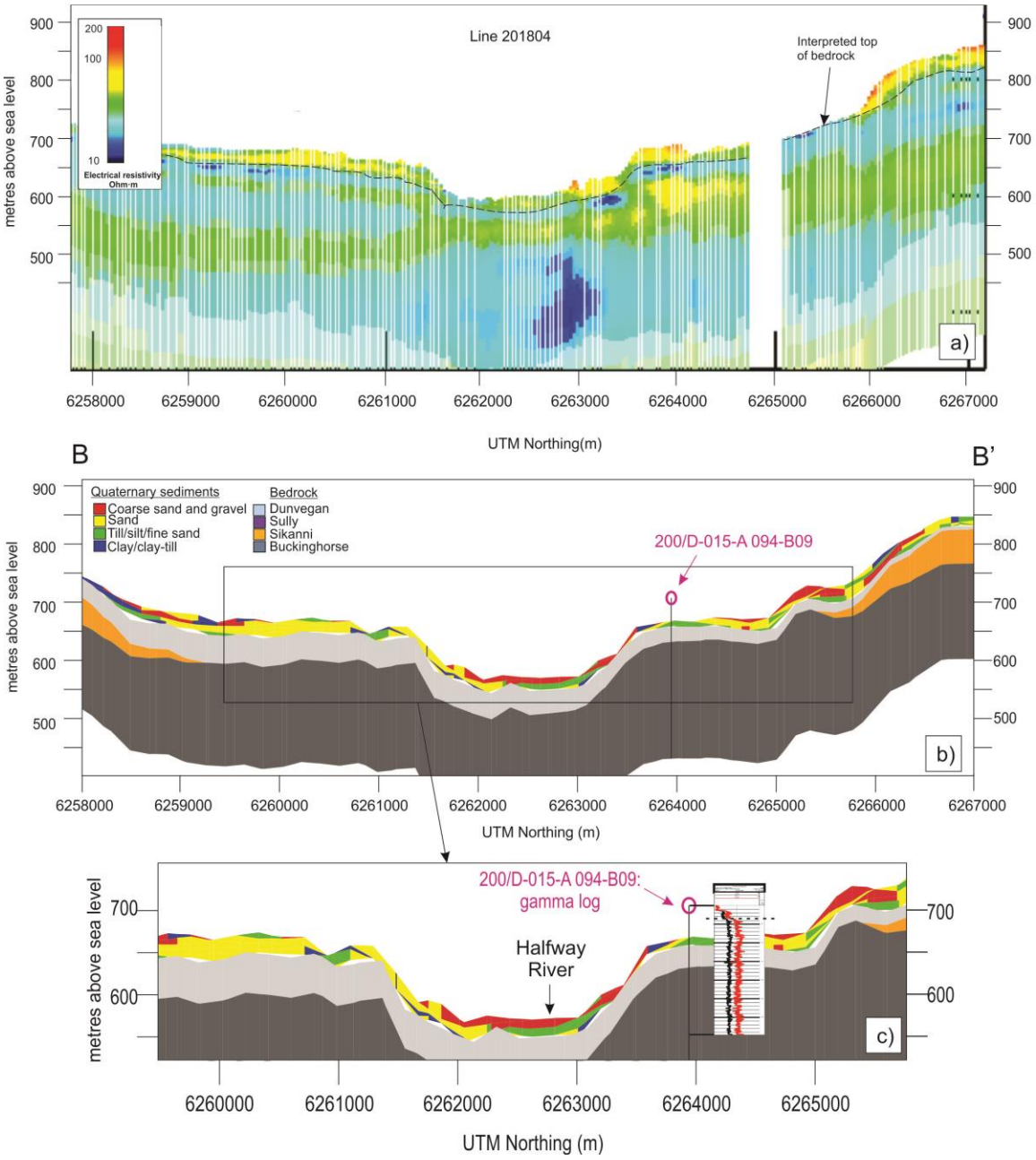

Figure 4.7. B-B' cross-section using Sequential Indicator Simulation (SIS) algorithm for Facies Modelling in Petrel. See Figure 4.3 for cross-section location.

Figure 4.8b shows the C-C' cross-section through the SIS GR 1 geological model. The cross-section was drawn through the model in approximately the same location and orientation as the resistivity section in Figure 4.8a (Line 118101).

The resistivity section shows a prominent and extensive highly resistive feature spanning approximately 3.5 km in width with a thickness of approximately 25 m (located

from approximately 567500-571000 m). This feature is represented in the geological model as a mostly sand and gravel facies that constitutes an extensive and continuous unit on the uplands near the Halfway River. At further distances from the river to the east, till/silt/fine sand facies become more prominent. This large deposit of permeable material is possibly terrace gravels or older deposits associated with a Halfway River paleovalley that were deposited and then later incised by the river, resulting in them being stratigraphically above the modern river level.

West, towards the Halfway River, Figure 4.8c shows alternating sands, silts/tills, and clays. This may be a deep paleovalley with heterogeneous fill, or may be floodplain deposits associated with the Halfway River. The resistivity section (Figure 4.8a) also indicates variable resistivity within this area. Underlying the large resistive feature, the resistivity section shows a very conductive unit approximately 20 m thick, underlain by a moderately resistive unit approximately 50 m thick. The top of the conductive unit may represent the top of bedrock in the resistivity section (as indicated in Figure 4.8a), corresponding with the top of bedrock in the geological cross-section around 650 metres above sea level (masl).

The bedrock geology shown in Figure 4.8b and c identifies several different formations, and is likely not representative of the actual bedrock, but rather again a result of the bedrock modelling algorithm in Petrel. However, the Sikanni Formation is present in the location of the moderate resistivity unit between 568000-571000 m below 650 masl. If the Sikanni is in fact the top of bedrock unit in this location, it is possible that the upper portion of the Sikanni has been extensively eroded from glacial and/or fluvial activity, resulting in fine-grained (low resistivity) gouge at the top of the formation. It is also possible that the conductive unit represents a shale-rich portion of the Sikanni, or remnant Sully. As described above, modelling the bedrock accurately is challenging.

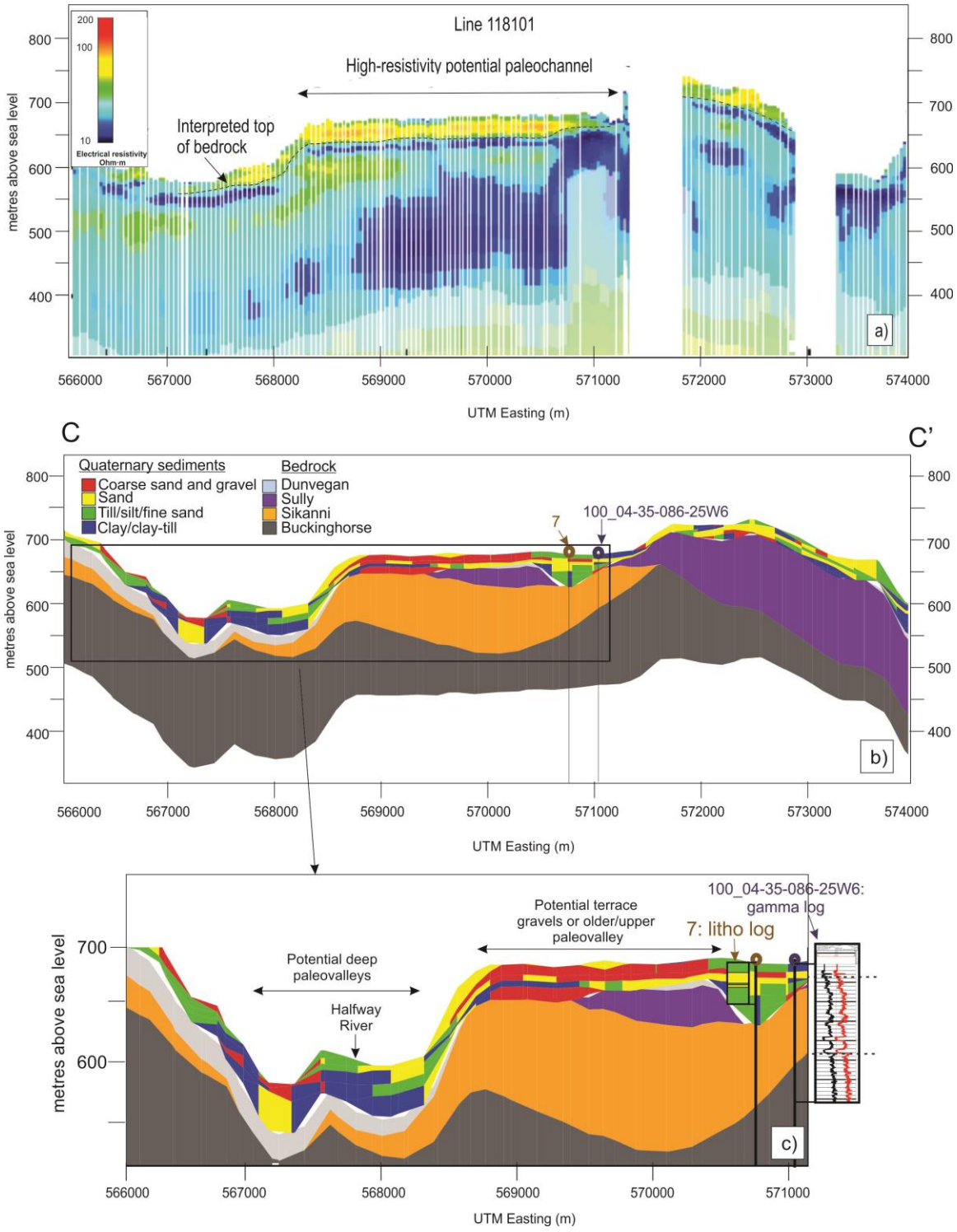

Figure 4.8. C-C' cross-section using Sequential Indicator Simulation (SIS) algorithm for Facies Modelling in Petrel. See Figure 4.3 for cross-section location.

The bedrock formations in the cross-sections also appear to be quite undulatory; however, these cross-sections have a fair amount of vertical exaggeration to allow for

visualization of the Quaternary material. As described in Chapter 2, the bedrock formations are mostly horizontal with a shallow regional dip to the southwest.

Well 7 from the Peace Project drilling program (see Chapter 2) is along the C-C' cross-section line. There are also three oil and gas wells near the cross-section with corrected gamma-ray logs; however, only one logged the Quaternary: 100/04-35-086-25W6. This well was projected onto the cross-section line from a distance of approximately 800 m to the southeast.

The detailed lithology log from Well 7, shown in Figure 4.8c, generally matches with the geological model. Alternating till/silt/fine sand and sand facies constitute the Quaternary materials in this area. The interpretation from the gamma-ray log (100_04-35-086-25W6) also matches the model with a low-moderate gamma-ray response suggesting alternating sand and silts. The bedrock contacts show some deviation, likely due to the distance the well was projected from.

Assign Values (AV) Results

As discussed in Chapter 3, the Assign Values (AV) algorithm is a deterministic Facies Modelling algorithm in Petrel. The AV algorithm assigns facies using trends as the primary input. The upscaled well log data are used in areas where they exist; however, interpolation between the wells is not performed. This results in the two AV models with the two different gamma-ray ranges being essentially the same, except where the cells are intersected by the wells. Therefore, only the GR 1 range was used in generating figures showing the results from AV. Figure 4.9 shows plan view maps of the facies distribution from AV throughout three different elevation intervals of the model: shallow (Figure 4.9a: 5-10 mbgs); intermediate (Figure 4.9b: 20-30 mbgs); and deep (Figure 4.9c: 580-520 masl). Figure C7 in Appendix C is a panel figure showing the full suite of plan view maps of facies distribution from AV for all elevation intervals of the model.

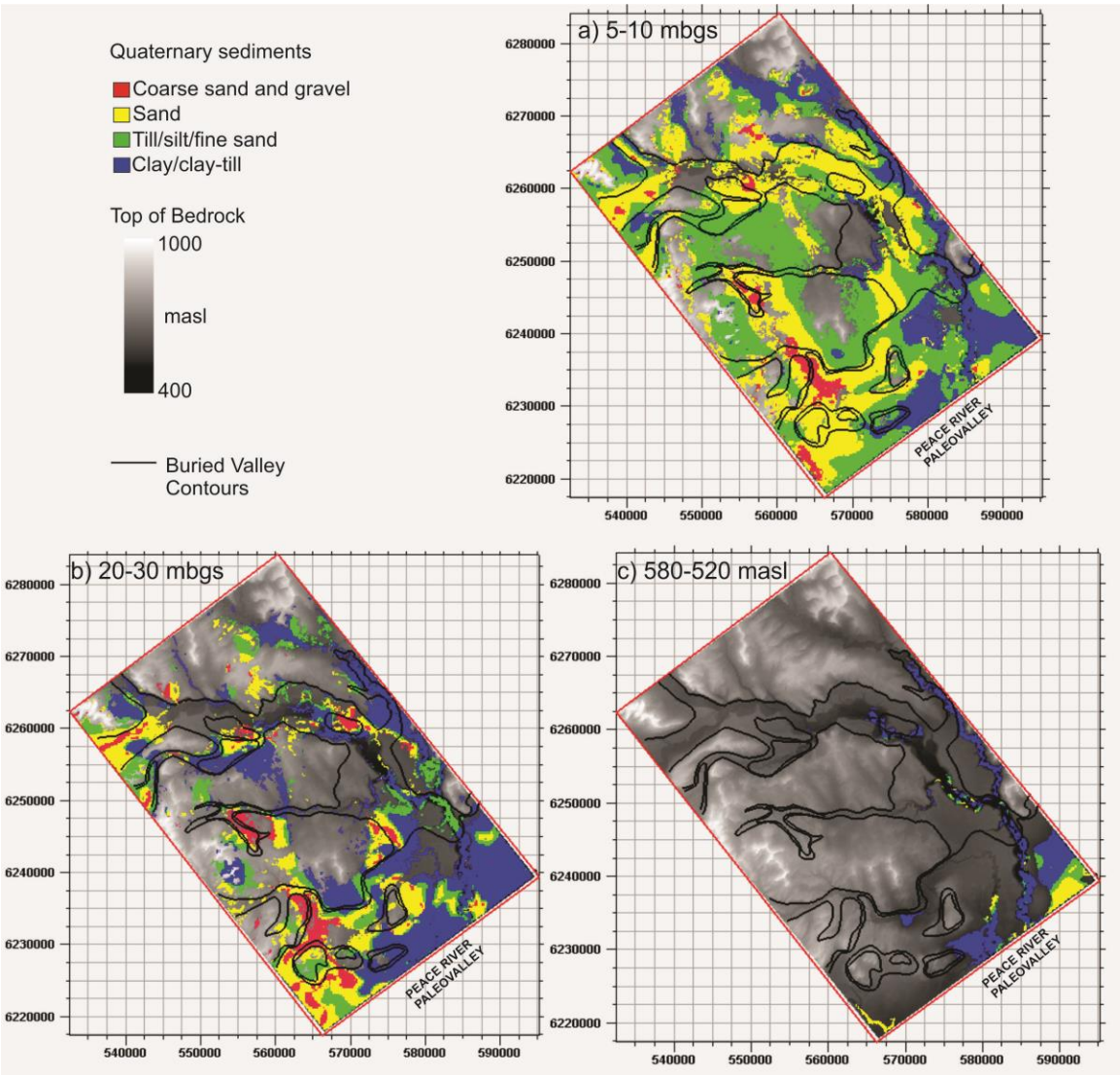

Figure 4.9. Plan view maps of facies distribution using Assign Values (AV). The outline of the buried valley network is shown in black (Levson in Petrel Robertson Consulting Ltd., 2015). Zones shown are from the generated elevation surfaces in Petrel in metres below ground surface (mbgs) and absolute elevation in metres above sea level (masl).

As the same volumetric grids were used in generating both the SIS and AV models (see Chapter 3), the presence of Quaternary material and bedrock outcrop is the same in both models. Similar to the SIS panel figures, Figure 4.9 and C7 illustrate that: 1) Quaternary material is present throughout most of the model area with some bedrock outcrops at surface, 2) with depth the Quaternary material becomes confined to the outline of the buried valleys, and 3) at greater depths Quaternary material is present along the Halfway River and to the southeast towards the Peace River paleovalley.

Figure 4.9 and C7 show that the AV algorithm results in a more homogeneous distribution of Quaternary sediments compared to SIS. Within Figure C7 it is much easier to assess continuity of geological material type within the buried valleys. In the shallower intervals of the panel figures, permeable sands (yellow) and coarse sands and gravels (reds) tend to be distributed more continuously, particularly throughout the northern part of the buried valley network along the Halfway River. In contrast, the southern part of the study area near the Peace River paleovalley is quite complex. There are no defined buried valley channels and Quaternary material is quite variable. With depth (>20 mbgs) the fill becomes more confined to the buried valley outlines and more clay-rich, with the exception of a few permeable deposits such as at the confluence of the Graham and Halfway Rivers (Figure C7e,f: 540000, 62600000 m), and along a bend of Farrell Creek (Figure C7d,e: 565000, 6240000 m). These permeable units persist to greater depths. The most extensive thick deposit is at the bottom southeast corner of the study area (Figure C7g-k: 590000, 62400000 m). A very thick (>100 m) deposit of sand was modelled here and may be a deep paleovalley leading into the larger Peace River paleovalley.

Overall, in terms of continuity of units within each of the zones, the most continuous permeable units appear to be within the buried valley network and along the Halfway River. These continuous units appear in the shallower intervals. At depth, permeable deposits appear more isolated.

Table 4.2 shows the percentages of each facies present throughout the two AV Quaternary models using the two different GR ranges. Similar to the results shown in Table 4.1, the different GR ranges result in different percentages of facies present in the upscaled cells. However, even though the percentages of the upscaled cells are different, the entire model facies percentages are essentially the same between the two GR ranges of the AV models.

Table 4.2. Statistics for Assign Values (AV) results in Petrel for the two different gamma-ray ranges.

AV Gamma-ray range 1		AV Gamma-ray range 2	
Facies	**%**	**Facies**	**%**
Entire Model		**Entire Model**	
Coarse sand and gravel	9.21	Coarse sand and gravel	9.19
Sand	30.48	Sand	30.51
Till/silt/fine sand	31.01	Till/silt/fine sand	31.01
Clay/clay-till	29.31	Clay/clay-till	29.29
Upscaled Cells		**Upscaled Cells**	
Coarse sand and gravel	26.37	Coarse sand and gravel	11.28
Sand	23.38	Sand	43.59
Till/silt/fine sand	29.37	Till/silt/fine sand	31.47
Clay/clay-till	20.88	Clay/clay-till	13.66

Four cross-sections through the AV GR 1 model were created to display the results of the AV Facies Modelling in Petrel. Two of the cross-sections correspond to the same lines shown for the SIS results (Figure 4.10 and Figure 4.11), and two are additional locations (Figure 4.12 and Figure 4.13).

The B-B' cross-section shown in Figure 4.10 appears to be quite similar to that from the SIS-GR1 algorithm in Figure 4.7. Both the valley fill and the surficial deposits on the uplands are fairly heterogeneous, although geological material type is slightly more homogeneous in Figure 4.10. Within the valley fill, permeable material is present in the shallow subsurface, but at depth the fill becomes more fine-grained. To the south of the Halfway River, some permeable material exists at depth. As described in the SIS results, permeable deposits on the uplands of the valley are likely terrace sands and gravels or an old and exposed paleovalley associated with the Halfway River, as this cross-section line spans a large mapped area of fluvial and glaciofluvial deposits (Figure 4.3).

As with Figure 4.7, the bedrock contacts identified from the gamma log projected onto the cross-section (200/D-015-A 094-B09) do not correlate well with the geological model, likely due to the far projection distance of 1.7 km to the west. However, the gamma response from the Quaternary interval matches well, in that the log shows low-

gamma sands overlying bedrock. In the vicinity of the well, Petrel generated sands with some till/silt/fine sands.

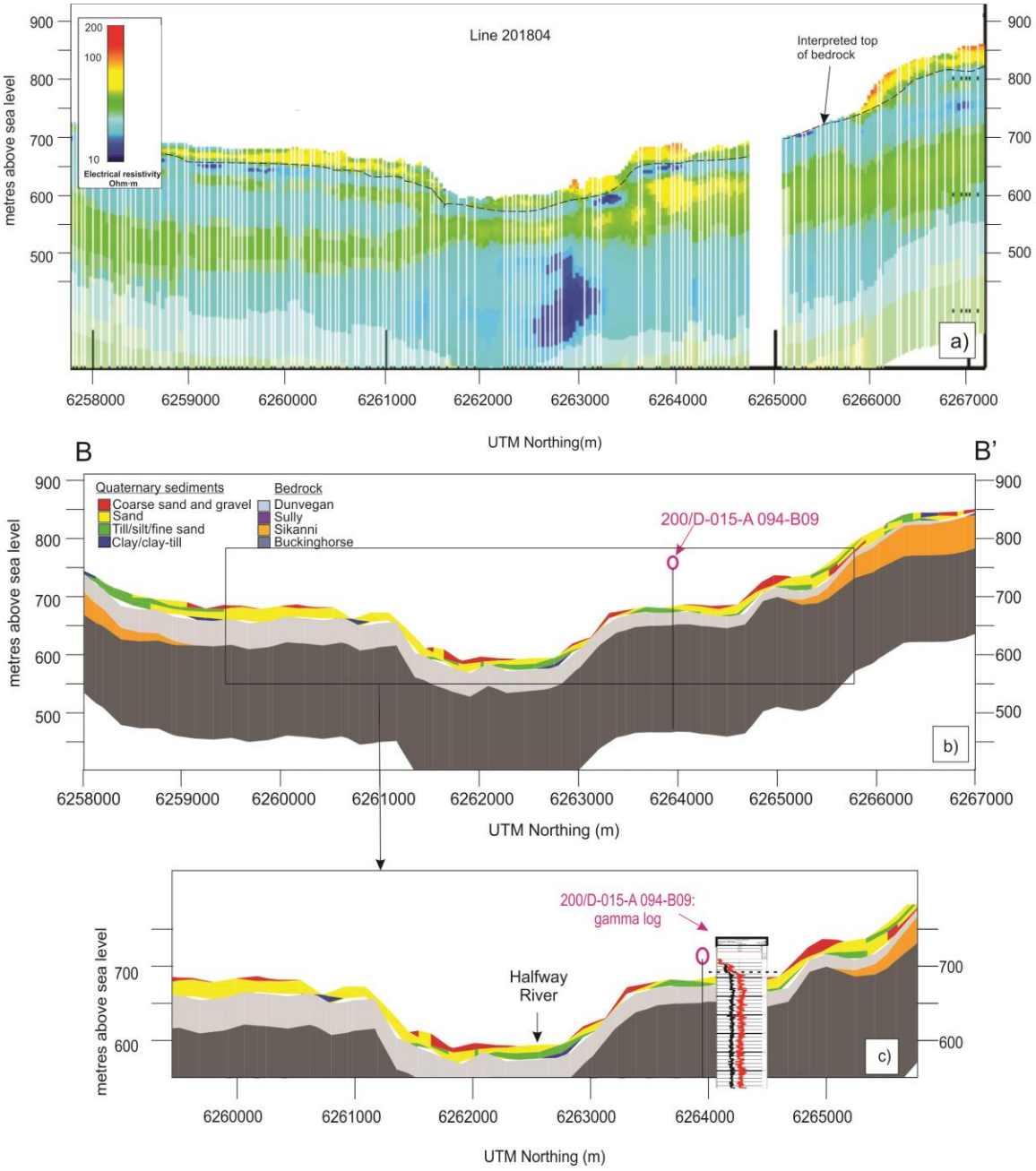

Figure 4.10. B-B' cross-section using the Assign Values (AV) algorithm for Facies Modelling in Petrel. See Figure 4.3 for cross-section location.

The C-C' cross-section line shown in Figure 4.11 corresponds to the SIS GR 1 line in Figure 4.8. Figure 4.11b shows that the AV algorithm results in a different and more homogeneous geological distribution compared to SIS. The high resistivity feature

on the uplands of the Halfway River valley (Figure 4.11a) is modelled as a thick unit of sands and coarse sands and gravels. Down into the valley, the fill becomes more fine-grained, with clays being dominant. There are some areas east of the river (Figure 4.11c) where sand is present representing a potential permeable paleovalley deposit. Figure 4.11 illustrates that these sands and gravels may be connected with other permeable deposits of potential older/upper paleovalleys, rather than as isolated buried, basal permeable units at the Quaternary-bedrock contact as suggested by the SIS results.

In the vicinity of Well 7, the modelled geology in Figure 4.11b and c shows some deviation from the lithology log. Petrel modelled the area as sands overlying coarse sands and gravels; however, the lithology log depicts alternating sand and silt sequences. It is likely that local-scale variations within the lithology are present, and they are not captured on the regional-scale resistivity sections. However, without drilling multiple wells along the section line it cannot be confirmed whether this lithology is extensive throughout the high resistivity feature shown in Figure 4.11a. A further discussion on this uncertainty in interpreting the resistivity data is provided in Section 4.3.

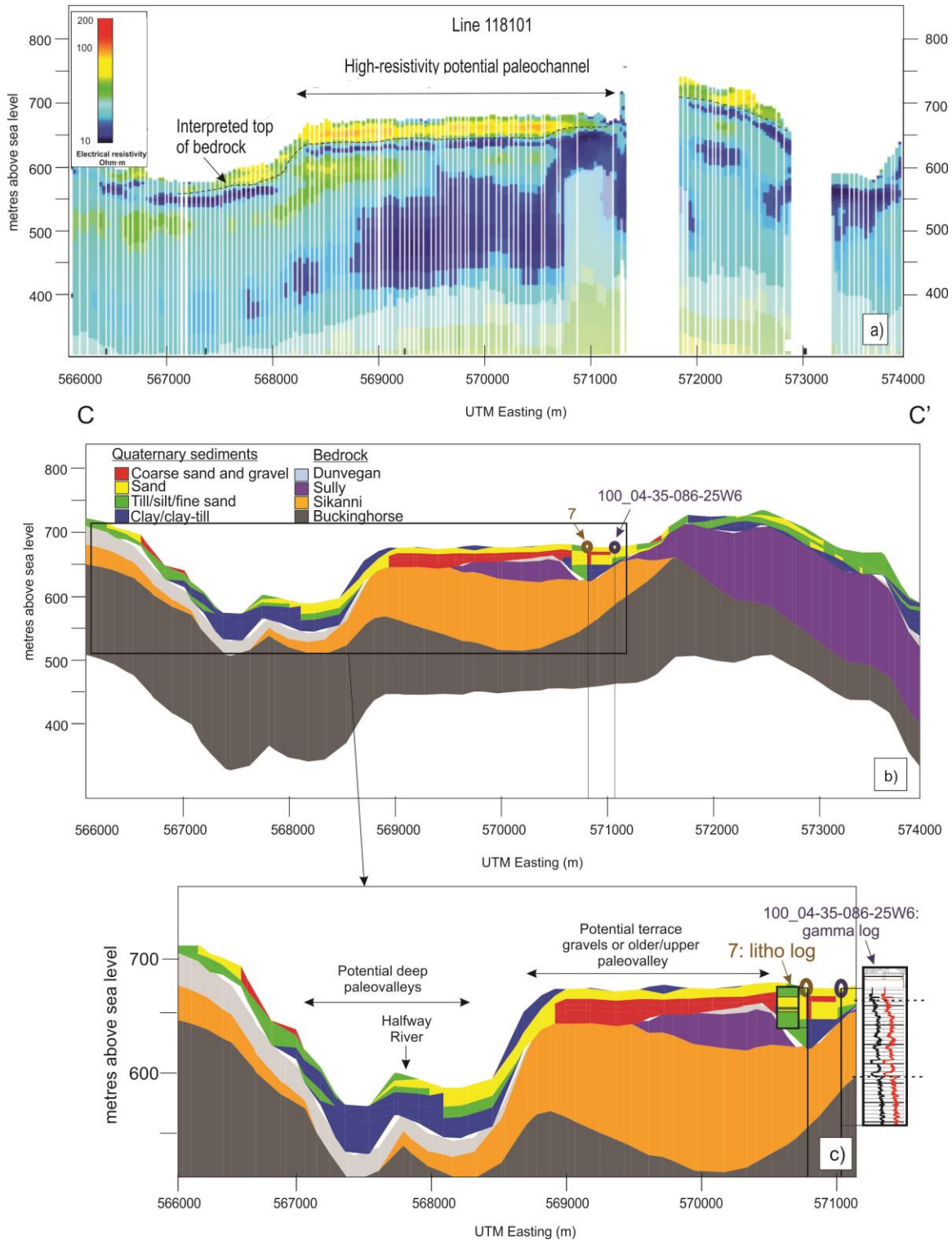

Figure 4.11. C-C' cross-section using the Assign Values (AV) algorithm for Facies Modelling in Petrel. See Figure 4.3 for cross-section location.

Figure 4.12b shows the D-D’ cross-section through the AV GR 1 geological model drawn in approximately the same location and orientation as the resistivity sections shown in Figure 4.12a (Lines 202703-202705).

This section line spans across two surface water features (Graham River and Kobes Creek) resulting in two valleys being captured in the cross-section. The resistivity line (Figure 4.12a) shows that within these valleys, high resistivity deposits are present, and are quite thick in the northern valley. These may be permeable paleovalley deposits. On both the southern and northern ends of the resistivity line, high resistivity units are present on the topographical highs, likely representing clastic bedrock units. The top of the bedrock surface on the resistivity line was interpreted as the base of the permeable materials within the valleys.

Figure 4.12b and c show the geological model generated in Petrel. The high resistivity deposits within the Graham and Kobes valleys were modelled as permeable deposits of sands and gravels. In the Graham River valley these deposits are quite thick (approximately 50 m). Permeable deposits are also within the Kobes Creek area, albeit thinner; however, overlying clays provide a confining layer whereas in the Graham River area the permeable deposits extend up to surface.

In the Graham River valley, there is a moderately thick clay unit at the base between 6255000 and 6257000 m. This corresponds to the low resistivity deposit in the same location in Figure 4.12a. Whether this is Quaternary clay or shale bedrock is uncertain. Although the algorithm used in Petrel to generate the bedrock surface may not be accurate in all locations, it was demonstrated from the Peace Project drilling that the top of bedrock is quite a bit deeper than expected in these valleys. Another bedrock discrepancy exists in the geological model as Petrel modelled the Sully Formation to the north of the Graham valley, while the resistivity line suggests a highly-resistive clastic unit.

The two wells projected onto the cross-sections are from moderate distances from the section lines (200/D-074-F 094 B-08: 200 m to the east; 200/D-094-F 094 B-08: 1 km to the east). The gamma log from 200/D-074-F094 B-08 matches the geology generated from Petrel with low gamma Quaternary sands overlying shales. The gamma log from 200/D-094-F094 B-08, however, is from quite a far distance away; therefore,

surface elevation and top of bedrock elevations do not correlate well. However, the gamma log suggests low-gamma Quaternary material overlying shales, which is consistent with the modelled geology along the cross-section in this location.

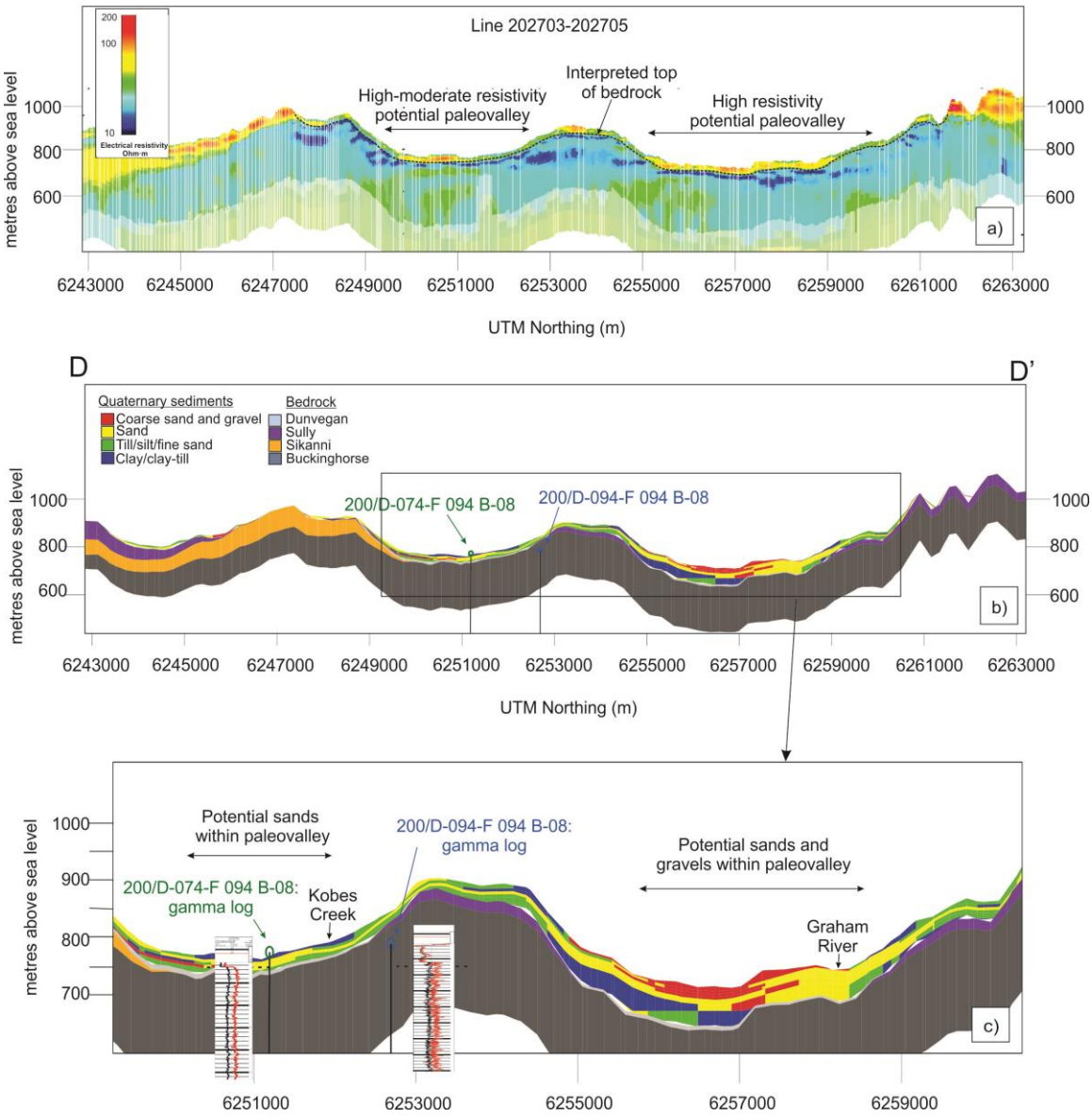

Figure 4.12. D-D' cross-section using the Assign Values (AV) algorithm for Facies Modelling in Petrel. See Figure 4.3 for cross-section location.

Figure 4.13b shows the E-E' cross-section through the AV GR 1 geological model drawn in approximately the same location and orientation as the resistivity section shown in Figure 4.13a (Line 121202).

The most obvious feature on the resistivity section is the highly resistive deposit at 564000 m. Based on the interpreted top of bedrock, this may be a broad, infilled paleochannel of Farrell Creek. However, the full extent of the top of bedrock is difficult to interpret in the resistivity section, especially to the west of the high-resistivity feature. There does not appear to be an extensive unit that could represent a bedrock formation to the west of Farrell Creek, except below approximately 700 masl.

Figure 4.13b and c show the geological modelling results. The high resistivity feature is represented by a thick package of coarse sands and gravels. As these are above the modern Farrell Creek, they may be terrace gravels or older paleovalley deposits that were further incised. To the east of Farrell Creek, the geological model matches the resistivity section in that it transitions to alternating sands and silts. To the west of the high resistivity feature, where the bedrock surface is uncertain, Petrel generated another valley structure which may be a potential paleotributary of Farrell Creek. This valley is filled with alternating sands, silts, and clays. It is also possible that bedrock should be present at surface here; however, as data are limited this is uncertain.

The wells projected onto the cross-section are from quite a far distance from the cross-section line; 200_B-049-D 094-A05 1.4 km from the northwest, and 100_16-12-084-26W6 1.2 km from the northwest. Again, as these wells are from such large distances, it is not surprising the bedrock contacts on the logs do not match with the geological cross-section. However, both gamma logs show similar responses, with low gamma Quaternary sediments overlying bedrock. This is consistent with the high resistivity feature suggesting it is continuous towards these wells. The gamma logs also indicate Sully as the top of bedrock formation and Sikanni within 100 m of the top of bedrock. However, Petrel generated a thin Dunvegan unit overlying the Sully. This is likely not the case in reality, but rather a result of the bedrock modelling algorithm as discussed previously.

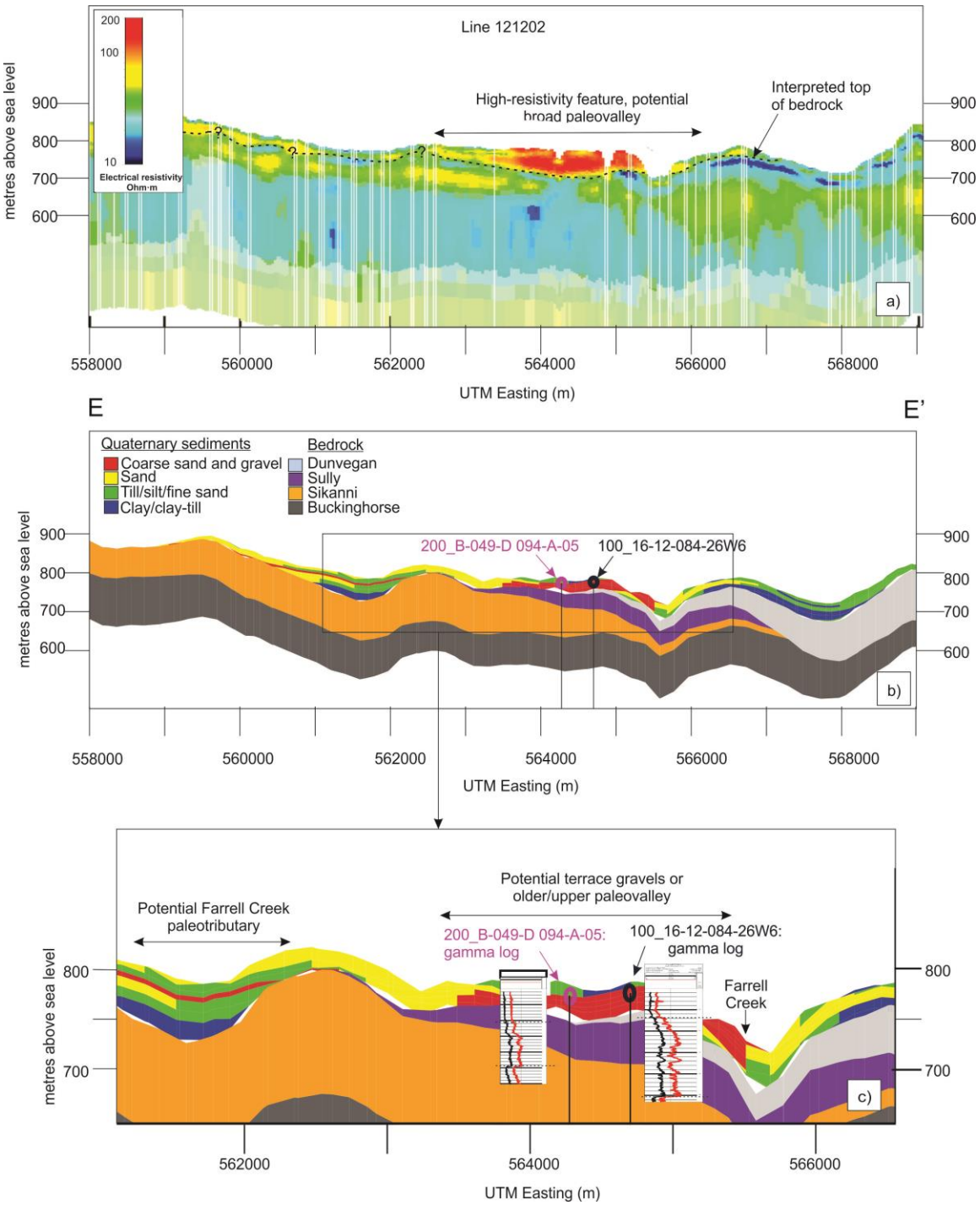

Figure 4.13. E-E' cross-section using the Assign Values (AV) algorithm for Facies Modelling in Petrel. See Figure 4.3 for cross-section location.

Justification for Selecting the Assign Values (AV) Model

To move forward with the numerical flow modelling, a single geological model had to be selected for designing the flow model. The previous section provided a discussion and comparison of the results of the two Facies Modelling algorithms in Petrel. Based on these results, the most suitable facies model upon which to base the Quaternary portion of the flow model is the Assign Values (AV) model. The justification for this selection is provided below.

The regional-scale nature of this investigation requires a simplification of the overall hydrostratigraphy. The modelling results of the SIS algorithms are extremely heterogeneous due to the different stochastic realizations of each SIS model run, resulting in it being very difficult to assess the continuity of units within the buried valley outlines. The cross-sections, plan view maps, and facies statistics presented in the previous sections all illustrate the larger emphasis that SIS puts on well log data compared to the resistivity trends. The statistics shown in Table 4.1 and Table 4.2 in particular highlight the impacts to the SIS modelling results if the well log data are altered (i.e. different gamma-ray ranges), whereas altering the well data has very little effect on the AV modelling results because trends (i.e. the continuous resistivity data) control the facies distribution. Selecting the AV algorithm offers a more conservative approach to modelling the geology as the model is not sensitive to gamma-ray classifications on lithology. While it is important to include the well log data, they are sparse throughout the study area and it is the resistivity data that offer a spatially extensive dataset in the region.

To verify that the AV algorithm is accurate in the areas where lithology logs are available, three additional cross-sections were created. These section lines intersect three different wells located within the buried valley outlines that had lithology logs available for thick Quaternary fill. The locations of the three wells selected can be found in Figure 4.3. All cross-sections were drawn in the same orientation; perpendicular to the buried valley network and in the same orientation as sections A-A', C-C', and E-E'. The horizontal scales on these cross-sections are smaller compared to all previous cross-sections, and the cell size for the Quaternary model (200 x 200 m) should be kept in mind when viewing these sections. Where well logs penetrate through cells of the model, the generated facies conform to the well log lithology data. The generated facies for cells

which do not have well logs are constrained by the resistivity trends. Units that are thinner than 5 m in the lithology logs could not be resolved in the regional geological model, and therefore lithology data were averaged over these smaller intervals. It should also be noted that in some locations (e.g. WTN 104450, 104451, 104452) multiple wells penetrate a single cell in the model. Therefore, at these locations Petrel averaged the lithology based on all well logs within the cell.

Figure 4.14 shows the comparison of the Well 13 lithology log (Peace Project drilling program) to the Petrel-generated AV GR1 Quaternary model. Overall, the lithology log generally matches with the geological model. The only exception is the approximately 10 m thick package of gravel in the lithology log, compared to the unit of clay/clay-rich till in the geology model. As the cell size in the model is 200 x 200 m, it seems that the lithology log cut into the western edge of the potential clay unit modelled in Petrel. It is possible that the gravel encountered during drilling is a part of the modelled sand unit (579700 m to the western edge of the section) from about 645-635 masl, and the trend from the resistivity data extended a bit too far in this location (i.e. there should be no small units of clay at 579700 m).

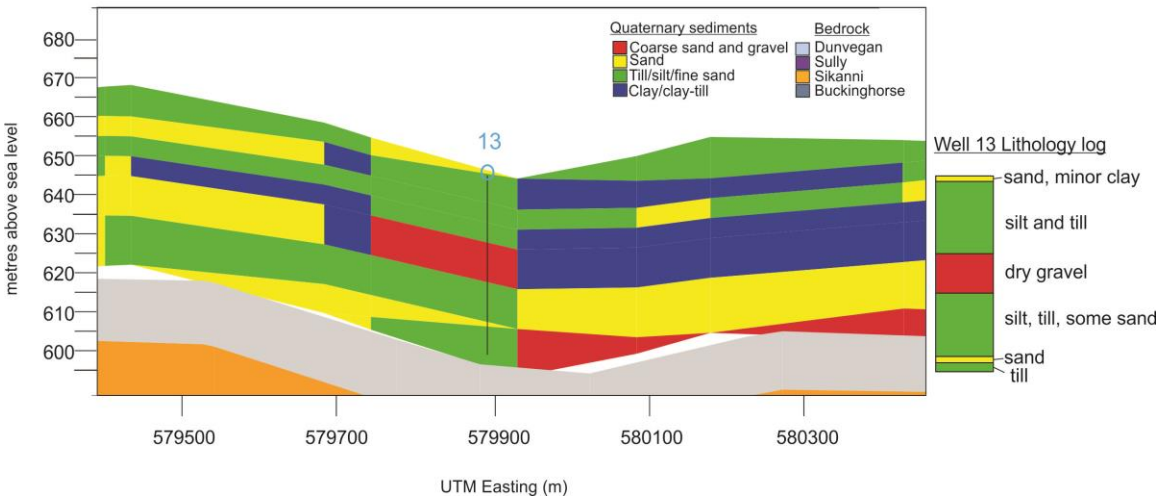

Figure 4.14. Cross-section comparing lithology log at well 13 to modelled geology from the AV GR 1 Quaternary model from Petrel. See Figure 4.3 for well location, and Table A9 in Appendix A for detailed lithology log.

Figure 4.15 shows the comparison of WTN 104451 lithology log (BC Ministry of Environment, 2017; WELLS database) to the Petrel-generated AV GR 1 Quaternary model. As with Figure 4.14, there are both similarities and differences between the

geological model and the lithology log. The near-surface geology in the lithology log is quite variable; with material type changing between three different facies types over about 15 m. The thicker unit of overlying sand seems to line up with the upper gravel and underlying silt of the geological model. Perhaps it is a fining-downwards unit of sand logged just as sand by the driller, and the small unit of clay is actually fine silt. Or, the resistivity trends are a result of averaging the TEM data. The basal Quaternary unit of clay in the geological model may in fact be silt, as the resistivity values of these two material types can be quite similar. Nonetheless, they both serve as aquitards from a hydrostratigraphic perspective. The thin unit of gravel in the lithology log could not be resolved in the geological model; however, the higher resistivity signature of gravel may have been modelled as a sand unit as seen in the cross-section. It should also be noted that there are three wells located within 50 m of each other in this location; all with varying Quaternary surficial deposits (104450, 104451, 104452; see Table A2 in Appendix A). Therefore, Petrel averaged the facies logs from all three wells.

There is a bit of discrepancy with the bedrock surface modelled by Petrel; however, as there are three wells located so close to each other in this location, with top of bedrock contacts ranging from 24 to 47 mbgs, Petrel interpolated the top of bedrock in this location from all three measurements.

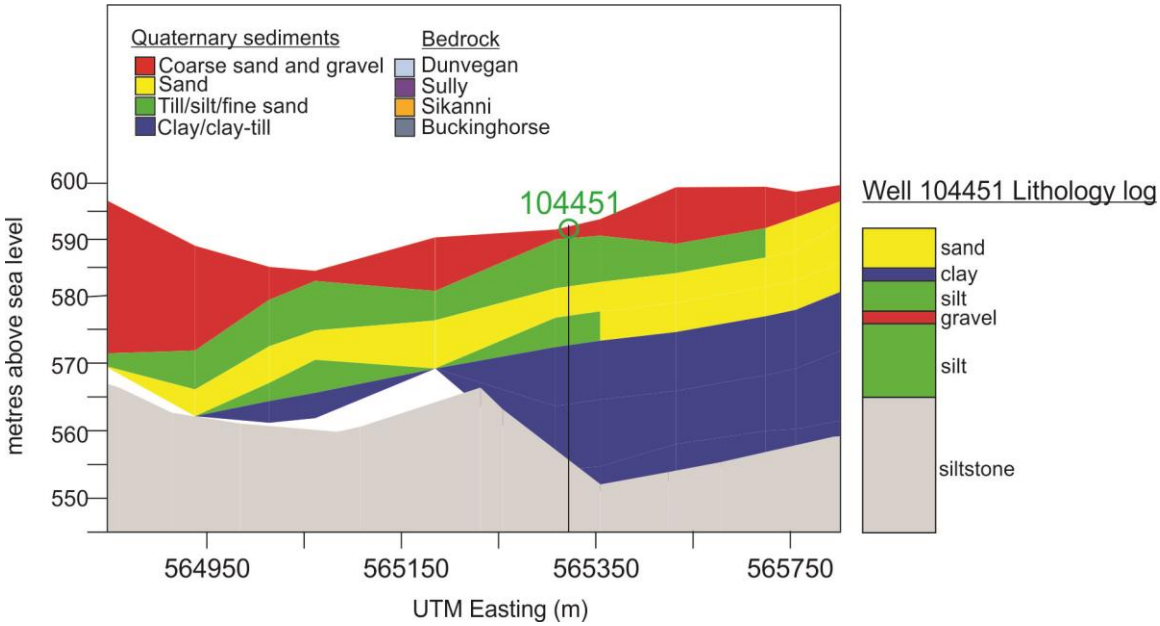

Figure 4.15. Cross-section comparing lithology log well 104451 to modelled geology from the AV GR 1 Quaternary model from Petrel. See Figure 4.3 for well location, and Table A2 in Appendix A for detailed lithology log.

Figure 4.16 shows the comparison of WTN 111527 lithology log (BC Ministry of Environment, 2017; WELLS database) to the Petrel-generated AV GR 1 Quaternary model. This section shows significant differences between the geology generated from the resistivity data compared to the lithology log. The lithology log depicts a 43 m thick package of silty clay overlying shale/siltstone bedrock. While the bedrock contact and underlying formation are correct, the Quaternary material is quite different from the AV GR 1 model. However, this particular well was drilled quite deep (>250 ft into bedrock) and was completed in the shale bedrock. It is possible that the driller overgeneralized or misinterpreted the Quaternary materials, or possibly that clay exists at this specific location.

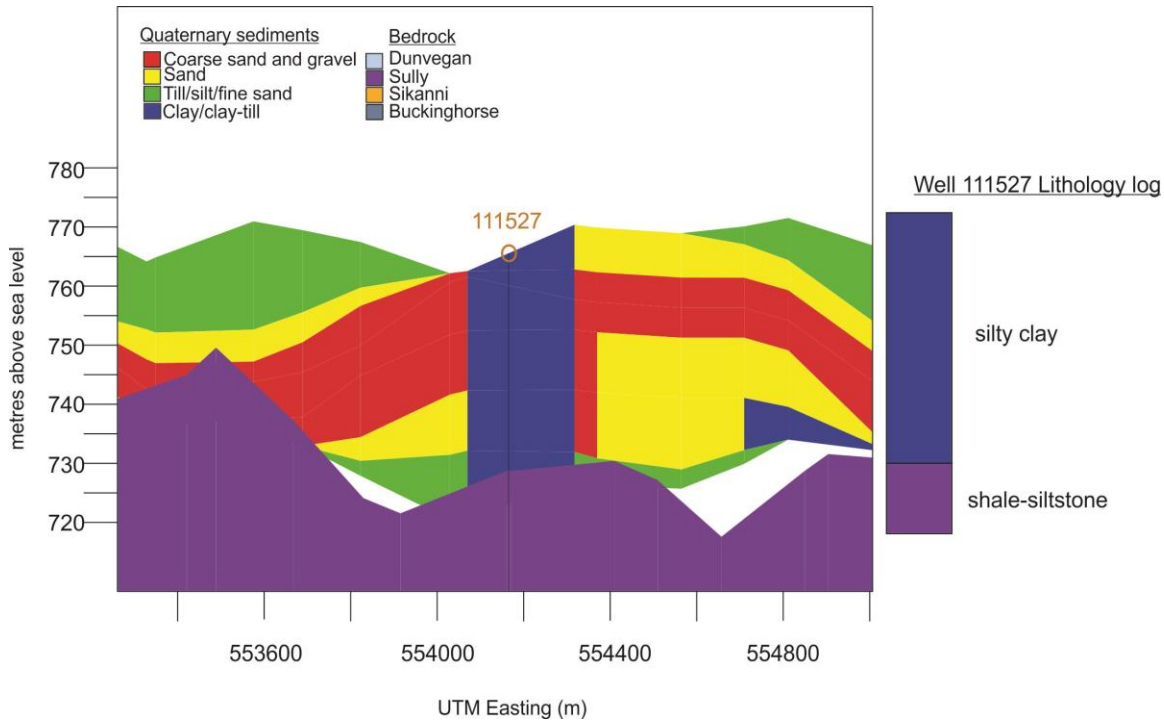

Figure 4.16. Cross-section comparing lithology log at well 111527 to modelled geology from the AV GR 1 Quaternary model from Petrel. See Figure 4.3 for well location, and Table A2 in Appendix A for detailed lithology log.

The three wells chosen to compare the AV GR 1 results to lithology logs all had thick Quaternary fill to enable a more detailed comparison. Other wells throughout the model area tend only to have a few metres of Quaternary materials logged, or bedrock within a few metres of the surface. While drillers' logs are useful, particularly for identifying top of bedrock, drillers normally are not geologists. The lithology logs from the Peace Project drilling program are more accurate as lithology was logged by a geologist. While it is important to consider how well lithology logs match the geology generated from the resistivity data, the AV algorithm does not place emphasis on the log data as in SIS algorithm. Overall, there are some lithology logs that do show some differences with the modelled geology; however, the majority of wells from the WELLS database and Peace Project drilling program correlate reasonably well with the geology generated from the resistivity data using the AV GR 1 model. Therefore, this model was chosen as the geological model to be imported into MODFLOW.

4.3. Geophysical Uncertainty

Uncertainty is a problem that plagues all modelling projects because it is impossible to know exactly what is in the subsurface at all locations without drilling everywhere. Therefore, researchers rely on geophysical surveys to gain an insight into the subsurface. However, when relying on geophysical surveys, uncertainty must be kept in mind.

The modelling conducted in this study relied heavily on the resistivity data, which were derived from one specific inversion scheme (Aarhus Geophysics ApS, 2016d). Airborne TEM data is also averaged over large volumes of material, with resolution decreasing with depth as a result of this averaging. Resistivity is also a function of multiple variables such as pore water salinity, water content, porosity, and texture (Oldenborger et al., 2014), and therefore, specific lithologies do not necessarily have a unique resistivity value, which leads to “non-uniqueness” in the interpretation. The resistivity results could be related to grain size (which is how they were interpreted in this research), or to other factors (e.g. dry versus wet, saline versus non-saline). Until calibration wells are drilled, the relationship is uncertain.

This issue was encountered during the Peace Project drilling program, specifically at Well 10-b. The preliminary interpretation of resistivity cross-sections and depth slices at this location suggested a thick package of glaciofluvial sands and gravels overlying bedrock, based on the highly resistive signature of the materials (Bemex Consulting International and Quaternary Geosciences Inc., 2016). However, very dry silts, fine sands, and till were logged during drilling and bedrock was not encountered (see Table A6 in Appendix A). The materials were resistive because they were very dry, relating to the fact that the water table was very deep as this location is on the uplands of a very steep river valley. This drilling location showed the most deviation from what was interpreted from the resistivity data and highlights the challenges in interpreting resistivity data when different variables may be influencing the measured resistivity.

It is also not possible to differentiate between a highly resistive gravel that is dry and a gravel that is wet using the airborne TEM data and gamma-ray logs. Similar difficulties exist in differentiating shale versus clay, and sand versus sandstone. The interpretation of the Quaternary-bedrock contact from single gamma-ray logs is also

highly questionable, as sands and sandstones, and clays and shales, may have similar gamma responses, respectively. A large portion of the gamma-ray logs also did not log all the way up to surface. Therefore, it was only possible to suggest a minimum depth to bedrock in these wells.

4.4. Conceptual Model of the Buried Valley Network

Previous studies have documented that the Quaternary sediments of the Peace Region are heterogeneous, but thick accumulations of permeable material may exist within buried valleys (Lowen, 2011). It has also been suggested that basal sands and gravels in the buried valley thalwegs may represent significant sources of groundwater (Cowen, 1998). The fill within these valleys typically contains pre-glacial and advance phase glaciofluvial sands and gravels, overlain by advance-phase glaciolacustrine silts, clays, and a thick package of glacial sediments, often capped by retreat-phase glaciolacustrine sediments (Levson et al., 2006).

The plan view maps and geological cross-sections illustrate that there are thick deposits of permeable material, mainly associated with the modern rivers and creeks in the study area including the Halfway River, Graham River, Kobes Creek, and Farrell Creek. Some of these permeable deposits also persist with depth, and in some locations can reach thicknesses of approximately 50 m. The cross-sections show that there are discontinuous sands and gravels at or near surface on plateaus and valley uplands, potentially formed by glacial meltwater channels at the end of the last glaciation, or representing older paleovalleys that have been further incised. Thick packages of heterogeneous Quaternary material including large packages of till can be found on valley uplands. The thickness of the Quaternary material is also quite variable; in some locations bedrock is exposed at surface whereas in other locations it is buried by >100 m of Quaternary sediments.

The cross-sections also highlight that some of the permeable deposits associated with the paleovalleys appear to be exposed at surface, and that confining, low-permeability units such as silts and clays are generally discontinuous in the northern portion of the model (most cross-sections are in the northern and central portion of the model where the buried valley outline is more narrow). In the southern portion of the model within the mapped thick Quaternary fill of the large Peace River paleovalley (see

Figure 4.3), overlying thick deposits of silts and clays deposited in Glacial Lake Peace are present (Vic Levson, personal communication December 2017). It is questionable whether the discontinuous nature of overlying silts and clays outside of the Peace River paleovalley is the case in reality. The geological distribution for the upper 5 m of the geological model was obtained from the surficial geology map compiled by Levson in Petrel Robertson Consulting Ltd. (2015). This map details the dominant surficial unit, and therefore thin and/or isolated deposits of silts/soils may not be included. Most wells drilled during the Peace Project drilling program recorded fine-grained silts, clays, and sometimes organics at surface (see Appendix A). However, these wells are only in a few localized areas. It also cannot be ruled out that high resistivity deposits at surface which may have been modelled as sands or gravels, are in fact dry vadose zone silts.

A synopsis on the hydrogeochemistry of the Peace Region by Dirk Kirste, SFU, in Baye et al. (2016) describes the differentiation of groundwater sourced from Quaternary versus bedrock aquifers using the relative proportion of sodium to calcium and the presence or absence of tritium. The majority of groundwater samples sourced from Quaternary aquifers had high calcium and low sodium content, and contained tritium, whereas most of the samples from bedrock aquifers had high sodium and contained no tritium. The presence of tritium indicates a mean groundwater residence time of less than approximately 50 years; therefore, groundwater sourced from Quaternary aquifers is very young, and originates as recent recharge while the bedrock groundwater is much older (Baye et al., 2016). This finding suggests a low degree of hydraulic connection between the Quaternary and bedrock aquifers; however, a higher degree of hydraulic connection between overlying units within the Quaternary deposits. However, the majority of water chemistry samples collected throughout the Peace Region are south of the Peace River (and south of the study area for this thesis), concentrated in the Dawson Creek area. As described above, within the southern portion of this study area in the Peace River paleovalley, overlying deposits of silts and clays are quite thick. These likely preclude recharge from precipitation infiltration. This may result in older groundwater ages and recharge coming from upland areas or areas where streams or tributary channels have incised deep into the Quaternary sediments and possibly shallow bedrock formations. Consequently, there may be differences in the recharge areas and flow regimes north (this research) and south (Baye et al., 2016) of the Peace River.

The plan view maps showing slices of the Quaternary models allow for investigation of the continuity of permeable deposits within the buried valleys. As described earlier, continuous permeable deposits are generally present at shallow-moderate depths mostly along modern river valleys, but with depth they appear to be present as localized and discontinuous sand and gravel bodies, perhaps isolated by glacial processes such as ice erosion. The discontinuous nature of unconsolidated sand and gravel aquifers has been encountered south of the study area, within the Montney Trend of the Dawson Creek area. In 2011, new provincial observation wells were drilled for the purpose of intercepting both unconsolidated and bedrock aquifers. The well locations were selected within the apparent boundary of an unconsolidated aquifer; however, five of the seven wells did not intercept any water-bearing sand and gravel zones (Wilford et al., 2012; Baye et al., 2016). From this drilling program, it was concluded that the previously mapped unconsolidated aquifer was not as aerially extensive or as continuous as previously suggested, but rather consists of discontinuous water-bearing zones (Baye et al., 2016). The findings of the Peace Project drilling program also highlight how heterogeneous and discontinuous Quaternary deposits are, as different lithologies were encountered at boreholes that were 5 m apart. Additionally, only two locations intercepted water-bearing units with high enough permeability to install monitoring wells, again suggesting discontinuous water-bearing zones, or, a deep water table. However, the primary objective of the Peace Project drilling was to confirm the interpretation of the TEM data, not locate water. Therefore, drilling targets were at the edges of valleys and not in the thalwegs, where encountering high-yield aquifers would be expected.

Although the deeper permeable deposits modelled by Petrel do not show a high degree of continuity at a regional scale, there are some locations that contain deposits of permeable material that are quite thick. Figure 4.17 shows an isopach map of the sand and coarse sand and gravel facies from the AV GR 1 model. Locations with thick deposits of permeable Quaternary fill are readily apparent.

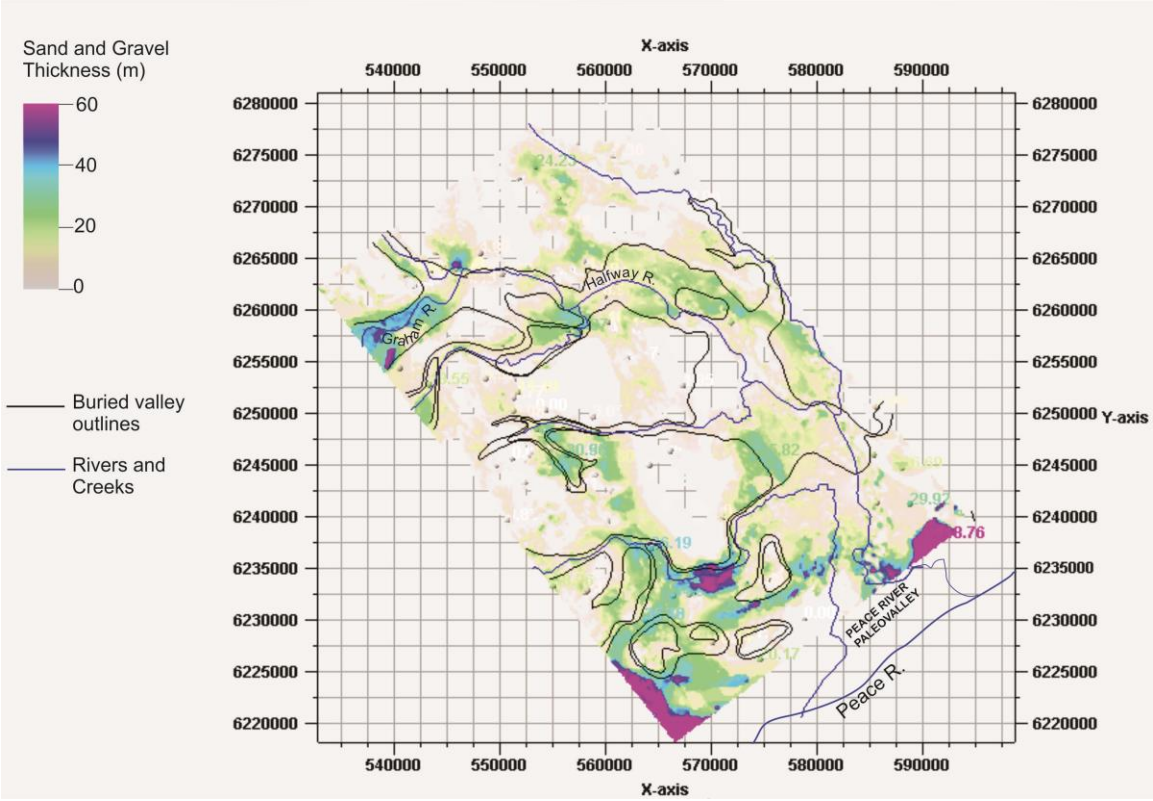

Figure 4.17. Isopach map of sand and coarse sand and gravel facies from the Assign Values Gamma-ray range 1 model generated in Petrel.

The isopach map shows that there are moderately thick continuous deposits, particularly along the Halfway River, and down in the south of the study area within the complex Peace River paleovalley (Levson in Petrel Robertson Consulting Ltd., 2015), towards the modern Peace River. The thickest sand and gravel deposits in the model area are somewhat isolated; one is within the northern narrow portion of the buried valley network (along the Graham River), and the rest are located in the south of the study area, within the thick Quaternary fill of the Peace River paleovalley. A well drilled into a deposit in this southern region during the Peace Project drilling program is located at the bottom left corner of the model (Well 10b; see Appendix A Table A6). The lithology encountered was a thick package of alternating silts and fine sands that were dry (described above in Section 4.3). It is unknown if these units are laterally extensive, but it was confirmed through drilling that the Quaternary deposits in this area are exceptionally thick as bedrock was not encountered (total well depth of 60 m). Another very thick deposit of sands present at the bottom right corner of the model may represent a paleotributary extending into the Peace River valley. Figure C7 shows that

this deposit is overlain by approximately 40 m of low-permeability clays/clay-rich tills (Glacial Lake Peace).

The isopach map can also help in identifying potential buried valleys that were not identified with the preliminary outline of the network (Levson in Petrel Robertson Consulting Ltd., 2015). Within the study area for this thesis, the buried valley outline was interpreted using somewhat limited data (only 199 oil and gas wells to identify Quaternary-bedrock contacts), and mainly follows the modern river valleys and creeks in the region. So it is possible that additional buried valleys exist that were not previously identified. Two potential areas with moderately thick permeable deposits were generated in Petrel: one extending northwards from Farrell Creek located at approximately 560000 m, 6240000 m (Figure 4.17); and, one extending northwards from the Halfway River at approximately 555000, 6265500 m (Figure 4.17). To suggest whether it is possible for these to be buried valleys, the DEM of the Peace Region and oil and gas wells in the areas were consulted. These two potential areas are in locations where although oil and gas wells are present, the gamma-ray logs do not extend up to surface; therefore it was only possible to determine a minimum depth to bedrock (see Petrel Robertson Consulting Ltd., 2015). Bedrock may be closer to surface, resulting in thinner Quaternary fill; however, this is unknown due to the missing shallow gamma-ray log intervals.

The surface topography over the potential paleovalley that extends from the Halfway River is a high ridge bounded to the east by the Cameron River and to the west by a minor creek. Therefore, it is unlikely that there is a buried valley here. The gamma-ray logs in this area also have variable minimum depth to bedrock picks ranging from 0 to 35 mbgs. The surface topography over the potential valley extending from Farrell Creek shows an alternating network of surface highs and lows, potentially representing old paleotributaries or paleochannels of Farrell Creek. While this suggests a buried valley in this location is more plausible, the gamma-ray logs in this area again have variable minimum depths to bedrock ranging from 0 to 39 mbgs. In both cases, the uncertainty associated with the gamma-ray logs results in an uncertain top of bedrock surface and therefore these areas of potential buried valleys were disregarded in further modelling. The bedrock surface, which defines the buried valleys, is challenging to model accurately, and therefore, the full extent of the paleovalleys remains uncertain.

The conceptual model of the buried valley network in the central Peace Region is that of a large network containing heterogeneous Quaternary material of variable thickness. Permeable deposits exist within these buried valleys, and thinner units show some degree of larger-scale connectivity at shallower depths. However, deep and/or thick permeable deposits tend to be isolated and show poor regional connectivity throughout the full study area. Although these results do not indicate that basal sands and gravels are present regionally throughout the area, their presence cannot be ruled out, particularly at smaller scales. Exposures of extensive sand and gravel deposits overlying bedrock have been observed at major river confluences north and south of the study area (e.g. Levson et al., 2006; Hartman and Clague, 2008).

The geological modelling conducted in this research relied heavily on the TEM data and supplemental borehole logs. These geophysical datasets have uncertainty associated with them due to averaging and inversion methods, and non-uniqueness of parameters being estimated (i.e. resistivity and gamma-ray response). Thus, it is questionable as to whether or not these buried valley aquifers do in fact contribute to regional flow. To more fully assess their potential hydraulic role in the regional flow regime of the central Peace Region, numerical models are required. The next chapter discusses the developed flow models, and investigates the role of buried valleys in the regional hydrogeologic regime of the area. The details of the export of the AV GR 1 Quaternary model and bedrock model from Petrel into MODFLOW are provided in Appendix D.

Chapter 5.

Investigating the Hydraulic Role of a Large Buried Valley Network on Regional Groundwater Flow

5.1. Introduction

Buried valleys are channel-form depressions, or paleovalleys, that have been infilled by sediment and buried following their formation (Cummings et al. 2012). Within these buried valleys, permeable material can form thick units that have the potential to store and transmit significant amounts of water, thus representing attractive targets for groundwater exploitation (Shaver and Pusc 1992, Andriashek 2000, Cummings et al. 2012, Oldenborger et al. 2013). Therefore, studying buried valleys and gaining an understanding of their internal hydrostratigraphic architecture, lateral extent, and continuity of the permeable units is crucial to managing groundwater resources (Hickin et al. 2016, Korus et al. 2017).

Buried valleys have been identified below glaciated terrains in North America and northern Europe, and several studies have explored the hydraulic role of buried valley aquifers through both field techniques (e.g. Troost and Curry 1991, Shaver and Pusc 1992, van der Kamp and Maathuis 2012) and numerical modelling (e.g. Shaver and Pusc 1992, Seifert et al. 2008, Seyoum and Eckstein 2014). Investigations into buried valley aquifers using numerical modelling have incorporated their three-dimensional hydrostratigraphic architecture and have explored the continuity of the permeable units within their fill, which are among the key factors that control the effect that buried valleys have on groundwater flow (Russell et al. 2004). These studies, however, tend to be localized (e.g. one buried valley). There has been limited investigation of the resource potential and hydraulic role of buried valley aquifers at a regional scale (Russell et al. 2004).

The objective of this study is to contribute to the knowledge of buried valley aquifer hydrogeology and explore the influence that buried valley aquifers have on regional groundwater flow. The study area is the central Peace Region of Northeast British Columbia (NEBC), where a large network of buried valleys has been identified

(Figure 5.1) (Levson in Petrel Robertson Consulting Ltd. 2015). In this study, a geological model of this buried valley network was created using the reservoir software, Petrel (Schlumberger 2016). This geological model was then used as a basis for developing two numerical models of the regional groundwater flow system; one with detailed geological complexity, and a simplified version. Because NEBC is a very data-sparse area, there were few hydraulic head data available for calibration. As such, a novel approach was used to estimate baseflow for model calibration. Notwithstanding, the models are interpretive in nature. Although interpretive models are uncalibrated (or only calibrated to a few measurements), they can still be used to conceptualize flow systems and investigate parameters and groundwater processes (Anderson et al. 2015). The two models were used to assess the water balance and the regional groundwater flow patterns and travel times within the buried valley network. Capture zones of potential abstraction wells completed in the buried valleys were also examined.

This study also extends the research conducted for Geoscience BC's Peace Project (e.g. Petrel Robertson Consulting Ltd. 2015, Aarhus Geophysics ApS 2016a-e, Bemex Consulting International and Quaternary Geosciences Inc. 2016, Levson and Best 2017a and b, Mykula 2017, Best and Levson 2017 unpublished report), which is aimed at contributing new information about the available groundwater resources in NEBC.

5.2. Study Area

The Peace Region is situated east of the Rocky Mountains and along the western edge of the Alberta Plateau (Figure 5.1) (Holland 1964). Within the central Peace Region, the terrain is generally low-relief with thick deposits of glacial drift (Levson 2008). The climate of the Peace Region is continental boreal and consists of long cold winters, and short warm summers. Throughout the year, average daily temperatures at Fort St. John (Climate Station ID: 1183000) range from 16 to -13°C, mean monthly precipitation ranges from 19 to 75 mm, and mean annual precipitation is 445 mm/year (Environment Canada 2017a). The Peace River is the major river in the Peace Region and drains an area of approximately 122,000 km^2 within BC; the Peace River extends into Alberta. There are several other rivers within the study area including the Halfway River, Cameron River, and Graham River (Figure 5.1), which together drain

approximately 9,260 km^2. There are also small creeks that are tributaries to these rivers including Farrell Creek, Groundbirch Creek, and Kobes Creek.

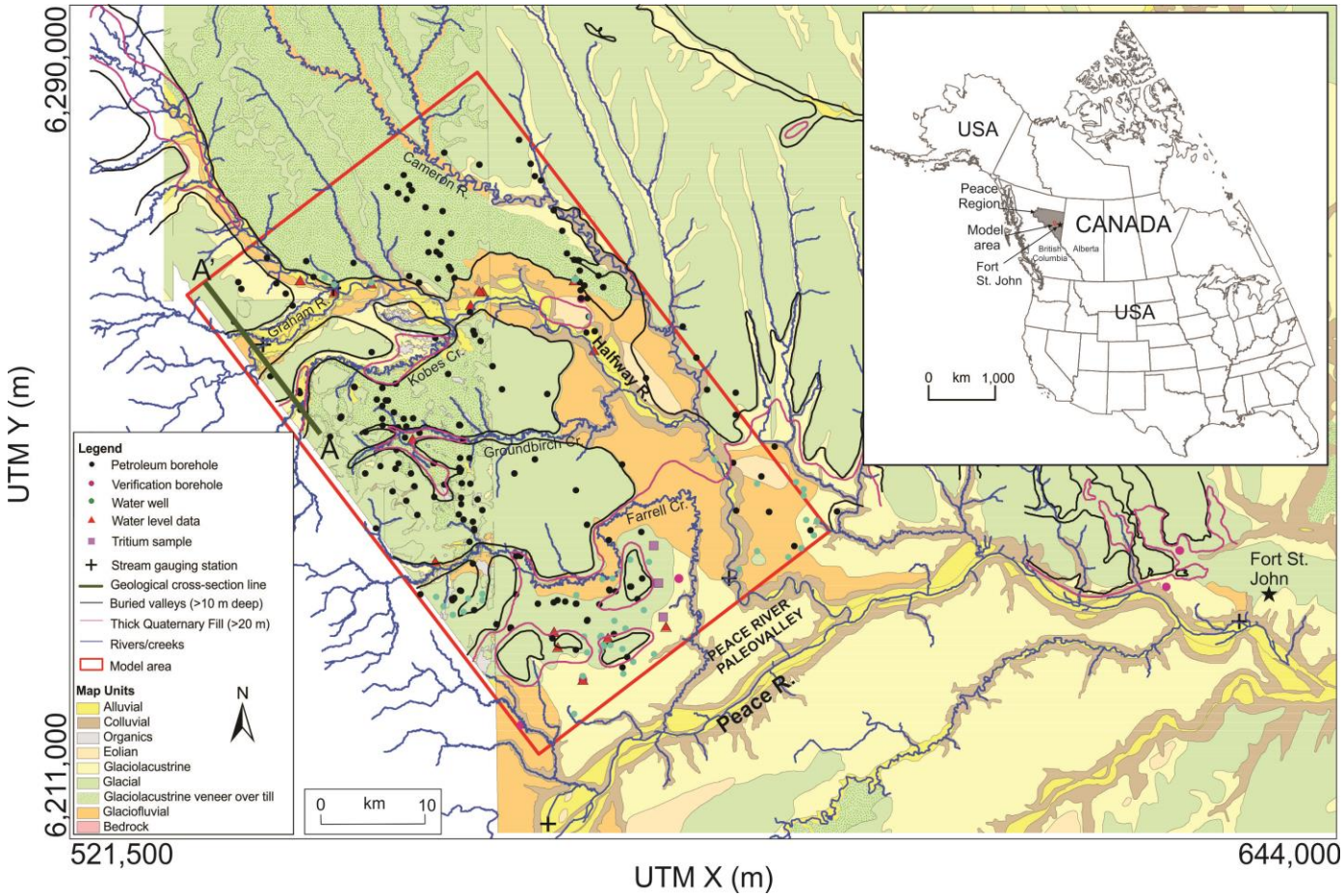

Figure 5.1. Surficial geology of the central Peace Region in Northeast BC. The model area outline is shown in red and the thick black lines represent outlines of buried valleys (generally >10 m deep). Green line A-A' shows the location of the cross-section in Figure 5.5. Locations of rivers/streams, gauging stations, water level and well data in the model area are shown. Inset map shows the outline of the Peace Region in British Columbia, the model area, and the location of Fort St. John. Modified from Levson in Petrel Roberston Consulting Ltd. (2015) with permission.

The bedrock strata underlying the Peace Region comprise Paleozoic to Tertiary age sedimentary rock overlying Precambrian basement (BC Ministry of Natural Gas Development 2011). Cretaceous sedimentary rocks outcrop at surface or directly underlie surficial sediments. They represent several marine transgression-regression-transgression cycles and are, for the most part, gently dipping towards the southwest (BC Ministry of Energy and Mines 2011). The marine shales and minor sandstones of the Fort Saint John Group, composed of the Lower Cretaceous Buckinghorse shales, Lower Cretaceous Sikanni sandstones, and Upper Cretaceous Sully shales, are overlain by the Upper Cretaceous Dunvegan sandstones (BC Ministry of Natural Gas Development 2011). A simplified stratigraphic section is shown in Figure 5.2.

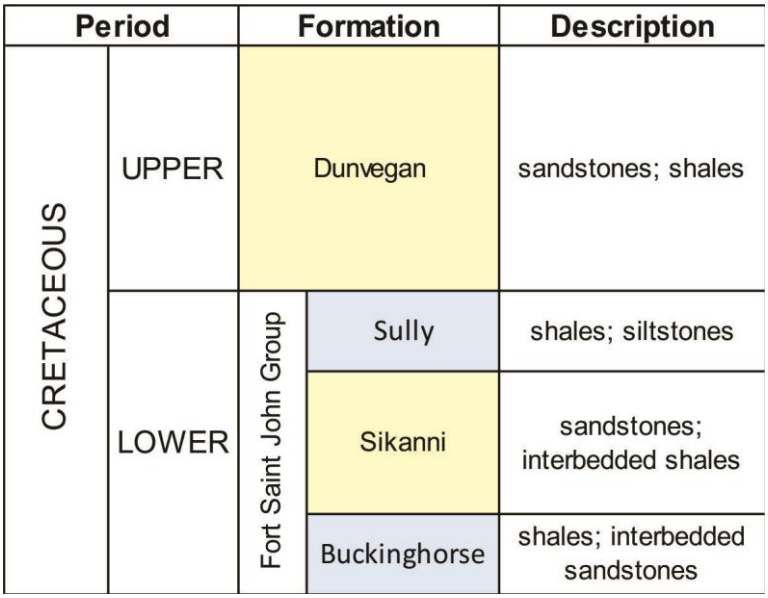

Figure 5.2. Simplified stratigraphy of the Cretaceous bedrock formations in the study area. Predominantly sandstone units are shown in yellow and predominantly shale units are shown in grey.

The Quaternary sediments of the Peace Region are lithologically heterogeneous due to several periods of the advance and retreat of both the Cordilleran and Laurentide ice sheets (Hartman 2005), and can range in thickness from <1 m to hundreds of meters (Hickin 2011). The surficial deposits left behind during these glacial periods are glaciolacustrine silts and clays, glaciofluvial sands and gravels, and till (Figure 5.1). Paleovalleys formed during both pre-glacial and glacial times were subsequently filled with this material, and glaciofluvial sand and gravel deposits within the valley fills may constitute productive aquifers (Lowen 2011). As this fill is more easily erodible than bedrock, the paleovalleys may have also been further eroded. Finally, these valleys

were buried during the Late Quaternary by processes such as aggradation. As a result, in many areas, these valleys have little to no surface expression due to thick accumulations of Quaternary sediments (Levson et al. 2006, Hickin et al. 2016).

Several studies have documented the existence of buried paleovalleys in the Peace Region (e.g. Mathews 1978, Levson et al. 2006, Hartman and Clague 2008, Lowen 2011, Hickin et al. 2016). Exposures along tributary valleys of large rivers, such as the Peace River (Figure 5.1), show large deposits of sands and gravels overlying bedrock (e.g. Hartman and Clague 2008), and thick and permeable deposits are expected at these confluences. It has been suggested that sand and gravel deposits within the valleys, such as basal deposits in the valley thalwegs, could potentially represent significant sources of groundwater (Cowen 1998). If these deposits are regionally connective, they may significantly affect the regional groundwater flow regime. However, glacial processes such as ice erosion may have isolated sand and gravel deposits, impacting the connectivity of the permeable paleovalley deposits. Moreover, the buried valley aquifers also need to be connected to a source of recharge in order to be a viable source of groundwater.

Water resources in this region support multiple users such as First Nations and local communities, agriculture and industry. The oil and gas sector, in particular, uses large quantities of water due to the recent increase in hydraulic fracturing in the area for shale gas development. The BC Oil and Gas Commission (BCOGC) is the regulator for the oil and gas industry in BC, and is responsible for water management. The Northeast Water Tool (NEWT; BCOGC 2017) is a GIS-based hydrological modelling tool used to support decision-making for short-term water use approvals and water licenses in the region. NEWT generates the monthly and annual runoff at any location in a watershed, and provides guidance on environmental flows and potential water availability (Chapman et al. 2012). As such, NEWT quantifies how much water is already allocated when new water license applications are submitted; however, it does not distinguish between surface water and groundwater. Currently, most of the water used for hydraulic fracturing in the region is surface water (e.g. rivers, streams, or lakes) or private acquisition and produced water (BCOGC 2015); however, increased development may increase the demand for groundwater stored in aquifers. Not only is there industrial interest in the potential for groundwater in buried valley aquifers, First Nations are also interested for their own land-planning use.

5.3. Materials and Methods

5.3.1. Geophysical Surveys

Buried valley geometry can be extremely complex (Oldenborger et al., 2014); therefore, high-resolution geophysical data are ideally suited for interpreting their architecture. This study incorporated the interpretations of data collected from two different geophysical techniques: airborne electromagnetic surveys and borehole gamma-ray logging. Additionally, seven boreholes were drilled to verify the geophysical data.

Airborne Electromagnetic Survey Data

As part of Geoscience BC's Peace Project, approximately 21,000 line-kilometers were flown with the SkyTEM system (Sørensen and Auken 2004) to collect airborne time-domain electromagnetic (TEM) data for the Peace Region. Airborne TEM surveys have proven to be efficient and accurate tools for hydrogeophysical investigations of buried valleys (e.g. Steuer et al. 2009, Høyer et al. 2011, Oldenborger et al. 2013). The TEM data were subject to one-dimensional (1-D) (SkyTEM Surveys ApS 2015) and three-dimensional (3-D) (Aarhus Geophysics ApS 2016a-e) inversions and were made available as interpreted horizontal subsurface resistivity slices (Figure 5.3a) and vertical resistivity cross-sections (Figure 5.3b). Generally, low resistivity is interpreted to represent fine-grained material such as clay or shale, or material containing saline water, whereas high resistivity is interpreted to represent coarse-grained material such as sand and gravel, or sandstone and conglomerate. The 3-D inverted TEM data for the study area were used to develop the geological model (see Section 5.3.2).

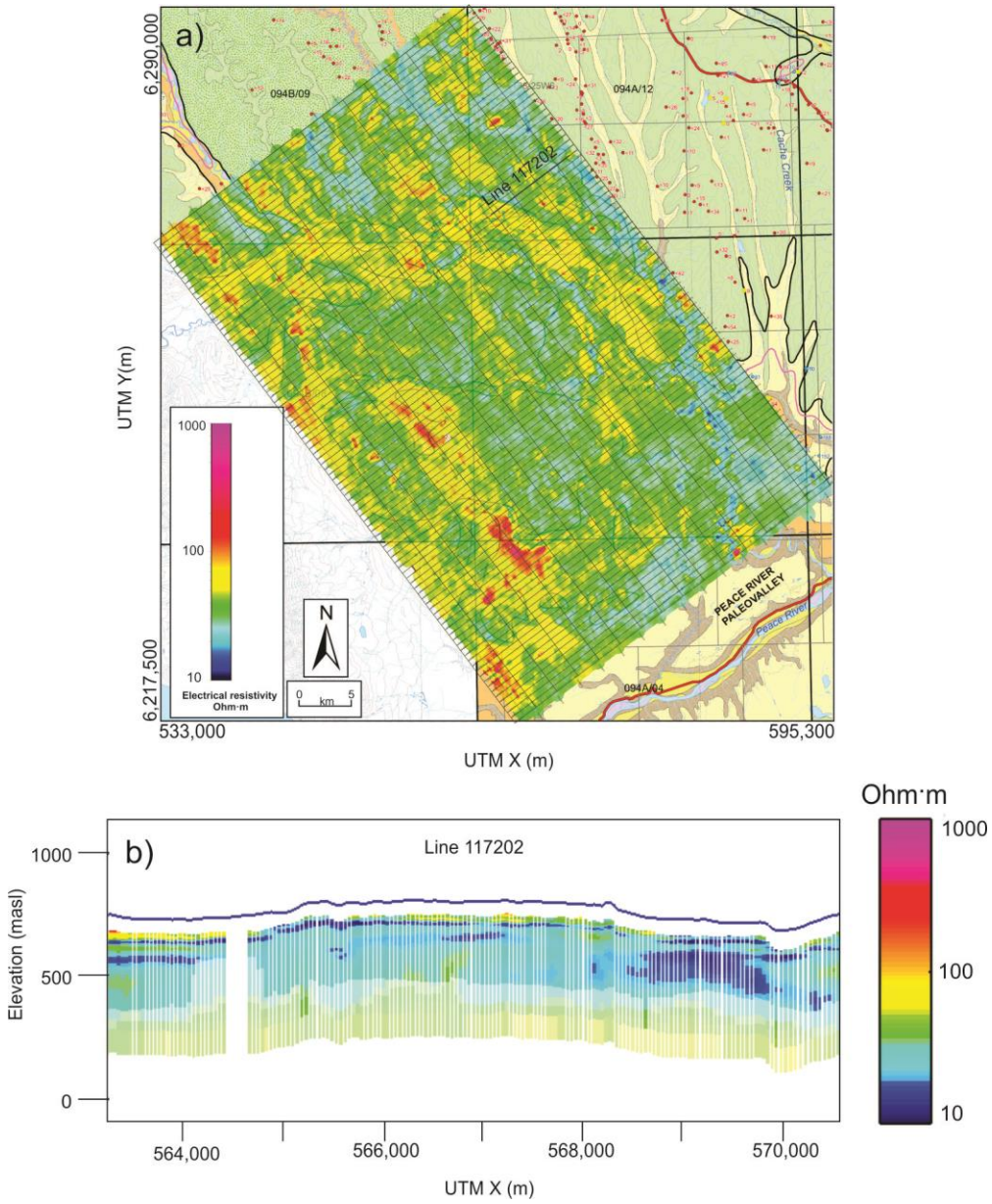

Figure 5.3. **Interpretation results of the 3-D inversion of TEM data collected from the SkyTEM survey for the Peace Main Phase 1 sub-area (coinciding with the study area for this study) of Geoscience BC's Peace Project derived from spatially constrained inversion. For the results in other areas of the Peace Project, refer to Aarhus Geophysics ApS (2016a-e). a) Example of a horizontal subsurface resistivity slice showing the resistivity distribution from 5 to 10 m below ground surface. Flight lines and section line for b) are shown. b) Example of a vertical resistivity section showing resistivity distribution along flight line 117202. Modified from Aarhus Geophysics ApS (2016d) with permission.**

Corrected Gamma-ray Logs

Gamma-ray logs are commonly used to determine subsurface lithology and identify stratigraphic picks between formations. Since 2010, all oil and gas wells in BC must be logged from surface (BCOGC 2010); however, the steel surface casing surrounding the well mutes the gamma-ray response from the formation, reducing the amplitude and variance of the data, and lowering the overall gamma-ray response (Quartero et al. 2014). While surface casing provides wellbore stability and protects shallow groundwater from surface contamination, the attenuation caused by the casing is problematic for geological interpretation.

As part of Geoscience BC's Peace project, the gamma-ray logs from 199 wells in the study area (see Figure 5.1) were corrected for the attenuation caused by the surface casing using the statistical correction technique developed by Quartero et al. (2014) (Petrel Robertson Consulting Ltd. 2015). This technique allows the cased and non-cased log intervals to be merged into one continuous gamma-ray curve for stratigraphic correlation. All available gamma-ray logs in the study area were used to constrain the geological modelling (see Section 5.3.2).

Verification Boreholes

Seven locations were selected to drill boreholes within the study area to verify the geophysical surveys (see Figure 5.1 for locations). The boreholes were drilled with a sonic rig, in which the drill bit vibrates up and down in addition to being pushed downwards, which allows for excellent core recovery compared to conventional rotary drilling. Core was collected and logged along the entire length of the borehole. The boreholes were completed with solid PVC pipe and backfilled with cement grout to enable geophysical logging (gamma-ray, resistivity, dipole sonic, neutron-porosity, and density-porosity). At two locations, a high-permeability water-bearing unit was intersected. The drill rig was moved less than 5 m away, and a new borehole was drilled to that particular depth. The borehole was then screened using slotted PVC pipe over the defined interval of the aquifer. Sediment samples were collected from the cores from the depth interval corresponding to the screened interval, and from other locations of coarse-grained units (i.e. sand), for grain size analysis to derive hydraulic conductivity estimates.

5.3.2. Geological Modelling

The reservoir software, Petrel (Schlumberger 2016), was used to design a 3-D geological model of the buried valley network (see Figure 5.1 for model outline), using a novel workflow for integrating these types of data in Petrel. The vertical extent of the geological model is from ground surface down to approximately 200 meters below the top of bedrock, below which there is likely limited groundwater flow. The model was created in two separate phases: a bedrock model and a Quaternary model.

Bedrock Model

The available corrected gamma-ray logs and supplemental water well lithology logs (WELLS database, BC Ministry of Environment 2017) were used to determine the outline of the buried valley network and Quaternary-bedrock contacts (Petrel Robertson Consulting Ltd. 2015), and to identify additional contacts between bedrock formations. The gamma-ray logs were imported into Petrel. The stratigraphic picks of the Quaternary-bedrock contact and contacts between bedrock formations were imported as well tops, which were used in a convergent interpolation algorithm to create surfaces representing the top of bedrock as well as top of Dunvegan, Sully, Sikanni, and Buckinghorse Formations (see Figure 5.2). In Petrel, surfaces can be specified as Erosional, Conformable, Discontinuous or Base. Since the top of the bedrock surface was created to show the Quaternary-bedrock contact and does not relate to a specific bedrock formation, it was set as Discontinuous. This means the surface is erosional, such that surfaces below will be truncated; however, surfaces above (i.e. Quaternary material) will lap onto it. The formation surfaces were set as Conformable, and a Base surface representing 200 m below the top of Buckinghorse was generated. The bedrock surfaces were then used as input in generating a 3-D grid of the bedrock, and each cell of the grid was populated with a code for the respective bedrock formation in between surfaces.

Quaternary Model

The horizontal resistivity slices (Aarhus Geophysics ApS 2016d) were the main dataset used to model the Quaternary sediments. The resistivity depth slices (i.e. maps of resistivity distribution at various depth intervals) were recreated in Petrel by digitizing them in ArcGIS, relating resistivity values to geological material type according to Table

5.1. These digitized resistivity slices were then converted to ASCII text files and imported into Petrel.

Table 5.1. Resistivity values for different geologic materials. Modified from Bemex Consulting International and Quaternary Geosciences Inc. (2016).

Geologic Material	Resistivity (ohm·m)
Clay/clay-till	<15
Till/silt/fine sand	15-50
Sand	50-100
Coarse sand and gravel	>100

A 3-D grid of the Quaternary was created using a digital elevation model (DEM) of the Peace Region (USGS 2014) and the top of bedrock surface. A deterministic facies modelling algorithm, specifically the 'Assign Values' algorithm in Petrel, was then used to populate each of the grid cells with a distinct facies (a stochastic algorithm was also used, but produced unfavourable results; that model was not carried further). The digitized resistivity surfaces were the main input, but were supplemented by facies logs derived from the corrected gamma-ray logs, water well lithology logs, and borehole logs from the Peace Project drilling. Four discrete facies were modelled: clay/clay-till, till/silt/fine sand, sand, and coarse sand and gravel. Figure 5.4 shows the resulting facies map for 5 to 10 m below ground surface in the geological model, and Figure 5.5 shows a cross-section from the geological model compared to a vertical resistivity section along a flight line in approximately the same location and orientation (see Figure 5.1 for location).

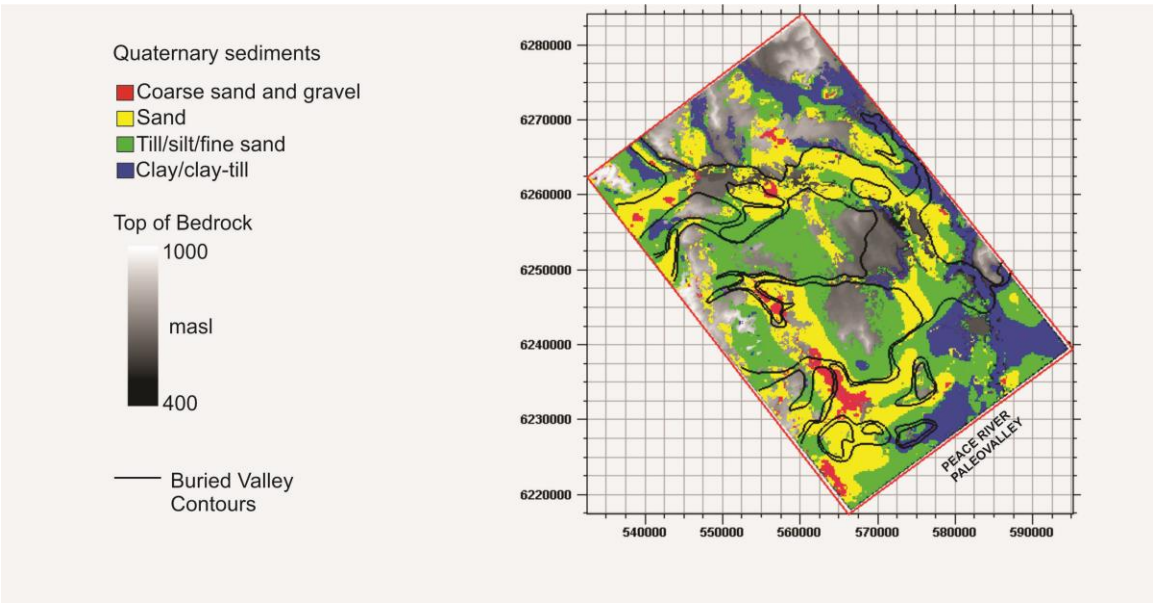

Figure 5.4. **Plan view map of facies distribution from 5 to 10 m below ground surface using the 'Assign Values' deterministic facies modelling algorithm in Petrel. The outline of the buried valley network is shown (Levson in Petrel Robertson Consulting Ltd. 2015) as well as the generated top of bedrock surface in m above sea level.**

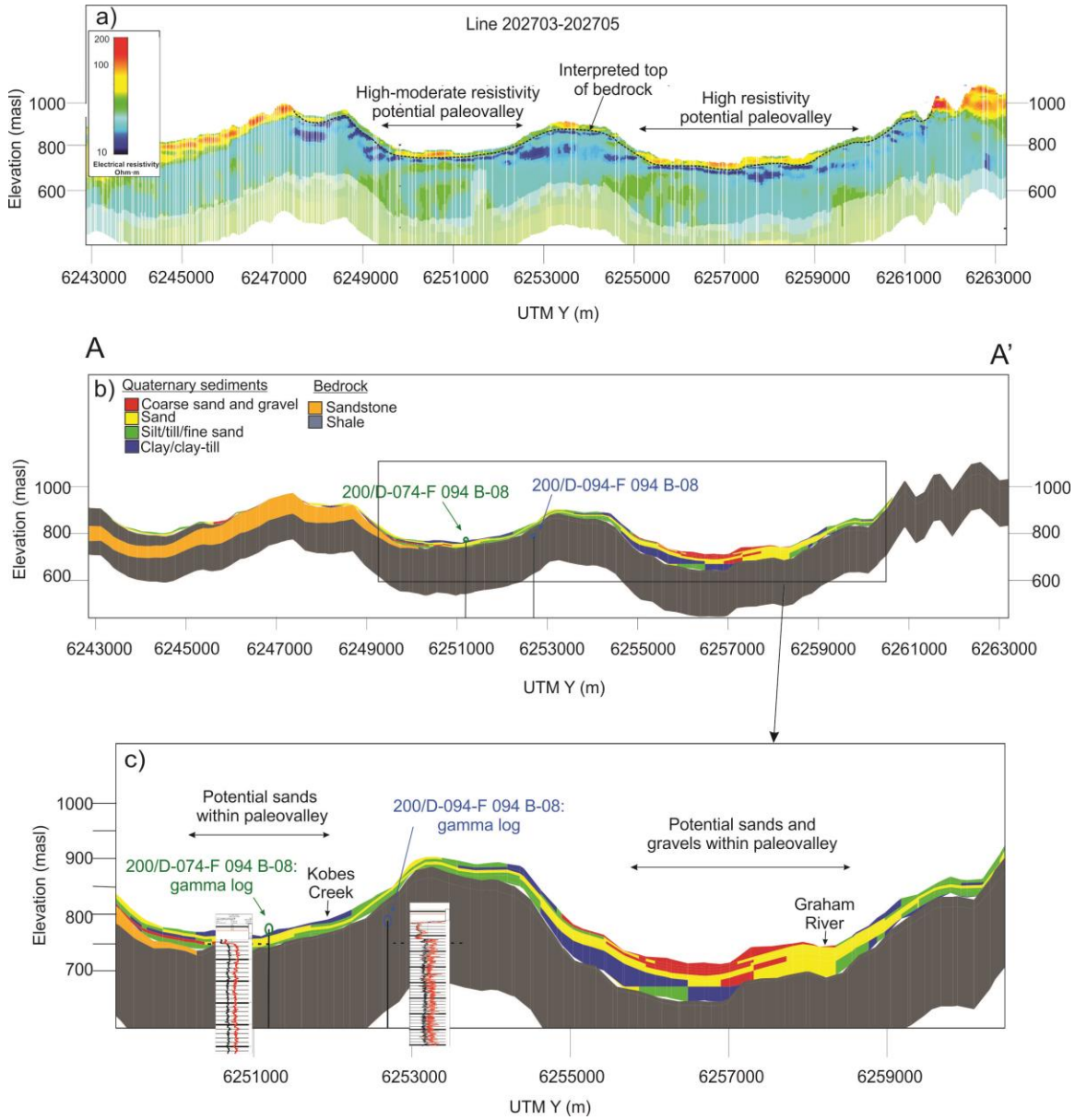

Figure 5.5. Results of the geological modelling in Petrel compared to the resistivity data. See Figure 5.1 for cross-section location. a) Resistivity section from flight lines 202703-202705. Modified from Aarhus Geophysics ApS (2016d) with permission. b) A-A'cross-section from geological model developed using the 'Assign Values' deterministic facies modelling algorithm in Petrel. c) Zoom-in of b).

5.3.3. Groundwater Flow Modelling

Two interpretive steady-state numerical flow models were constructed using MODFLOW (Harbaugh 2005): one detailed and one simplified. The same grid design and boundary conditions were used for consistency (Figure 5.7). The detailed model

captures the full complexity of the geological model as described below. The simplified model is a generic model of a large buried valley network in which large bedrock valleys are filled with thick deposits of till, overlying continuous sand and gravel deposits in the valley thalwegs at the Quaternary-bedrock contact.

The active model domain is approximately 2,000 km^2 (36 km x 56 km) and is oriented in a northwest-southeast direction to correspond to the location of the SkyTEM survey flight lines (Figure 5.3). As such, the length of the model domain is not oriented parallel to the likely regional groundwater flow direction (presumed to be southeast towards the Peace River following the main drainage features). Accordingly, the corners of the domain were assigned as inactive. The models were discretized to a uniform cell size of 200 m x 200 m, for a total of 2,014,320 cells, of which 981,240 are active. The vertical extent is from ground surface (Peace Region DEM: USGS 2014) down to approximately 200 m below the top of bedrock, below which, as stated above, there is likely limited groundwater flow. Both models have 20 layers, and the bottom elevations for each layer were determined using geometric progression within Matlab (refer to Appendix D for details).

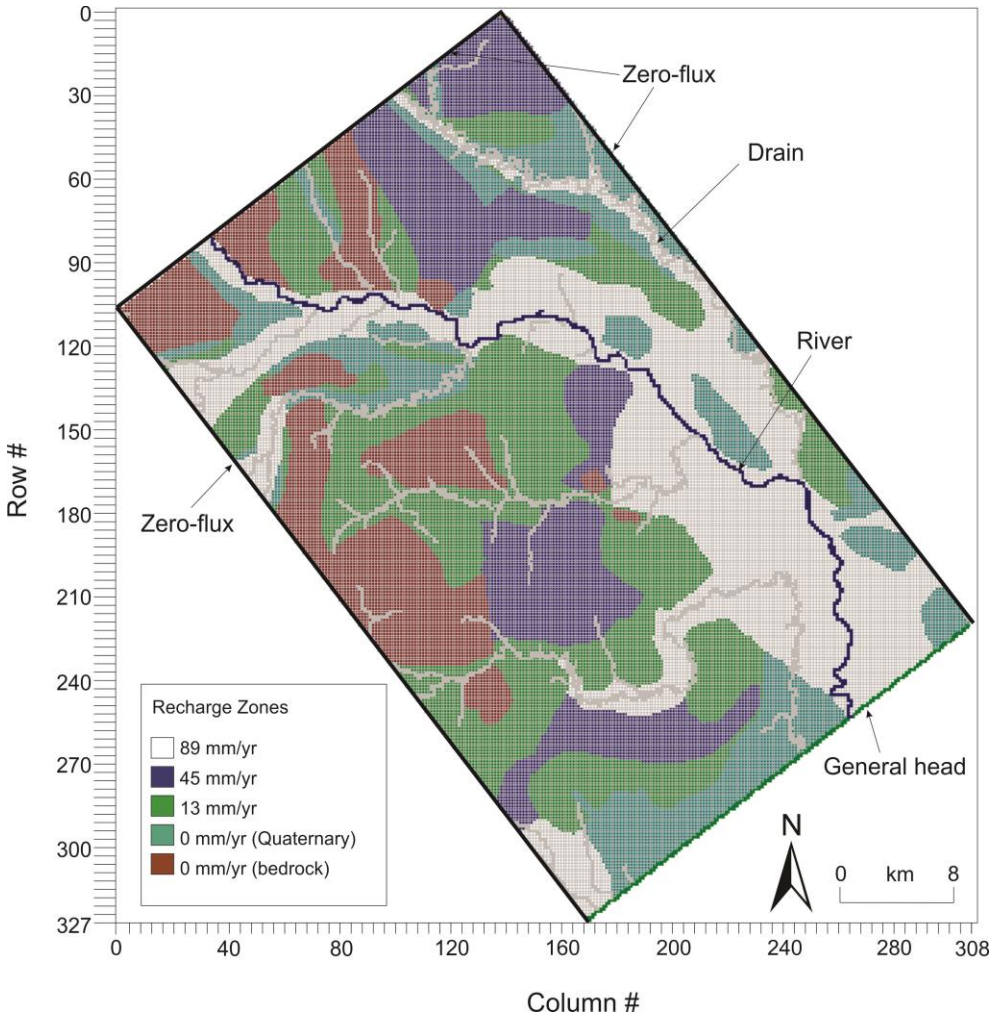

Figure 5.6. The model domain showing all boundary conditions as viewed from the top layer. Model domain boundary conditions (zero-flux and general head) were applied to all layers. Drain boundaries were applied only to layer 1. Due to the input values for riverbed bottom and thickness, some cells in layers 2 and 3 were also assigned river boundaries. Recharge zones were applied to the uppermost active layer.

Detailed Model: K Distribution

The geological model was exported from Petrel and imported into MODFLOW using a custom Matlab script. Any inconsistencies or artifacts identified during the import process were manually adjusted in MODFLOW.

Four different Quaternary facies (clay/clay-till, till/silt/fine sand, sand, and coarse sand and gravel) and two different bedrock lithologies (sandstone and shale) were modelled, resulting in six hydraulic conductivity (K) zones. The Dunvegan and Sikanni Formations were grouped as sandstone aquifers and the Sully and Buckinghorse shales

were grouped as shale aquitards for simplicity. K estimates were derived from a combination of grain size analyses on sediment samples taken during the Peace Project drilling (see Appendix A), estimates reported in consulting reports (BGC Engineering Inc. and Hemmera Envirochem Inc. 2012), and literature values (Freeze and Cherry 1979). K estimates reported in Baye et al. (2016) for the Kaskapau shale formation were not used as they were not within the literature range, and were thus deemed too high to represent shale in this regional numerical modelling. The values and range of uncertainty (i.e. based on ranges reported in the literature) are shown in Table 5.2.

Table 5.2. Hydraulic conductivity values for the six different geological material types modelled in this study. Literature ranges from Freeze and Cherry (1979) provide a range of uncertainty.

Geological Material	Model K_x	Model K_y	Model K_z	Literature Range[a]	
				Min	Max
	(m/s)	(m/s)	(m/s)	(m/s)	(m/s)
Coarse sand and gravel[bd]	$3x10^{-3}$	$3x10^{-3}$	$1x10^{-3}$	10^{-3}	1
Sand[bd]	$5x10^{-5}$	$5x10^{-5}$	$1x10^{-5}$	10^{-6}	10^{-2}
Till/silt/fine sand[c]	$4x10^{-7}$	$4x10^{-7}$	$2x10^{-8}$	10^{-10}	10^{-5}
Clay/clay-till[d]	$1x10^{-8}$	$1x10^{-8}$	$1x10^{-10}$	10^{-12}	10^{-7}
Sandstone[c]	$1x10^{-5}$	$1x10^{-5}$	$1x10^{-6}$	10^{-10}	10^{-5}
Shale[c]	$7.7x10^{-10}$	$7.7x10^{-10}$	$7.7x10^{-12}$	10^{-13}	10^{-9}

[a] Freeze and Cherry (1979)
[b] K estimated from grain size analysis (see Appendix A)
[c] K estimated from BGC Engineering Inc. and Hemmera Envirochem Inc. (2012)
[d] K estimated from literature values from Freeze and Cherry (1979)

The output from Petrel is a distribution of geological facies for different depth slices. Therefore, the model layers do not coincide with specific K zones. Rather each model layer has a distribution of K zones.

Simplified Model: K Distribution

The K distribution of the simplified model was as follows: layers 1-3 reflect the surficial geology map by Levson in Petrel Roberston Consulting Ltd. (2015); cells in layers 4-6 within the buried valley outline were assigned till/silt/fine sand, and cells at the confluences of rivers and major creeks were assigned coarse sand and gravel to facilitate recharge to the basal sands and gravels, and all other cells outside the buried valley network were assigned sandstone; cells in layers 7-10 within valley thalwegs were assigned coarse sand and gravel, and all other cells assigned sandstone; all cells for

layers 10-14 were assigned sandstone, and; all cells for layers 14-20 were assigned shale.

Boundary Conditions

The physical extent of the model resulted in boundary conditions being somewhat challenging to assign because the model domain is constrained to the area where the SkyTEM survey was undertaken (see Figure 5.3). Boundary conditions were based largely on generalizations of the regional flow system due to the limited hydraulic head data in the study area. Figure 5.6 shows the distribution of the various boundary conditions. A description of each is provided below.

The lateral boundaries of the model were assigned zero-flux boundaries due to the likely regional southeast groundwater flow direction towards the Peace River. The northern boundary of the model was also assigned as zero-flux. As such, it is assumed that there is no regional groundwater flow entering the domain from the northwest; the only source of water to the model is recharge and river leakage. As shown in Figure 5.1, this boundary intersects the mapped paleovalley outline, so there is likely to be some flux across this boundary; however, this flux is not known. The bottom of the model (200 m below top of bedrock) was also assigned zero-flux.

The southern boundary of the model domain was assigned a general head boundary to account for the influence of the Peace River on the model. This boundary condition requires an input of the boundary head, distance from the boundary to the river, and the average K of the material between the boundary and the river. Stage measurements from Environment Canada stream gauging stations (Environment Canada 2017c and 2017f) and the DEM of the Peace Region were used to estimate an average water level of the river for the boundary of 441 meters above sea level. The distance from the boundary to the river was determined using the measure tool in ArcGIS, and the boundary was applied in segments to account for the variable distance from the model domain to the Peace River. To facilitate flow to the Peace River, a K value of 1×10^{-5} m/s was initially used for all layers. However, during model calibration it was necessary to reduce this K value for layers 14 through 20 (the bedrock layers) to 1×10^{-7} m/s.

As can be seen in Figure 5.1, there are several surface water features in the model domain. A shapefile of all rivers and creeks was obtained from iMap BC (the provincial GIS and data warehouse), and imported into MODFLOW. The Halfway River was modelled as a head-dependant river boundary, with a riverbed thickness of 1 m, riverbed bottom of 2 m below ground surface, and river stage 1 m above the river bottom. For simplicity during calibration, two initial riverbed K_z values were assigned. With the exception of river cells at major confluences, all river cells were assigned a conductance value of 1.7×10^3 m^2/day (corresponding to a sandy-silt K_z value of 5×10^{-7} m/s). Those cells at confluences of the Halfway River with other rivers and creeks were assigned a conductance of 3.5×10^5 m^2/day (corresponding to a K_z value of 1×10^{-4} m/s), due to the assumption that these confluences have thick accumulations of fluvial sands and gravels, allowing for more exchange. All other rivers and creeks were modelled as head-dependant drain boundaries, with a drain elevation of 1 m below ground surface. Drain conductance values were based on the underlying surficial material identified from the surficial geology map by Levson in Petrel Robertson Consulting Ltd. (2015). Rivers and creeks flowing over mapped glaciolacustrine deposits and till were assigned 3.5×10^2 m^2/day (corresponding to a K value of 1×10^{-7} m/s). Those flowing over mapped fluvial deposits were assigned 3.5×10^5 m^2/day. Conductance values were varied during the sensitivity analysis.

Recharge varies spatially and is dependent on precipitation, evapotranspiration, geological material type, and depth to water table (Holding and Allen 2015). Mean annual recharge for the study area is estimated to range from 0-32% of mean annual precipitation (Holding and Allen 2015). For this study, recharge rates within this range were tested and applied to the uppermost active layer of the models. Recharge was distributed in different zones based on the K distribution of the near-surface layers, with the assumption that there is limited recharge to clays and till, but high recharge to permeable fluvial material and sandstone bedrock. The map of recharge zones and associated recharge values is shown in Figure 5.6.

Model Calibration

Calibration was performed on the detailed model using a trial and error process in which model parameters (i.e. K, conductance values, and recharge rates) were altered within the range of uncertainty. As the simplified model is a very homogenized

distribution of K, it was not calibrated and thus is just used for comparison of the hydraulic head distribution and particle tracking simulations.

There are no long-term monitoring wells in the study area that provide a hydraulic head record that can be used for calibration. Within the model domain, there are only 20 wells with water level data available (Table E1 in Appendix E). These data are from driller's reports from the BC WELLS database (BC Ministry of Environment 2017) and represent static water level at the end of drilling, and thus may not represent equilibrium conditions. These reports also span over approximately 40 years (1980-2017), and drilling likely occurred at different times of the year (seasonally).

For this study, the statistical measure used in assessing the error in model-calculated heads was the normalized root mean square error (RMSE). The RMSE gives the standard deviation of the model prediction error, and through normalizing the value the error is given as a percentage. Normalizing RMSE also allows for the comparison of models with different scales. Typically, the target for RMSE is less than 5%. However, due to the limited and potentially unreliable water level measurements in the model domain, the RMSE achieved through calibration of the detailed model was 27%. Considering all 20 wells, the model both over and under-calculates hydraulic head, slightly favoring under-calculating hydraulic head especially at the southern end of the model in deeper layers. This may be due to the assignment of the general head boundary condition at the southern boundary drawing water out of the model laterally. In reality, the water table has a steep gradient leading into the Peace River valley, with bedrock outcropping above the river level. Therefore, this outflow is likely a seepage face, which was not able to be reproduced in this model.

Streamflow data, specifically estimates of baseflow, were also used for model calibration. The approach for estimating the baseflow follows Beck et al. (2013). The authors estimated baseflow indices (BFI) by modelling numerous heterogeneous catchments worldwide. The BFI is the ratio of long-term mean baseflow to total discharge, based on climatic and physiographic characteristics of the catchment. As the BFI includes both baseflow and interflow (e.g. streamflow originating from channel bank storage, wetlands), it provides an upper bound of the baseflow component. Based on the climate and physiography of the Peace Region (cold, no dry season), the median BFI for the region is estimated to be 74% of discharge (Beck et al. 2013). The lower bound for

the baseflow component was estimated as the median of annual minimum daily discharge, following the methodology of Sonnenborg et al. (2003) and Seifert et al. (2008). Hydrometric data from five gauging stations in the vicinity of the study area (see Figure 5.1 for locations) were obtained from Environment Canada (Environment Canada 2017b-f). The average median of annual minimum daily discharge was determined to be 20% of mean annual discharge (MAD).

In the absence of streamflow data within the model area, the Northeast Water Tool (NEWT) was used to estimate the baseflow for calibration. To quantify the potential uncertainty with estimates from NEWT, MAD values from NEWT were compared to MAD values from the five gauging stations shown in Figure 5.1. The associated error was determined to be ± 3.5%. NEWT was used to determine the MAD for all rivers and creeks within the model area by generating MAD estimates and hydrographs for the locations where the river or creek both enters and leaves the model domain (NEWT Inflow and Outflow in Table 5.3). With these two values, the component of MAD corresponding only to the model domain could be determined (NEWT Model Domain in Table 5.3). To estimate the amount of baseflow for each river or creek within the model domain, the rivers and creeks were all assigned a unique zone in Zone Budget, and the upper and lower bounds of 74% and 20%, respectively, were applied to the MAD estimates from NEWT. This produced a range for baseflow (± 3.5%) for calibration. These ranges and the baseflow results for all rivers and creeks are provided in Table 5.3.

Table 5.3. Baseflow estimates from rivers and creeks in model derived using the Northeast Water Tool (NEWT) and Zone Budget. MAD refers to mean annual discharge.

River/Creek	NEWT Inflow (m^3/s)	NEWT Outflow (m^3/s)	NEWT Model Domain MAD (m^3/s)	NEWT Model Domain MAD (m^3/d)	Lower Bound (20% of MAD) m^3/d	Upper Bound (74% of MAD) m^3/d	Model Simulated Baseflow (m^3/d)	% of MAD
Halfway River	35	75	40	3,416,256	683,251	2,528,029	1,005,700	29
Graham River	26	27	1	84,672	16,934	62,657	30,779	36
Cameron River	5	7	2	173,664	34,733	128,511	73,061	42
Groundbirch Creek	Full watershed within model			137,000	27,400	101,380	51,575	38
Kobes Creek	1	2	0	35,424	7,085	26,214	13,242	37
Farrell Creek	1	3	2	173,664	34,733	128,511	69,542	40

Sensitivity Analysis

A sensitivity analysis of conductance values, recharge rates, and K values of the permeable sands and gravels suggested that the model is most sensitive to conductance values and K values. As one could expect, lowering the conductance values significantly reduces the outputs to the river and drain boundaries; much lower than the 20% of MAD lower bound of baseflow ranges. Increasing the conductance values significantly increases the outputs to greater than 74% of MAD. However, varying the conductance values only has a slight impact on the RMSE.

Higher rates of recharge resulted in a decrease in RMSE and a slight increase in baseflow outflows of the rivers and drains; however, the hydraulic head in some areas of the model was too high, with some areas of the model flooding. Lower recharge rates resulted in an increase to the RMSE and a slight decrease in baseflows. Increasing the K value of the gravel and sand units resulted in a slight increase in RMSE; however, baseflows significantly increased to as much as 87% of MAD. Conversely, decreasing the hydraulic conductivity of the gravel and sands resulted in a decrease in RMSE, but baseflows decreased to as low as 15% of MAD.

5.4. Results

5.4.1. Hydraulic Head Distribution

The hydraulic head distribution is fairly similar throughout all layers in both models. The simulated head distribution for layer 7 of the detailed model is shown in Figure 5.7a. Regionally, groundwater flows east-southeast, discharging to the Halfway River and the Peace River to the south (i.e. the general head boundary). Areas of high hydraulic heads with steeper gradients coincide with areas of higher topography and areas where shale bedrock is close to surface, and lower values of head with lower gradients occur within the large mapped paleovalley of the Halfway River, and along the river itself.

The hydraulic head distribution for the simplified model is shown in Figure 5.7b. Overall, there is a similar trend in groundwater levels as in the detailed model (Figure 5.7a), but with smoother, somewhat reduced gradients. The similarities in head distributions between the two models suggest that neither conceptualization (simplified or detailed) can be ruled out. This introduces the issue of equifinality (model non-uniqueness), a problem commonly encountered in flow modelling (e.g. Harrar et al. 2003, Troldborg et al. 2007, Seifert et al. 2008), that requires further simulations such as particle tracking and groundwater age dating to identify the most appropriate model.

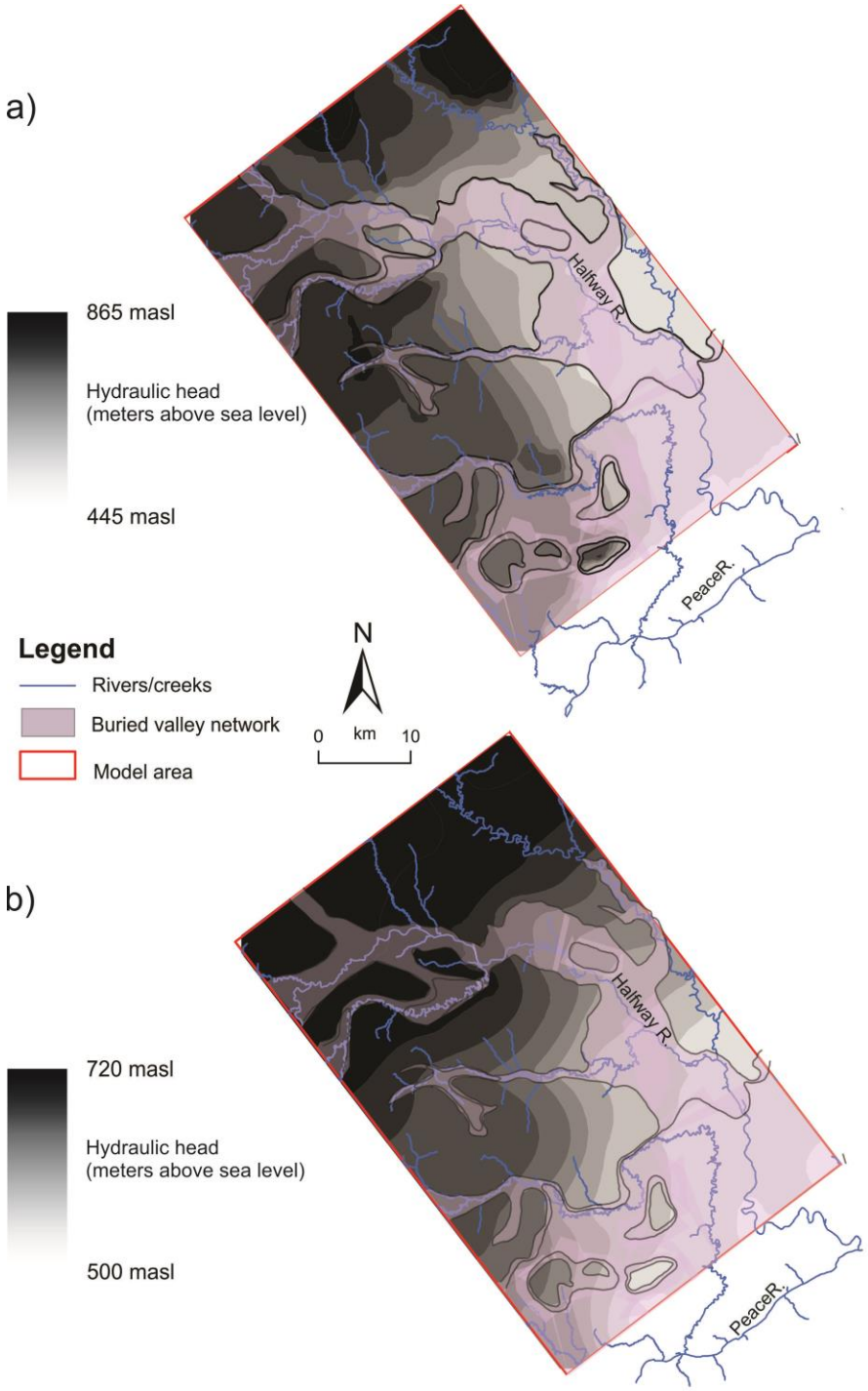

Figure 5.7. Distribution of hydraulic head for layer 7. The outline of the buried valley network (Levson in Petrel Robertson Consulting Ltd. 2015) is shown. a) Detailed model. b) Simplified model. Note different scales for hydraulic head.

5.4.2. Water Balance

The water balance for the detailed model is presented in Table 5.4. The largest component of the water balance is river leakage, followed by recharge, drains, and the general head boundary. River leakage (along the Halfway River) accounts for almost all of the inflow to and outflow from the model. While this seems unrealistic, in reality, the Halfway River may be fed by deep groundwater entering from the north through a narrow mapped paleovalley (see Figure 5.1). But this boundary was assigned as zero-flux in the model, so all of the baseflow to the Halfway River must derive from the model domain. Given the narrow width of the mapped paleovalley, it is unlikely that any appreciable amount of groundwater flow derives from outside the domain. There may also be regional-scale flow in the bedrock entering the model that is not accounted for. Nevertheless, these potential fluxes are unknown and thus could not be modelled.

The water balance for the simplified model is also shown in Table 5.4. Inflow and outflow rates for the drain and river boundaries are higher in the simplified model; however, because more water is being removed by the drains, and recharge rates are the same between the two models, river leakage accounts for even more of total inflow in the simplified model. The higher rates are attributed to the change in K distribution, as water is able to more easily recharge and move through the simplified model due to the greater continuity of units.

The Zone Budget tool within MODFLOW was used to compare the flow within the buried valleys to flow in the bedrock. Grid cells with K values representing Quaternary material were designated as ‘Quaternary’ and those with K values representing bedrock were designated ‘bedrock’. The Quaternary zone was then further divided into “shallow Quaternary” (layers 1-3) and “buried valley sediments”. The results of the Zone Budget analysis for the detailed model indicate that 63% of the flow is within the shallow Quaternary, 28% within the buried valleys, and 8% within the bedrock. For the simplified model, the assigned zones were: shallow Quaternary (layers 1-3), buried valley sediments, and bedrock. The results of the Zone Budget analysis indicate that for the simplified model, 68% of the flow is within the shallow Quaternary, 17% of the flow is within the buried valleys, and 14% of the flow is within the bedrock. This is likely due to the higher proportion of shallow permeable material and sandstone bedrock in the simplified model.

Table 5.4. Water balance for the detailed and simplified models.

	Inflow (m^3/day)	Outflow (m^3/day)	Inflow (%)	Outflow (%)
Detailed Model				
River leakage (Halfway River)	433,049	535,934	70	86
Drains (all other rivers/creeks)	0	75,906	0	12
Recharge	189,514	0	30	0
General head boundary	0	10,991	0	2
Total flow	622,563	622,831		
In flow-Out flow	-268			
% error	-0.043			
Simplified Model				
River leakage (Halfway River)	1,016,318	1,005,297	85	84
Drains (all other rivers/creeks)	0	165,906	0	14
Recharge	181,360		15	0
General head boundary	0	26,034	0	2
Total flow	1,197,678	1,197,237		
In flow-Out flow	441			
% error	0.037			

5.4.3. Particle Tracking

The locations of recharge and discharge areas within the buried valley network were investigated using MODPATH (Pollock 1989) for both the detailed model and simplified model. Table 5.5 lists the effective porosity values used for each geologic material type. These values were estimated from the literature (Morris and Johnson 1967).

Table 5.5. Effective porosity values used for Particle Tracking. Estimated from the literature (Morris and Johnson 1967).

Geologic Material	Effective Porosity (%)
Coarse sand and gravel	30
Sand	30
Till/silt/fine sand	20
Clay/clay-till	10
Sandstone	25
Shale	10

Lines of 100 particles were added to both models and forward-tracked to identify discharge locations. The lines were placed in a shallow (layer 1) and intermediate (layer 6) layer to observe where recharge from precipitation infiltration, or potential flow within the buried valleys, would travel within 100 years. The particles were placed in the northwest corner of the model, near the Graham River, and in the east-northeast area of the model near the Halfway River, within deposits of permeable material. In the detailed model, the particles released near the Graham River travel through the shallow Quaternary and deposits within the buried valleys, and discharge at the confluence of the Graham and Halfway Rivers (Figure 5.8). The particles released along the Halfway River, however, mostly travel through a thick deposit of permeable material adjacent to the river (shallow Quaternary and buried valley deposits) down to the confluence of the Halfway and Cameron Rivers, a distance of approximately 20 km. Although it appears that these pathlines are outside of the buried valley network, the results from the geological modelling suggest that the network outline in this location should be extended east, incorporating the pathlines, as thick sands and gravels were modelled here in Petrel.

In contrast, particles released in the simplified model show different pathlines than the detailed model. Particles that are released near the Graham River travel through the shallow Quaternary permeable material to the confluence of the Graham and Halfway Rivers, where thick permeable fill allows recharge to the basal sands and gravels, and then travel down into the basal units, quickly travelling towards the southern general head boundary. The particles released near the Halfway River, however are not near a confluence, whereby they could easily enter the basal sands and gravels. Therefore, the particles travel through the shallow Quaternary and discharge at the

Halfway River, rather than travelling down through the thick till to reach the basal sands and gravels. It is apparent that discharge locations are significantly affected by the K distribution and connectivity of permeable material. However, water will not reach basal sands and gravels in the buried valleys unless there is a “window” (e.g. a river confluence with thick sands and gravels) in which it can recharge through to get to the basal deposits.

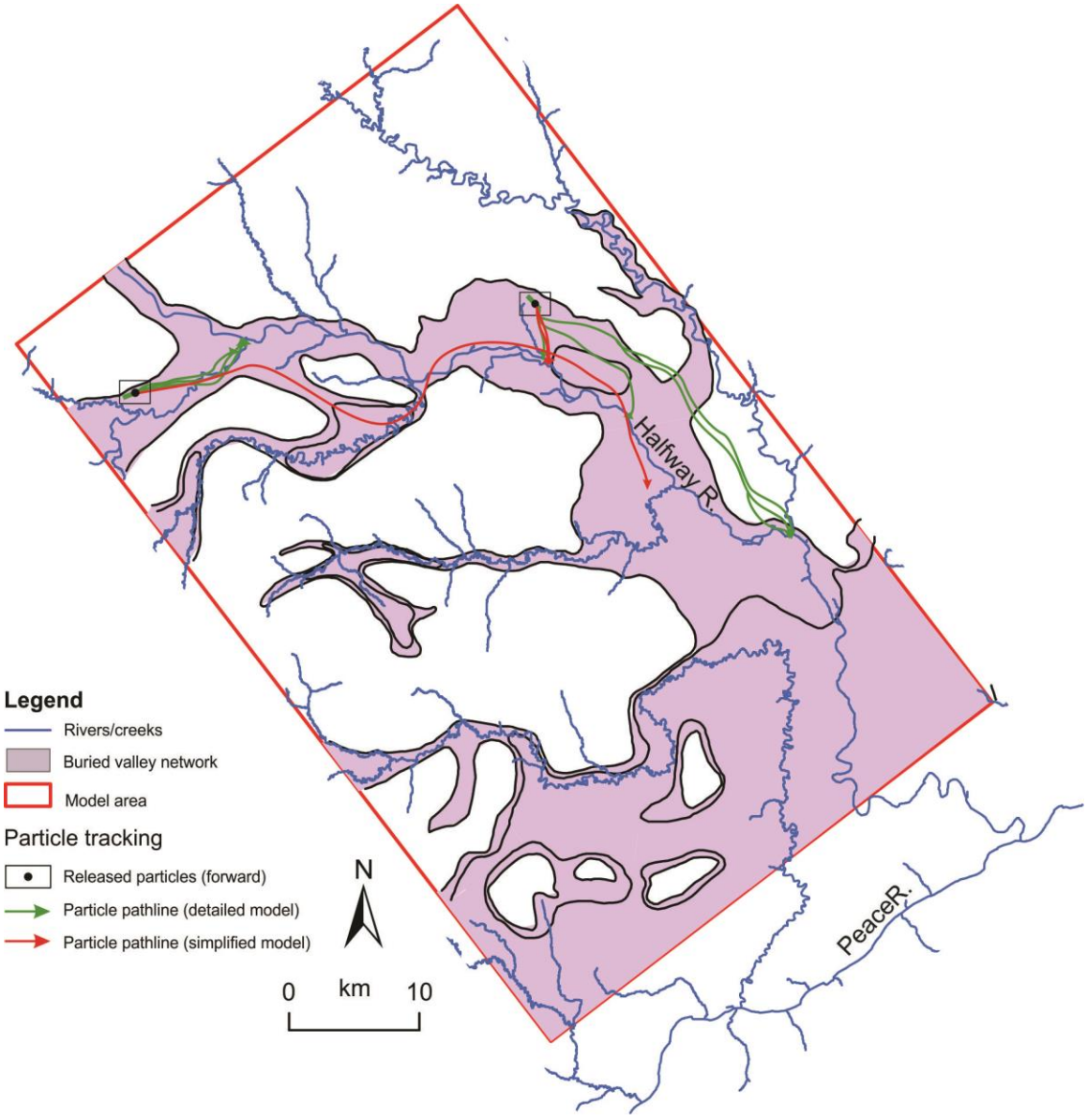

Figure 5.8. 100-year travel time pathlines for forward-tracking particles applied to both the detailed and simplified models in the buried valley network.

To identify recharge areas, particles were distributed as rings around the screens of five observation wells (four are screened in the Quaternary: Well ID 102672, 10x-2, 6a-MW, and 102658; see Table E1 in Appendix E. One is screened in sandstone bedrock: Well ID 109909; see Table E1 in Appendix E), within a deep and permeable deposit within the buried valley outline in the southern portion of the model, and at the locations of domestic wells with geochemical and tritium data available (tritium sample location pathlines were only observed for the detailed model). Figure 5.9 shows the locations of the released particles.

One hundred particles were allocated to each ring at a diameter of 200 m. The particles were backward-tracked and the pathlines viewed at different travel times to identify the recharge areas. Initially, the pathlines were displayed for a travel time of 100 years; however it was observed that particles travelled very slowly, particularly those in thick Quaternary material at far distances from the Halfway River. Therefore, the travel time was set to 1000 years.

For wells near the Halfway River, the particles track back to the river (Figure 5.9). However, for those wells that are not close to the river, particles track back to permeable deposits within the buried valley network, such as near the Graham River or Farrell Creek, although at longer travel times (particularly for well 10x-2 and the tritium sample locations), or in some cases to topographic highs where sandstone bedrock is at surface. For both models, where sandstone is in contact with permeable Quaternary material, pathlines indicate some exchange between bedrock and Quaternary. The pathlines for the particles placed in the deep buried valley deposits are different between the two models. The particles in the detailed model track back along Farrell Creek, where sandstone bedrock is near surface along a topographic high. However, in the simplified model the particles track back through the basal sands and gravels in the Halfway River valley thalweg, and recharge from the Halfway River and sandstone bedrock outside of the buried valley network.

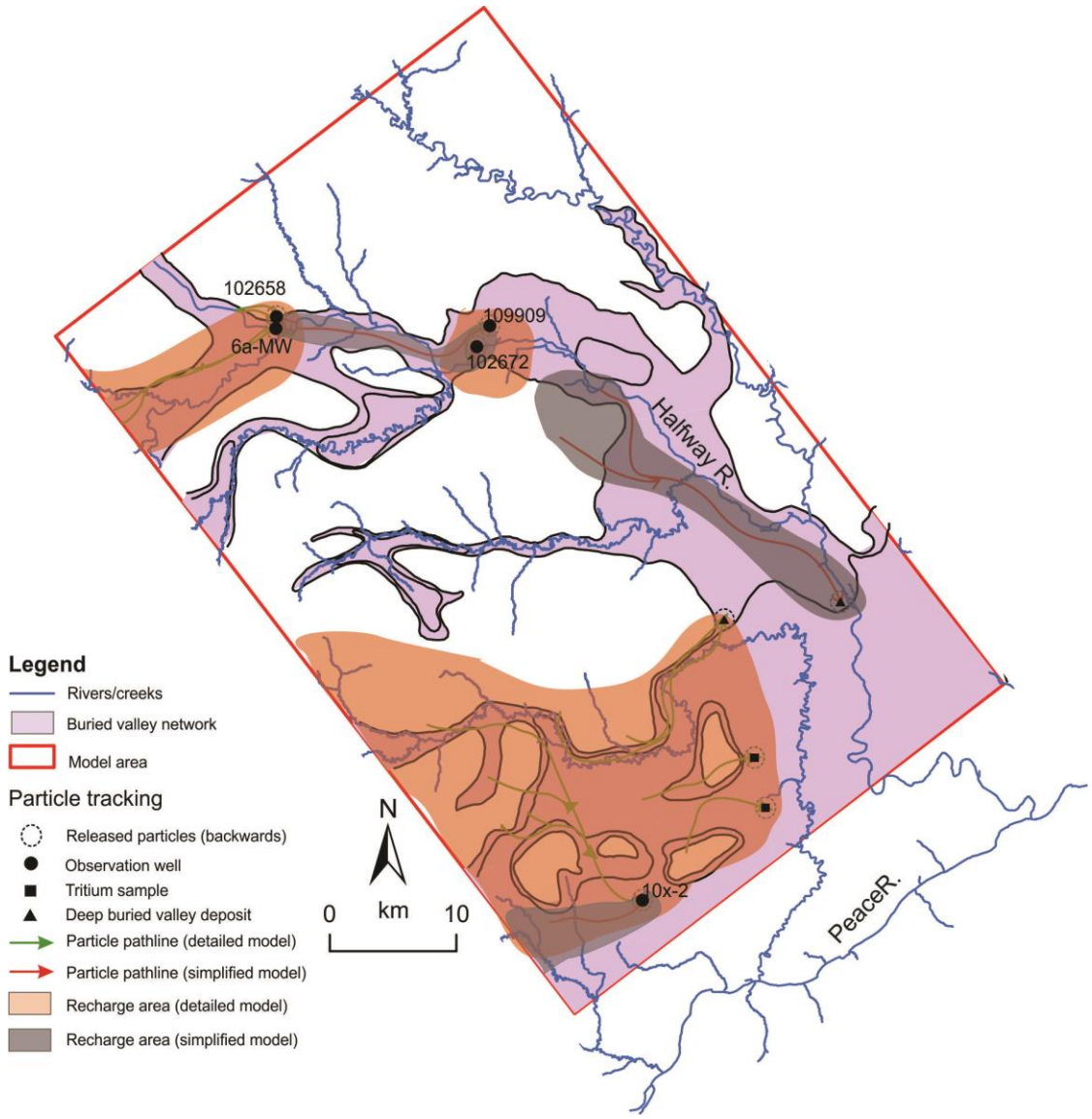

Figure 5.9. 1000-year travel time pathlines for backward-tracking particles applied to both the detailed and simplified models in the buried valley network.

Geochemical and tritium data were available from three domestic wells within the model area. These samples are all located in the southern part of the model area, near Farrell Creek and within the thick Quaternary fill of the large Peace River paleovalley (see Figure 5.9 for locations). Two samples came from wells completed in the Quaternary, and one in the bedrock. The well screen depths are unknown, so rings of particles were placed in the detailed model around the well locations in the deepest permeable Quaternary layer, and a sandstone bedrock layer for particle backward-tracking.

The presence of tritium in water samples indicates a mean residence time of less than approximately 50 years, suggesting relatively “young” groundwater (Kirste in Baye et al. 2016). All three samples contained essentially no tritium (0.04 tritium units for all samples). The pathlines for the wells indicate very slow travel times, with a minimum of 500 years to reach the recharge locations. While this result might be expected for the bedrock well, it indicates very slow groundwater flow rates through the Quaternary material in this area.

The results of the particle tracking highlight the impact of connective high K material when observing groundwater flow paths. In the simplified model, when particles are able to reach the basal sands and gravels they move quickly in these high K units. However, if there is no “window” for particles to recharge into the basal units, the particles will stay in the shallow flow system, interacting with the Halfway River. As the K distribution in the detailed model is fairly heterogeneous, permeable deposits in the buried valleys do not show full regional connectivity as in the simplified model. This results in some of the forward particles discharging to the Halfway River as opposed to flowing within the valleys, and some of the backwards particles showing long travel times. Nonetheless, there are still some areas where extensive permeable deposits exist, such as indicated by the forward pathlines of the detailed model in Figure 5.8. Although the geological and numerical modelling results do not show a fully connective network of basal sands and gravels at a regional scale, their presence is still possible as exposures of extensive sand and gravel deposits overlying bedrock have been observed at major river confluences both north and south of the model area (e.g. Levson et al. 2006, Hartman and Clague 2008).

The geological model, and subsequent K distribution, relied heavily on interpretations from resistivity data. Resistivity is a function of multiple variables such as pore water salinity, water content, porosity, and texture (Oldenborger et al. 2014), and thus specific lithologies do not necessarily have a unique resistivity value. The thickness of Quaternary fill, and consequent presence of basal sands and gravels, is also completely controlled by the top of bedrock surface. The top of bedrock surface was generated using stratigraphic picks from sparse gamma-ray and lithology logs throughout the model area, combined with surface topography, and thus is uncertain. More bedrock contacts, primarily within the buried valley network in the valley thalwegs are needed for a more well-constrained bedrock surface. However, this is challenging

due to the high costs of drilling into deep valley thalwegs. The uncertainty associated with the bedrock model may also result in larger volumes of shale or sandstone units being modelled than what may be the case in reality, which will affect how groundwater flows through the numerical models.

5.4.4. Simulating Abstraction

Given the high demand for water for hydraulic fracturing in the region, industry has been increasingly recycling water and using deep brackish groundwater. But shallow groundwater supplies offer an attractive alternative to lessen impacts to surface water, especially during periods of low streamflow. To investigate the potential for exchanging surface water sources for groundwater sources in the model area, abstraction wells were added to the detailed model in a hypothetical simulation. In addition, to evaluate permeable deposits within the buried valleys as a groundwater source, the impact of additional abstraction wells was simulated.

Figure 5.10 shows a map of all short term (up to 24 months) water licenses that have been approved by the BCOGC within the study area as of April 2017. These licenses are either for rivers/streams or water source dugouts; the latter act as a means to alleviate impacts on surface water during periods of low flow. The total withdrawal amount approved for licenses in the model area to rivers/streams is 1,934,980 m^3, and 662,345 m^3 for dugouts. The approved daily total for abstraction from the eight locations of river/stream withdrawals is approximately 18,000 m^3/day.

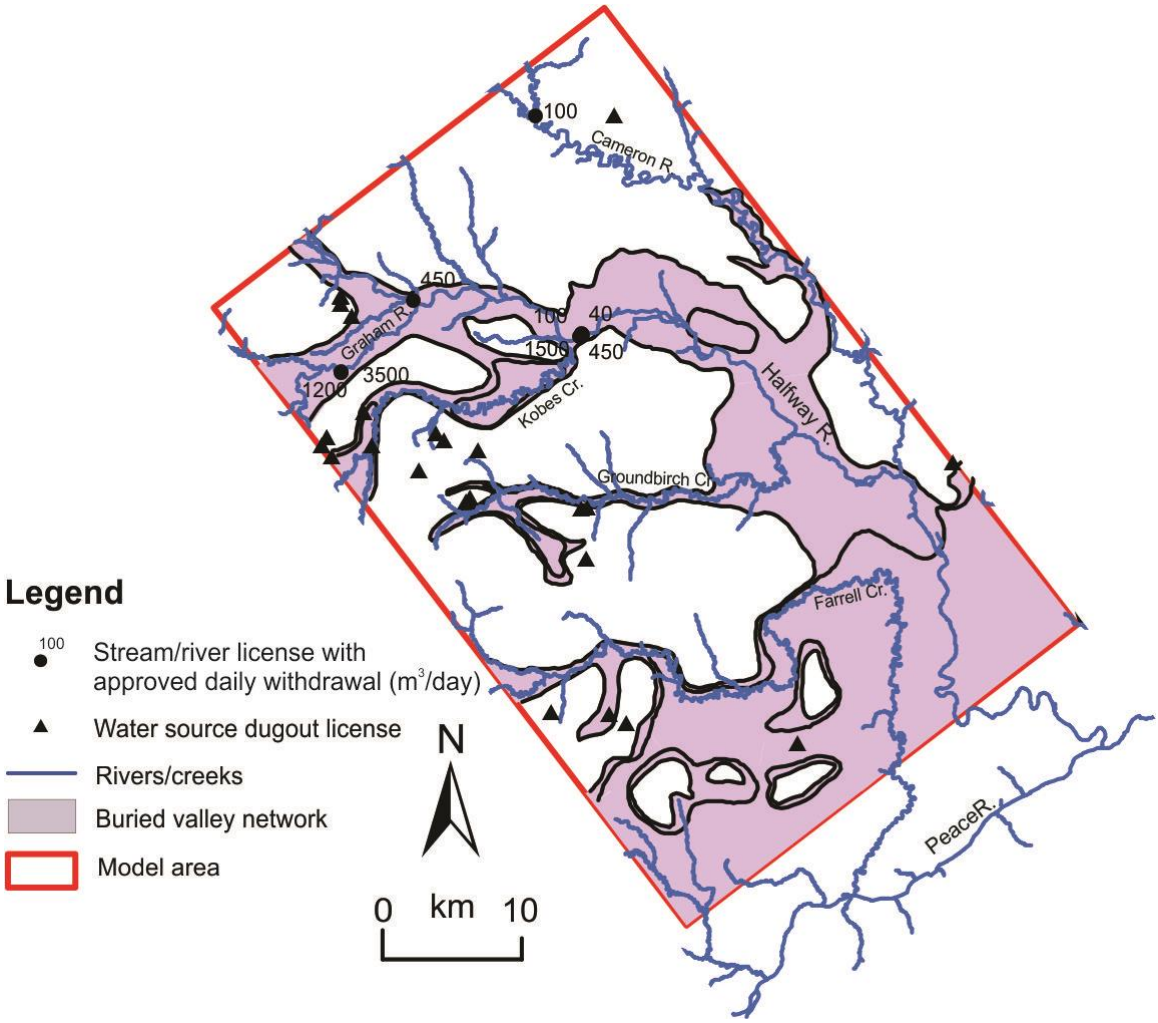

Figure 5.10. Short-term (up to 24 months) water licenses approved by the British Columbia Oil and Gas Comission (BCOGC) within the model area as of April 2017. Approved daily total withdrawals are shown for stream/river licenses. The outline of the buried valley network (Levson in Petrel Robertson Consulting Ltd. 2015) is shown.

Pumping wells were added to the model in the locations of these eight river/stream withdrawal licenses, 200 m away from the river/creek (i.e. a cell width away from the cells assigned boundary conditions for each water body), and screened in the deepest layer of permeable Quaternary material. The same abstraction volume of the surface water license was allocated to the well. It should be noted that this is a theoretical simulation and abstraction volume, as surface water and groundwater licences require different applications and thus are not transferable under the Water Sustainability Act (Government of British Columbia, 2017).

Simulation results indicate very minimal (<1%) decreases to baseflows of the Halfway and Cameron Rivers (most authorizations are for these two rivers), and the tributary Groundbirch and Farrell Creeks (which are south of the wells). Although, a 29% decrease in baseflow is seen in the Graham River, and 3.6% in Kobes Creek, as two licences are located along the Graham River. However, these wells are located close to the zero-flux boundary, which is likely the cause for this large decrease.

To assess the buried valleys as a new water source, the river/stream license replacement wells were turned off, and several pumping wells were added to the northern and southern areas of the buried valley network in two separate simulations in order to assess potential impacts to baseflow. The wells were completed in basal permeable deposits within the buried valleys, in locations where these deposits are most continuous (see Figure 5.11 for locations).

In the north, six wells were added in relatively similar locations to the surface water licenses near the Halfway River. The wells were added in two well fields consisting of three pumping wells. The total abstraction rate of approximately 18,000 m^3/day from the surface water licenses was distributed evenly among the six wells. Again it should be noted that this is a hypothetical simulation as it is unrealistic to have such high abstraction rates from source wells. According to Accumap (IHS Energy, 2017), typical rates for industry source wells in BC are approximately 200 m^3/day; although, these are almost all bedrock wells. However, this would have required 90 pumping wells to be added to the model to simulate the same total abstraction rate. Due to the large cell size and hypothetical nature of the simulation, it was deemed acceptable to use only a small number of wells but allocate a larger abstraction rate to each well.

Rings of particles were placed around the well screens at a diameter of 200 m and backward-tracked to identify capture zones. The pumping results indicate minimal impacts to baseflow as decreases for all rivers/creeks were <1%, due in part to the greater distance between the well and the rivers/creeks. The 50 and 100 year capture zones for the two northern well fields are shown in Figure 5.11. The source areas for these wells mostly coincide with the permeable material within the buried valleys and the Halfway River, with the eastern well field also drawing from a high sandstone ridge to the north in the 100 year capture zone. The particle pathlines also show that there is

exchange between the Quaternary and bedrock, as some particles travel through sandstones and then back into the Quaternary to reach the pumping wells.

In the south, five wells were added and completed in other basal permeable units within the buried valleys. The same total volume (18,000 m^3/day) was distributed to two well fields composed of 2 (southeast) and 3 (southwest) wells. Backwards particles were similarly placed around the wells. The 50 and 100 year capture zones for the southern wells are also shown in Figure 5.11. These capture zones are much smaller compared to those for the northern wells, suggesting that travel times are even slower for groundwater to reach these potential abstraction wells. Within 100 years, the southwestern wells draw water from permeable material within the buried valley outline near Farrell Creek; however, the southeastern wells draw from higher topography areas to the west in which sandstone is at or near surface. Results of the pumping simulation indicate small, yet slightly greater decreases to baseflows compared to the pumping simulation for the northern wells in the buried valleys. All rivers and creeks, with the exception of Farrell Creek, have a decrease in baseflow of 0.7-3.5%. In Farrell Creek, there is 17% reduction in baseflow. While a larger decrease in Farrell Creek baseflows is expected due to the locations of the pumping wells, the no-flow boundary that intersects Farrell Creek is likely exaggerating the degree to which the pumping wells impact flows to the creek.

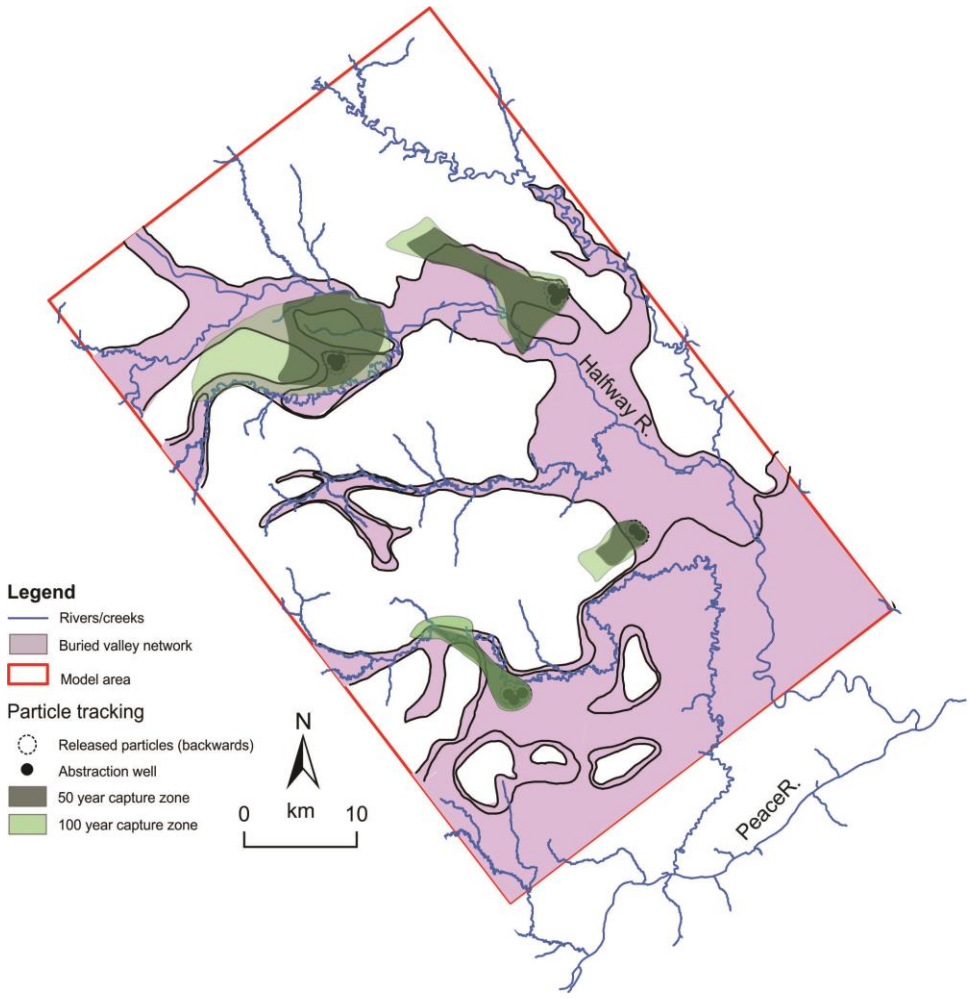

Figure 5.11. Capture zones for abstraction wells completed in basal permeable deposits of the buried valleys. The outline of the buried valley network (Levson in Petrel Robertson Consulting Ltd. 2015) is shown.

5.5. Conclusion

The high demand for water for hydraulic fracturing in Northeast British Columbia has led to a growing interest in using groundwater (rather than surface water) as a water source, and buried valleys present throughout the region may contain high-yield aquifers. However, similar to other regions, Northeast British Columbia is data-sparse, which led to the development of two interpretive models to conceptualize the regional groundwater flow system in a buried valley network.

The detailed model was based on the best available geophysical and geological data. Interpreted 3-D airborne TEM data were constrained to some degree by borehole gamma-ray logs and borehole lithology data. However, geophysical surveys can have associated uncertainty, and further interpretation of the architecture of the buried valley network and its fill through facies modelling is equally uncertain. So, this prompted the development of a simplified model based solely on a conceptual understanding of the extent and architecture of buried valleys. Both geological models were used to simulate groundwater flow with the same parameterization and boundary conditions. The lack of hydraulic head data in the study area also meant that the flow model (only the detailed model) be calibrated using creative means – here the use of the Northeast Water Tool (NEWT) to estimate the net amount of groundwater within the model area that contributes to baseflow. While the baseflow estimates are themselves uncertain, they provided some constraint to the flow model.

The results of this study suggest that both models result in similar head distributions, although that of the simplified model is more smoothed. Due to insufficient head data for calibration, the head calibration results were rather poor (RMSE of 27%), but the outflow to rivers and creeks were within the range of uncertainty of the NEWT estimates of baseflow. Thus, both models appear to be reasonable interpretive models.

Use of the models for practical applications, including pathline mapping and travel time estimation, however, showed important differences. Connective high K units in the simplified model facilitate quick flow through the basal sand and gravel units. However, windows in which permeable material connect the shallow Quaternary deposits to the basal units are necessary for groundwater to reach the deep sands and gravels. In contrast, the heterogeneous K distribution in the detailed model results in mostly disconnected particle pathlines and long travel times. However, some areas of extensive permeable deposits exist in the detailed model, resulting in areas of quicker flow.

The detailed model was used to simulate abstraction to explore potential extents of capture zones and impacts to baseflow. While the results are uncertain (for the range of reasons described above), the results suggest minimal impacts (relatively small 100-year capture zones and little impact on baseflow), suggesting the groundwater may be a viable water source in this area. However, utilizing particle tracking in a regional model

with large grid cells and employing uncertain boundary conditions leads to uncertainty. To more fully evaluate specific locations of permeable deposits within the buried valleys as groundwater sources, localized investigations using smaller model domains is necessary.

Chapter 6.

Conclusions

The purpose of this research was to contribute to the knowledge of buried valley aquifer hydrogeology, and explore the influence that buried valley aquifers have on groundwater flow at a regional scale. The study area was the central Peace Region in Northeast British Columbia (BC), where the approximate extent of a large network of buried valleys had been delineated by Levson in Petrel Robertson Consulting Ltd. (2015). Assessing the potential of buried valley aquifers as a water source for the region is of critical importance, as water resources support multiple users such as First Nations and local communities, agriculture, and industry. The oil and gas sector, in particular, uses large quantities of water due to the recent increase in shale gas development and hydraulic fracturing in the area.

The goals of this research were accomplished by: 1) determining the nature of the continuity of the permeable deposits within the buried valleys by developing a robust geological model of the study area using high-resolution geophysical and geological datasets; 2) characterizing the regional groundwater flow system of the study area through the creation of numerical flow models based on the geological model; and, 3) analyzing the impact of buried valley aquifers on the regional water budget, and assessing the potential of the buried valley network as a groundwater source.

Northeast BC is a very data sparse area, and thus limitations were encountered throughout this research. The following sections summarize the main findings of each objective, and discuss the limitations and sources of uncertainty. The final section of this chapter proposes recommendations for future work.

6.1. Geological Modelling

An understanding of the three-dimensional hydrostratigraphic architecture of a buried valley network, in particular the continuity of permeable units within their fill, is needed to evaluate the resource potential and role of buried valley aquifers in regional groundwater flow. In this research, the reservoir software, Petrel, was used to design a

3-D geological model of the buried valley network. The interpretations of geophysical and geological data collected as part of Geoscience BC's Peace Project were used to develop the geological model. These datasets included airborne time-domain electromagnetic (TEM) interpretations from a SkyTEM survey (Aarhus Geophysics ApS, 2016a-e), corrected gamma-ray logs from oil and gas wells (Petrel Robertson Consulting Ltd., 2015), borehole lithology logs (Levson and Best 2017a), and supplementary lithologic information from water wells (WELLS database; BC Ministry of Environment, 2017).

Both a bedrock and Quaternary model were created in Petrel. The bedrock model was created using surface topography, stratigraphic picks from the corrected gamma-ray logs (Petrel Robertson Consulting Ltd., 2015) and water well lithology logs (BC Ministry of Environment, 2017) in the study area. To evaluate the results of the bedrock modelling in Petrel, a compilation of bedrock geology maps from Northeast BC was used for comparison (MapPlace, 2017). While there were both similarities and differences between the bedrock model and bedrock maps, neither the model nor the mapped bedrock are certain due to the lack of lithology data in the area. As this study was mostly concerned with the Quaternary geology, the Petrel-generated bedrock model was considered to be a reasonable representation of the shallow bedrock in the study area.

The Quaternary model was created primarily using the airborne TEM interpretations; specifically, horizontal resistivity slices showing the resistivity distribution at various depth intervals (Aarhus Geophysics ApS 2016d). These were recreated in Petrel through digitizing them in ArcGIS by relating distinct resistivity values to geological material types. The TEM interpretations were supplemented by upscaled facies logs derived from borehole gamma-ray logs and lithology data. Two different facies modelling algorithms in Petrel were used to generate Quaternary models of the buried valley network, and were compared to assess differences in how the modelling algorithms honour input data and how the resultant facies models differ. The Sequential Indicator Simulation (SIS) algorithm was chosen to create a stochastic Quaternary model, and the Assign Values (AV) algorithm was chosen to create a deterministic Quaternary model. The SIS model results were extremely heterogeneous due to different stochastic realizations of each SIS model run, resulting in difficulties assessing the continuity of buried valley deposits. The SIS algorithm also placed a larger emphasis on well log data

compared to the resistivity data, which was investigated by comparing the statistics of generated facies types when gamma-ray classifications of the upscaled facies logs were varied. This was considered problematic for this study area, as well data in the region are quite sparse. In contrast, the facies distribution for the AV model was controlled by the resistivity data, and well log data were only used in areas where they existed. This resulted in the AV model being more homogeneous, which allowed for easier inspection of the continuity of permeable deposits within the buried valley network. While selecting the more homogeneous model may not be appropriate at a local scale, for regional-scale investigations this helps to simplify complex systems.

Due to the variability and uncertainty of the SIS results, the AV algorithm was selected as the most suitable facies modelling algorithm upon which to base the Quaternary model. The results of the AV Quaternary model indicate that the buried valley network is filled with heterogeneous Quaternary material of variable thickness. Permeable deposits exist within these buried valleys; however, based on the available data, they are not connected throughout the whole network, and do not form a regionally connective network of basal sands and gravels, as was originally hypothesized. This isolation of permeable deposits may be a result of glacial processes, such as ice erosion. Nevertheless, there are still areas within the network in which the modelling displayed thick deposits of permeable material with continuity at smaller scales. The presence of connective basal sands and gravels throughout the network cannot be ruled out, however, because exposures of extensive sand and gravel deposits overlying bedrock have been observed at major river confluences both north and south of the model area (e.g. Levson et al., 2006; Hartman and Clague, 2008).

The geological modelling conducted in this study relied heavily on interpretations from resistivity data. Resistivity is a function of multiple variables such as pore water salinity, water content, porosity, and texture (Oldenborger et al., 2014), and thus specific lithologies do not necessarily have a unique resistivity value. It is also not possible to differentiate between a highly resistive gravel that is dry and a gravel that is wet using the TEM data, and similar difficulties exist in differentiating shale versus clay, or sand versus sandstone. While different interpretations of the resistivity data were not performed in this research due to scope and time constraints, analyses were performed to look at different classifications of facies based on different gamma-ray ranges.

The thickness of Quaternary fill and the presence of basal permeable deposits are also completely governed by the top of bedrock surface. The top of bedrock surface was generated using sparse well data throughout the model area, combined with surface topography, and thus is uncertain. Most of the gamma-ray logs with top of bedrock picks were also outside of the buried valley outline (Levson in Petrel Robertson Consulting Ltd., 2015), and the results of the Peace Project drilling campaign highlighted how challenging it is to determine depth to bedrock with sparse gamma-ray logs and TEM data, as only one borehole encountered the Quaternary-bedrock contact. The Peace Project drilling results also emphasized how heterogeneous the Quaternary geology of the Peace Region is, as different lithologies were encountered at boreholes that were 5 m apart. The regional-scale nature of this investigation, however, limited the discretization of model grid cells to 200 x 200 m, enforcing a large generalization of lithology type.

As a first integration of this kind in Petrel, this modelling acted as an initial regional interpretation of these geophysical and geological datasets. As more data become available, the geological model can be refined.

6.2. Numerical Flow Modelling

The geological model developed in Petrel was used as a basis for constructing two numerical flow models of the regional groundwater flow system that incorporated the buried valley network; a model with detailed geological complexity derived from the facies modelling, and a simplified model based on the original conceptualization of the buried valley network (i.e. large bedrock valleys filled with thick packages of till overlying regionally connective basal sands and gravels). The two models were constructed in MODFLOW and had the same parameterization and boundary conditions. As Northeast BC is very groundwater data-limited, there were few hydraulic head data available for calibration. Therefore, an approach was designed to estimate baseflow for model calibration with the use of the Northeast Water Tool (NEWT). The limited calibration data resulted in the flow models being interpretive in nature; however, they could still be used to characterize the regional flow regime and understand the influence of permeable deposits within the buried valley network on regional groundwater flow.

The results of the numerical modelling suggest that both models result in similar head distributions, although that of the simplified model is more smoothed, due to the homogeneous hydraulic conductivity distribution which allows groundwater to flow more easily through the model. The similarities in hydraulic head distributions suggest that neither model (simplified or detailed) can be ruled out. This issue of equifinality (model non-uniqueness) is commonly encountered in flow modelling (e.g. Harrar et al., 2003; Troldborg et al., 2007; Seifert et al., 2008). Groundwater flow directions were east-southeast, from topographic highs at the northern edge of the model towards the Halfway River valley and the general head boundary representing the Peace River. Due to insufficient head data for calibration, the head calibration results were rather poor (RMSE of 27%), but the outflow to rivers and creeks were within the range of uncertainty of the NEWT estimates of baseflow, and were all around the lower bound of their respective baseflow estimates (i.e. 30-40% of mean annual discharge).

The water balance results identified the main component as exchange with the river boundary assigned to the Halfway River. While it is possible this exchange may be significant, the model did not consider any other inflows besides recharge. Therefore, it is possible that lateral inflows, such as from mapped paleovalleys intersecting the zero-flux boundaries of the model domain or regional-scale groundwater flow in the bedrock, could contribute to the total water entering the model, reducing the effect of river leakage on the water balance. Nevertheless, these potential fluxes are unknown and thus could not be modelled.

The results of using Zone Budget to compare flows within the shallow Quaternary, buried valleys, and bedrock indicated that in both models flow is primarily through the shallow Quaternary (63% in the detailed model and 68% in the simplified model), which is to be expected due to the large amount of river leakage from the water balance results. However, flow within the buried valleys in the detailed model was 28%, compared to 17% in the simplified model. This is likely due to the higher proportion of shallow permeable material and sandstone bedrock in the simplified model. Additionally, heterogeneities within the bedrock units such as local-scale high permeability zones within the shale units were not considered in this modelling. These high hydraulic conductivity zones could increase the proportion of flow within the bedrock in both the detailed and simplified models.

Particle tracking was used to identify potential recharge and discharge locations for the buried valleys, and estimate travel times. Recharge areas for both the detailed model and the simplified model appear to be focused around topographic highs, the river boundary, and permeable sediments within the valleys that received diffuse recharge; however, the discharge locations vary significantly between the two models. Within the simplified model, particles travel quickly from the shallow Quaternary into the basal gravels and through the entire network, travelling towards the southern general head boundary; however, “windows” in which permeable material connect the shallow Quaternary deposits to the basal units are necessary for groundwater to reach the deep sands and gravels. In the absence of these windows, particles will stay in the shallow flow system, interacting with the Halfway River. The limited regional connectivity of permeable units due to the heterogeneous hydraulic conductivity distribution of the detailed model resulted in particles travelling more slowly and discharging at confluences of the Halfway River and other creeks, as opposed to flowing within the buried valleys. However, the few locations with extensive permeable deposits (as described above in section 6.1) do show some particles travelling large distances within the buried valleys.

The detailed model was used to simulate abstraction to explore potential extents of capture zones and impacts to baseflow. While the results are uncertain (for the range of reasons described throughout this chapter), the results suggest minimal impacts (relatively small 100-year capture zones and little impact on baseflow), suggesting the buried valleys may be a viable water source in this area. However, utilizing particle tracking in a regional model with large grid cells and employing uncertain boundary conditions leads to uncertainty. Additionally, the low impacts to baseflow may simply be due to the fact that total baseflow is large relative to the abstraction volume of the wells, as other abstractions such as private domestic, or existing water licences (which were turned off during the simulation to evaluate the buried valley aquifers as a water source) were not included during the pumping simulation. To more fully evaluate specific locations of permeable deposits within the buried valleys as groundwater sources, localized investigations using smaller model domains is necessary.

In summary, the results of the modelling conducted in this study suggest that permeable deposits within the large buried valley network in the central Peace Region of Northeast BC are not regionally connected throughout the whole network, and do not

play a significant role in the regional groundwater flow regime. However, this conclusion is based on regional-scale modelling that relied heavily on the interpretations from an airborne TEM survey combined with supplementary borehole data. Disconnected particle pathlines and long travel times supported by a few tritium samples suggest regional isolation of sand and gravel deposits; however, areas of extensive permeable deposits within the buried valleys still exist in the model at smaller scales, and flow within the buried valley sediments accounts for approximately one third of total flow in the detailed model. Deep sand and gravel units at the bedrock contact may exist, particularly at the confluences of major rivers and creeks, as has been observed in the field by other researchers.

6.3. Recommendations for Future Work

In this study, the impact of buried valley aquifers on regional groundwater flow was investigated mainly with the use of interpretations from an extensive airborne TEM survey. As electrical resistivity does not uniquely define lithology, it is recommended that other geophysical surveys, such as seismic, which has proven very useful in geological modelling of buried valleys (e.g. Jørgensen et al., 2003; Ahmad et al., 2009; Oldenborger et al., 2016), be incorporated to more accurately investigate the hydrostratigraphic architecture of the valley-fills. The isopach map of sand and gravel facies generated in this thesis could be used to identify locations of interest for further investigation and geophysical surveys: particularly along the Halfway River near the Halfway River First Nations area, where further work has already been conducted on evaluating locations for proposed water well locations (e.g. Levson and Best, 2017b), and along Farrell Creek where thick permeable deposits seem to be present.

Future research should also include different interpretations of the resistivity data, in order to address how variables such as pore fluids, porosity, and texture, might influence resistivity, and analyze how these might alter the geological model. Within the facies modelling procedure, it is also suggested that multiple stochastic models be used to generate geological models (e.g. Refsgaard et al., 2012; He et al., 2013), and each one be carried through the flow modelling stage to quantify the sensitivity of the flow model to geology. Conducting local-scale investigations across single buried valleys may also help further refine the geological architecture of individual buried valleys, and the subsequent hydrostratigraphic framework. Incorporating the TEM data, particularly the

resistivity sections, in interpreting the bedrock formations in these local-scale investigations can also help further refine the regional bedrock model.

The top of bedrock surface generated in the geological modelling for this study is uncertain. As this controls the thickness of fill and presence of basal permeable material within the buried valleys, it is highly recommended that more bedrock contacts, primarily within the buried valley network in the valley thalwegs, be collected to better constrain the top of bedrock surface. While the most accurate method to collect these contacts would be drilling boreholes, this is challenging due to the high costs of drilling into deep valley thalwegs. Collecting more bedrock contacts along the perimeter of the buried valley outline can also help in confirming whether areas of additional buried valleys outside of the current interpreted outline exist. As gas production is likely to increase in this region, new regulations could be developed to require depth to bedrock be recorded in new oil and gas wells and uploaded to a database such as AccuMap (IHS Energy, 2017). Additionally, reporting of depth to bedrock could be required for new water wells and made available in the WELLS database. Not only would bedrock tags be beneficial for geological modelling, but they would also be useful in investigations such as hydrogeological modelling, Quaternary geology mapping, and geomorphology.

Finally, numerical flow models are highly parameterized. With the limited data in the region, numerous properties and boundaries had to be estimated based on the literature and best available data for the study area. Therefore, the regional numerical model should be used only as a preliminary screening tool or initial conceptual model for evaluating specific locations of permeable deposits within the buried valley network as groundwater sources. The collection of more hydraulic data, such as water level data and information to inform model boundary conditions is needed to better constrain numerical modelling of this area. As stated above, the generated isopach map could be used to identify areas where further hydrogeological investigations could be carried out (e.g. additional drilling and subsequent pumping tests). Again, areas such as the Halfway River First Nations area and along Farrell Creek are recommended to further evaluate the potential of permeable deposits within buried valleys in these locations as a water source for the region. As test wells would have to be drilled to directly assess these deposits as a water supply, collected bedrock contacts and lithology data could be further incorporated in the regional geological and hydrogeological models from this thesis.

References

Aarhus Geophysics ApS (2016a). *Processing and inversion of SkyTEM data. Charlie Lake Area- Phase 1*. Geoscience BC, Report 2016-09b, 28 pp.

Aarhus Geophysics ApS (2016b). *Processing and inversion of SkyTEM data. DOIG Area- Phase 1*. Geoscience BC, Report 2016-09c, 27 pp.

Aarhus Geophysics ApS (2016c). *Processing and inversion of SkyTEM data. Peace River "Conoco" Area- Phase 2*. Geoscience BC, Report 2016-09d, 33 pp.

Aarhus Geophysics ApS (2016d). *Processing and inversion of SkyTEM data. Peace River Main Area- Phase 1*. Geoscience BC, Report 2016-09a, 28 pp.

Aarhus Geophysics ApS (2016e). *Processing and inversion of SkyTEM data. Peace River "Sikanni" Area- Phase 2*. Geoscience BC, Report 2016-09e 27 pp.

Ahmad, J., Schmitt, D. R., Rokosh, C. D., & Pawlowicz, J. G. (2009). *High-resolution seismic and resistivity profiling of a buried Quaternary subglacial valley: Northern Alberta, Canada*. Geological Society of America Bulletin, 121(11–12), 1570–1583.

Anderson, M. P., Woessner, W. W., and Hunt, R. J. (2015). *Applied groundwater modelling: simulation of flow and advective transport. 2nd edition*. Kidlington, Oxford: Academic press.

Andriashek, L. D. D. (2000). *Quaternary stratigraphy of the buried Birch and Willow bedrock channels, NE Alberta*. Alberta Energy and Utilities Board, EUB/AGS Earth Sciences, Report 2000-15, 61 pp.

Andriashek, L. D., & Atkinson, N. (2007). *Buried channels and glacial-drift aquifers in the Fort McMurray region, northeast Alberta*. Alberta Energy and Utilities Board, EUB/AGS Earth Sciences, Report 2007-01,169 pp.

Auken, E., Christiansen, A. V., Jacobsen, L. H., and Sørensen, K. I. (2008). A resolution study of buried valleys using laterally constrained inversion of TEM data. *Journal of Applied Geophysics, 65*(1), 10-20. doi:10.1016/j.jappgeo.2008.03.003

Baye, A., Rathfelder, K., Wei, M., & Yin, J. (2016). *Hydrostratigraphic, hydraulic and hydrogeochemical descriptions of Dawson Creek-Groundbirch areas, Northeast BC*. Victoria, Province of B.C. Water Science Series 2016-04, 58 pp.

BC Ministry of Energy and Mines. (2011). *Diagrammatic S.W. – N.E. geologic section through Northeastern British Columbia.* BC Ministry of Energy and Mines. Retrieved from http://www2.gov.bc.ca/gov/content/industry/natural-gas-oil/petroleum-geoscience/sedimentary-basins-of-bc/northeastern-bc-basin (May, 2017).

BC Ministry of Environment (2017). *WELLS database*. BC Ministry of Environment. Retrieved from https://a100.gov.bc.ca/pub/wells/public/indexreports.jsp (July, 2017).

BC Ministry of Natural Gas Development. (2011). *Stratigraphic correlation chart: Northeastern British Columbia and adjacent parts of Alberta, Yukon and Northwest Territories.* BC Ministry of Natural Gas Development. Retrieved from http://www2.gov.bc.ca/gov/content/industry/natural-gas-oil/petroleum-geoscience/sedimentary-basins-of-bc/northeastern-bc-basin (May, 2017).

BCOGC (2010). *Oil and gas activities act. Drilling and production regulation.* Victoria, B.C.: British Columbia Oil and Gas Commission.

BCOGC. (2015). *Water management for oil and gas activity: 2015 annual report.* Victoria, B.C.: British Columbia Oil and Gas Commission. 33 pp.

BCOGC. (2017). *NEWT: Northeast Water Tool.* Victoria, B.C.: British Columbia Oil and Gas Commission. Retrieved from https://water.bcogc.ca/newt (November, 2017).

Beck, H.E., Van Dijk, A.I.J.M., Miralles, D.G., De Jeu, R.A.M., Bruijnzeel, L.A., McVicar, T.R., & Schellekens, J. (2013). Global patterns in base flow index and recession based on streamflow observations from 3394 catchments. *Water Resources Research, 49*(12), 7843–7863. doi:10.1002/2013WR013918

Bemex Consulting International and Quaternary Geosciences Inc. (2016). *Peace area project – well selection for testing geological model based on gamma and airborne electromagnetic (AEM) studies*. Geoscience BC, Report 2016-18, 42 pp.

Best, M., & Levson, V. (2017). *Peace area project- comparison of resistivity, gamma, and geological logs with airborne EM inversions.* Geoscience BC, unpublished report, 27 pp.

BGC Engineering & Hemmera Envirochem. (2012). *Site C clean energy project: volume 2 appendix F- groundwater regime technical data report*. Prepared for: BC Hydro Power and Authority, 204 pp.

Catto, N. R. (1991). *Quaternary geology and landforms of the Eastern Peace River Region, British Columbia, NTS 94A/1, 2, 7, 8.* BC Ministry of Energy, Mines and Petroleum Resources, Mineral Resources Division, Geological Survey Branch, 18 pp.

Chapman, A., B. Kerr, D. Wilford. (2012). *Hydrological modelling and decision-support tool development for water allocation, Northeastern British Columbia*. Geoscience BC Summary of Activities 2011, Geoscience BC, Report 2012-1, 81-86.

Cowen, A. (1998). *BC Peace Region groundwater initiative interim report 1998.* Agriculture and Agri-Food Canada, Prairie Farm Rehabilitation Administration, Northern Alberta/BC Region. 25 pp.

Cummings, D. I., Russell, H. A. J., & Sharpe, D. R. (2012). Buried-valley aquifers in the Canadian prairies: geology, hydrogeology, and origin. *Canadian Journal of Earth Sciences, 49*(9), 987–1004. doi:10.1139/E2012-041

Danielsen, J. E., Auken, E., Jørgensen, F., Søndergaard, V., & Sørensen, K. I. (2003). The application of the transient electromagnetic method in hydrogeophysical surveys. *Journal of Applied Geophysics, 53*(4), 181–198. doi:10.1016/j.jappgeo.2003.08.004

Di Salvo, C., Di Luzio, E., Mancini, M., Moscatelli, M., Capelli, G., Cavinato, G. P., & Mazza, R. (2012). GIS-based hydrostratigraphic modelling of the city of Rome (Italy): analysis of the geometric relationships between a buried aquifer in the Tiber Valley and the confining hydrostratigraphic complexes. *Hydrogeology Journal, 20*(8), 1549–1567. doi: 10.1007/s10040-012-0899-2

Environment Canada. (2017a). Fort St. John station results - climate normals 1981-2010. Retrieved from http://climate.weather.gc.ca/climate_normals/results_1981_2010_e.html?searchType=stnName&txtStationName=Fort+St+John&searchMethod=contains&txtCentralLatMin=0&txtCentralLatSec=0&txtCentralLongMin=0&txtCentralLongSec=0&stnID=1413&dispBack=1 (July, 2017).

Environment Canada. (2017b). Historical hydrometric data: Halfway River above Graham River station 07FA003. Retrieved from https://wateroffice.ec.gc.ca/download/index_e.html?results_type=historical (July, 2017).

Environment Canada. (2017c). Historical hydrometric data: Peace River above Pine River station 07FA004. Retrieved from https://wateroffice.ec.gc.ca/download/index_e.html?results_type=historical (July, 2017).

Environment Canada. (2017d). Historical hydrometric data: Graham River above Colt Creek station 07FA005. Retrieved from https://wateroffice.ec.gc.ca/download/index_e.html?results_type=historical (July, 2017).

Environment Canada. (2017e). Historical hydrometric data: Halfway River near Farrell Creek station 07FA006. Retrieved from https://wateroffice.ec.gc.ca/download/index_e.html?results_type=historical (July, 2017).

Environment Canada. (2017f). Historical hydrometric data: Peace River at Hudsons Hope station 07EF001. Retrieved from https://wateroffice.ec.gc.ca/download/index_e.html?results_type=historical (July, 2017).

Exprodat Consulting Limited. (2017). *Data Assistant v223 user guide for ArcGIS 10.x. version 1.0 – April 2017,* Exprodat Consulting Limited, GIS for Petroleum.

Fitterman, D. V, & Stewart, M. T. (1986). Transient electromagnetic sounding for groundwater. *Geophysics, 51*(4), 995–1005.

Freeze, R.A. & Cherry, J.A. (1979). *Groundwater*. Englewood Cliffs, New Jersey: Prentice-Hall Inc.

Gibling, M. R. (2006). Width and thickness of fluvial channel bodies and valley fills in the geological record: a literature compilation and classification. *Journal of Sedimentary Research, 76*(5), 731–770. doi: 10.2110/jsr.2006.060

Government of British Columbia (2017). *Water Sustainability Act*. Water Sustainability Regulation, Statutes of British Columbia 2014, Chapter 15. Retrieved from http://www.bclaws.ca/civix/document/id/complete/statreg/14015#section9 (December 2017).

Green, T. R., Taniguchi, M., Kooi, H., Gurdak, J. J., Allen, D. M., Hiscock, K. M., Treidel, H., & Aureli, A. (2011). Beneath the surface of global change: impacts of climate change on groundwater. *Journal of Hydrology, 405*(3), 532–560. doi:10.1016/j.jhydrol.2011.05.002

Harbaugh, A.W. (2005). *MODFLOW-2005, the U.S. Geological Survey's modular ground water flow model - the groundwater flow process*, U.S. Geological Survey Techniques and Methods 6-A16. U.S. Geological Survey, 253 pp.

Harrar, W.G., Sonnenborg, T.O., & Henriksen, H.J. (2003). Capture zone, travel time, and solute-transport predictions using inverse modelling and different geological models. *Hydrogeology Journal, 11*(2003), 536-548. doi: 10.1007/s10040-003-0276-2

Hartman, G. M. D., & Clague, J. J. (2008). Quaternary stratigraphy and glacial history of the Peace River valley, northeast British Columbia. *Canadian Journal of Earth Sciences, 45*(5), 549–564. doi:10.1139/E2012-041

Hartman, G. M. D. (2005). *Quaternary stratigraphy and geologic history of Charlie Lake (NTS 94A)* (MSc Thesis). Simon Fraser University, Burnaby, Canada.

Hartz, M., Malone, D., & Nelson, R. (2016). Three-dimensional geologic model of glacial outwash in McLean County, Illinois, based on seismic refraction studies. *Geosciences, 6*(1), 9. doi:10.3390/geosciences6010009

He, X., Sonnenborg, T.O., Jørgensen, F., Høyer, A.-S., Møller, R.R., & Jensen, K.H. (2013). Analyzing the effects of geological and parameter uncertainty on prediction of groundwater head and travel time. *Hydrology and Earth System Sciences 17*(2013), 3245-3260. doi:10.5194/hess-17-3245-2013

Hickin, A. S., Kerr, B., Turner, D. G., & Barchyn, T. E. (2008). Mapping Quaternary paleovalleys and drift thickness using petrophysical logs, northeast British Columbia, Fontas map sheet, NTS 94I. *Canadian Journal of Earth Sciences, 45*(5), 577–591. doi: 10.1139/E07-063

Hickin, A. S. (2011). *Preliminary bedrock topography and drift thickness of the Montney Play area*. BC Ministry of Energy and Mines, Energy Open File 2011-1, Geoscience BC Report 2011-07, 2 maps, 1:500 000.

Hickin, A. S., & Best, M. E. (2016). *Geometry and valley-fill stratigraphic framework for aquifers in the Groundbirch paleovalley assessed through shallow seismic and ground-based electromagnetic surveys*. BC Ministry of Energy and Mines, British Columbia Geological Survey Open File 2016-5, 46 pp.

Holding, S. & Allen, D.M. (2015). *Shallow groundwater intrinsic vulnerability mapping in Northeast British Columbia*. Simon Fraser University, Final report prepared for Pacific Institute for Climate Solutions and BC Ministry of Energy and Mines, 41 pp.

Holland, S.S. (1964). *Landforms of British Columbia, a physiographic outline*. British Columbia Department of Mines and Petroleum Resources, Bull. No. 48, 136 pp.

Høyer, A.-S., Lykke-Andersen, H., Jørgensen, F., & Auken, E. (2011). Combined interpretation of SkyTEM and high-resolution seismic data. *Physics and Chemistry of the Earth, 36*(16), 1386–1397. doi:10.1016/j.pce.2011.01.001

Høyer, A.-S., Jørgensen, F., Sandersen, P. B. E., Viezzoli, A., & Møller, I. (2015). 3D geological modelling of a complex buried-valley network delineated from borehole and AEM data. *Journal of Applied Geophysics, 122* (2015), 94–102. doi: 10.1016/j.jappgeo.2015.09.004

Huuse, M., & Lykke-Andersen, H. (2000). Overdeepened Quaternary valleys in the eastern Danish North Sea: morphology and origin. *Quaternary Science Reviews, 19*(12), 1233–1253.

IHS Energy (2017). *IHS AccuMap®, version 26.06*, IHS Energy, mapping, data management and analysis software.

Jørgensen, F., Sandersen, P. B. E., & Auken, E. (2003). Imaging buried Quaternary valleys using the transient electromagnetic method. *Journal of Applied Geophysics, 53*(4), 199–213. doi:10.1016/j.jappgeo.2003.08.016

Jowett, D. M. S., Schröder-Adams, C. J., & Leckie, D. (2007). Sequences in the Sikanni Formation in the frontier Liard Basin of northwestern Canada—evidence for high frequency late Albian relative sea-level changes. *Cretaceous Research, 28*(4), 665–695. doi:10.1016/j.cretres.2006.10.005

Kolm, K. E. (1996). Conceptualization and characterization of ground-water systems using Geographic Information Systems. *Engineering Geology, 42*(1996), 111-118.

Korus, J.T., Joeckel, R.M., Divine, D.P., & Abraham, J.D. (2017). Three-dimensional architecture and hydrostratigraphy of cross-cutting buried valleys using airborne electromagnetics, glaciated Central Lowlands, Nebraska, USA. *Sedimentology, 64*(2017), 553-58. doi: 10.1111/sed.12314

Lau, J., Thomason, J. F., Malone, D. H., & Peterson, E. W. (2016). Three-dimensional geological model of Quaternary sediments in Walworth County, Wisconsin, USA. *Geosciences, 6*(3), 32, 14 pp. doi:10.3390/geosciences6030032

Levson, V. (2008). Geology of northeast British Columbia and northwest Alberta: diamonds, shallow gas, gravel, and glaciers. *Canadian Journal of Earth Sciences*, *45*(5), 509–512. doi:10.1139/E08-022

Levson, V., & Best, M. (2017a) *North-east BC sonic drilling project physical log descriptions and interpretations.* Geoscience BC, Report 2017-16, 35 pp.

Levson, V., & Best, M. (2017b) *Summary report on proposed water well locations for Halfway River First Nation area.* Geoscience BC, Report 2017-17, 21 pp.

Levson, V. M., Hickin, A. S., Ferbey, T., & Best, M. (2006). Mapping high resistivity buried channel deposits with airborne electromagnetic surveys and other methods. In *19th Symposium on the Application of Geophysics to Engineering and Environmental Problems (SAGEEP 2006): Geophysical Applications for Environmental and Engineering Hazards – Advances and Constraints. [pp.152-16].* Environmental and Engineering Geophysical Society (EEGS).

Lowen, D. (2011). *Aquifer classification mapping in the Peace River Region for the Montney Water Project*. Lowen Hydrogeology Consulting Ltd., 51 pp.

MapPlace (2017). *BCGS Geoscience Map*; British Columbia Geological Survey MapPlace website, BC Ministry of Energy, Mines and Petroleum Resources. Retrieved from http://www.empr.gov.bc.ca/Mining/Geoscience/MapPlace/MainMaps/Pages/geology.aspx (September 2017), scale 1:250 000.

Mathews, W. H. (1978). *Quaternary stratigraphy and geomorphology of Charlie Lake (94A) map area, British Columbia*. Geological Survey of Canada, Paper 76-20, 32 pp.

Mathews, W. H. (1980). *Retreat of the last ice sheets in Northeastern British Columbia and adjacent Alberta*. Geological Survey of Canada, Bulletin 331, 28 pp.

Morris, D.A., & A.I. Johnson, 1967. *Summary of hydrologic and physical properties of rock and soil materials as analyzed by the Hydrologic Laboratory of the U.S. Geological Survey*, U.S. Geological Survey Water-Supply Paper 1839-D, 42 pp.

Mykula, Y. (2017). *Petrophysical interpretation on six shallow wells in the Peace Region of BC.* Geoscience BC, Report 2017-18, 7 pp.

Odong, J. (2007). Evaluation of empirical formulae for determination of hydraulic conductivity based on grain-size analysis. *Journal of American Science*, *3*(3), 54-60.

Oldenborger, G. A., Logan, C. E., Hinton, M. J., Pugin, A.-M., Sapia, V., Sharpe, D. R., & Russell, H. A. J. (2016). Bedrock mapping of buried valley networks using seismic reflection and airborne electromagnetic data. *Journal of Applied Geophysics*, *128*(2016), 191–201.

Oldenborger, G. A., Logan, C. E., Hinton, M. J., Sapia, V., Pugin, A. J. M., Sharpe, D. R., Calderhead, A.I., & Russell, H. A. J. (2014). 3D hydrogeological model building using airborne electromagnetic data. In *Near Surface Geoscience 2014-20th European Meeting of Environmental and Engineering Geophysics*. [5 pp.]. European Association of Geoscientists and Engineers (EAGE).

Oldenborger, G. A., Pugin, A.-M., & Pullan, S. E. (2013). Airborne time-domain electromagnetics, electrical resistivity and seismic reflection for regional three-dimensional mapping and characterization of the Spiritwood Valley Aquifer, Manitoba, Canada. *Near Surface Geophysics*, *2013*(11), 63–74.

Peterson, E. W., & Malone, D. H. (2016). Three-dimensional geologic modelling and groundwater flow modelling above a CO_2 sequestration test site. *Open Journal of Modern Hydrology, 2016*(6), 182-193.

Petrel Robertson Consulting Ltd. (2015). *Interpretation of Quaternary sediments and depth to bedrock through data compilation and correction of gamma logs*. Geoscience BC, Report 2015-04, 24 pp.

Pollock, D.W. (1989). *Documentation of computer programs to compute and display pathlines using results from the U.S. Geological Survey modular three-dimensional finite difference ground-water flow model*. US Geological Survey, Open File Report, pp. 89-381.

Pugin, A. J.-M., Oldenborger, G. A., Cummings, D. I., Russell, H. A. J., & Sharpe, D. R. (2014). Architecture of buried valleys in glaciated Canadian Prairie regions based on high resolution geophysical data. *Quaternary Science Reviews, 86*(2014), 13–23. doi: 10.1016/j.quascirev.2013.12.007

Quartero, E. M., Bechtel, D., Leier, A. L., & Bentley, L. R. (2014). Gamma-ray normalization of shallow well-log data with applications to the Paleocene Paskapoo Formation, Alberta. *Canadian Journal of Earth Sciences, 51*(5), 452–465.

Refsgaard, J.C., Christensen, S., Sonnenborg, T.O., Seifert, D., Højberg, A.L., & Troldborg, L. (2012). Review of strategies for handling geological uncertainty in groundwater flow and transport modelling. *Advances in Water Resources 36*(2012), 36-50. doi:10.1016/j.advwatres.2011.04.006

Riddell, J. (2012). Potential for freshwater bedrock aquifers in northeast British Columbia: regional distribution and lithology of surface and shallow subsurface bedrock units (NTS 093I, O, P; 094A, B, G, H, I, J, N, O, P), British Columbia Ministry of Energy and Mines, Geoscience Reports 2012, pp. 65–78.

Ritzi, R. W., Dominic, D. F., Slesers, A. J., Greer, C. B., Reboulet, E. C., Telford, J. A., Masters, R.W., Klohe, C.A., Bogle, J. L., & Means, B. P. (2000). Comparing statistical models of physical heterogeneity in buried-valley aquifers. *Water Resources Research, 36*(11), 3179–3192.

Ritzi, R. W., Jayne, D. F., Zahradnik, A. J., Field, A. A., & Fogg, G. E. (1994). Geostatistical modelling of heterogeneity in glaciofluvial, buried-valley aquifers. *Ground Water, 32*(4), 666–674.

Rosas, J., Lopez, O., Missimer, T. M., Coulibaly, K. M., Dehwah, A. H. A., Sesler, K., Lujan, L.R., & Mantilla, D. (2014). Determination of hydraulic conductivity from grain-size distribution for different depositional environments. *Groundwater, 52*(3), 399–413.

Ross, M., Parent, M., & Lefebvre, R. (2005). 3D geologic framework models for regional hydrogeology and land-use management: a case study from a Quaternary basin of southwestern Quebec, Canada. *Hydrogeology Journal, 13*(5–6), 690–707.

Russell, H.A.J., Hinton, M.J., van der Kamp, G., & Sharpe, D.R. (2004). An overview of the architecture, sedimentology and hydrogeology of buried-valley aquifers in Canada. In *Geo-Engineering for Society and Its Environment, 57th Geotechnical Conference and the 5th Joint CGS-IAH Conference*. [pp. 26-33].

Sandersen, P. B. E., & Jørgensen, F. (2003). Buried Quaternary valleys in western Denmark—occurrence and inferred implications for groundwater resources and vulnerability. *Journal of Applied Geophysics, 53*(4), 229–248.

Sapia, V., Viezzoli, A., Jørgensen, F., Oldenborger, G. A., & Marchetti, M. (2014). The impact on geological and hydrogeological mapping results of moving from ground to airborne TEM. *Journal of Environmental and Engineering Geophysics, 19*(1), 53–66.

Schlumberger. (2016). *Petrel*. Petrel 2016 for Windows, online help (not available in libraries).

Schroder-Adams, C. J., & Pedersen, P. K. (2003). Litho-and biofacies analyses of the Buckinghorse Formation: the Albian Western Interior Sea in northeastern British Columbia (Canada). *Bulletin of Canadian Petroleum Geology, 51*(3), 234–252.

Seifert, D., Sonnenborg, T. O., Scharling, P., & Hinsby, K. (2008). Use of alternative conceptual models to assess the impact of a buried valley on groundwater vulnerability. *Hydrogeology Journal, 16*(4), 659–674.

Seyoum, W. M., & Eckstein, Y. (2014). Hydraulic relationships between buried valley sediments of the glacial drift and adjacent bedrock formations in northeastern Ohio, USA. *Hydrogeology Journal, 22*(5), 1193–1206.

Sharpe, D. R., Pugin, A., Pullan, S. E., & Gorrell, G. (2003). Application of seismic stratigraphy and sedimentology to regional hydrogeological investigations: an example from Oak Ridges Moraine, southern Ontario, Canada. *Canadian Geotechnical Journal, 40*(4), 711–730.

Sharpe, D. R., & Russell, H. A. J. (2004). Basin analysis applied to modelling buried valleys in the Great Lakes Basin. In Berg, R. C. (ed.), Russell, H.A.J. (ed.), & Thorleifson, L.H. (ed.), *Three-Dimensional Geological Mapping for Groundwater Applications Workshops*, Illinois State Geological Survey, Open File Series 2004-8. [pp. 81-84].

Shaver, R. B., & Pusc, S. W. (1992). Hydraulic barriers in Pleistocene buried-valley aquifers. *Ground Water, 30*(1), 21–28.

SkyTEM Surveys ApS (2015). *SkyTEM survey: British Columbia, Canada, Data report*. Geoscience BC, Report 2016-03, 62 pp.

SoilVision Systems Ltd. (2017). *SVOFFICE 5 Help Manual*. SoilVision Systems Ltd. Saskatoon, SK, Canada.

Sonnenborg, T. O., Christensen, B. S. B., Nyegaard, P., Henriksen, H. J., & Refsgaard, J. C. (2003). Transient modelling of regional groundwater flow using parameter estimates from steady-state automatic calibration. *Journal of Hydrology, 273*(2003), 188–204. doi: 10.1016/S0022-1694(02)00389-X

Sørensen, K. I., & Auken, E. (2004). SkyTEM–a new high-resolution helicopter transient electromagnetic system. *Exploration Geophysics, 35*(3), 194–202.

Springer, A. E., & Bair, E. S. (1992). Comparison of methods used to delineate capture zones of wells: 2. stratified-drift buried-valley aquifer. *Ground Water, 30*(6), 908–917.

Steuer, A., Siemon, B., & Auken, E. (2009). A comparison of helicopter-borne electromagnetics in frequency-and time-domain at the Cuxhaven valley in Northern Germany. *Journal of Applied Geophysics, 67*(3), 194–205.

Stott, D. F. (1982). *Lower Cretaceous Fort St. John Group and Upper Cretaceous Dunvegan Formation of the Foothills and Plains of Alberta, British Columbia, District of Mackenzie and Yukon Territory*. Geological Survey of Canada, Bulletin 328, 136 pp.

Toews, M. W., & Allen, D. M. (2007). *Modified BC WELLS database and interface*. Simon Fraser University, Burnaby, BC, unpublished report, 7 pp.

Troldborg, L., Refsgaard, J.C., Jensen, K.H., & Engesgaard, P. (2007). The importance of alternative conceptual models for simulation of concentrations in a multi-aquifer system. *Hydrogeology Journal 15*(2007), 843-860. doi: 10.1007/s10040-007-0192-y

Troost, K. G., & Curry, B. B. (1991). Genesis and continuity of Quaternary sand and gravel in glacigenic sediment at a proposed low-level radioactive waste disposal site in east-central Illinois. *Environmental Geology and Water Sciences, 18*(3), 159–170.

United States Geological Survey (USGS). (2014). USGS SRTM 1 Arc-Second Global: Digital elevation model of the ground surface of the Peace Region in Northeast British Columbia (25 m resolution). Retrieved from https://earthexplorer.usgs.gov/ (2015).

van der Kamp, G., & Maathuis, H. (2012). The unusual and large drawdown response of buried-valley aquifers to pumping. *Ground Water, 50*(2), 207–215.

Walton, W.C. (1970). *Groundwater resource evaluation*. Toronto, Canada: McGraw-Hill Book Company.

Weissmann, G. S., Zhang, Y., Fogg, G. E., & Mount, J. F. (2004). *Influence of incised-valley-fill deposits on hydrogeology of a stream-dominated alluvial fan*. Society for Sedimentary Geology Special Publication No. 80, pp. 15-28.

Wilford, D., Hickin, A. S., Chapman, A., Kelly, J., Janicki, E. P., Kerr, B., van Geloven, C., Dessouki, T., Henry, K., Heslop, K., Kirste, D., McCarville, M., Ronneseth, K., Sakals, M., & Wei, M. (2012). *Collaborative interagency water projects in British Columbia: introduction to the Northeast British Columbia aquifer project and streamflow modelling decision support tool*. BC Ministry of Energy and Mines, Geoscience Reports 2012, pp. 79-89.

Appendix A.

Data Sources for the Geological and Numerical Models

Description:

The accompanying PDF includes data that were used as inputs into the geological and numerical models created in Petrel and MODFLOW, respectively. These data sources include water well databases, oil and gas well locations, the data collected during the field verification of the geophysical data, and the results of the grain size analyses. Interpretations of the data sources are provided where necessary.

Filename:

SMorganMSc2018_AppendixA_Data sources.pdf

Appendix B.

Resistivity Depth Slice Comparisons

The accompanying PDF contains the comparisons of the original resistivity depth slices as PDFs from Aarhus Geophysics ApS (2016d) to the Petrel recreated resistivity slices.

Filename:

SMorganMSc2018_AppendixB_Depth slice comparisons.pdf

Appendix C.

Additional Petrel Figures

The accompanying PDF includes figures of the bedrock and Quaternary models generated in Petrel (Schlumberger, 2016).

Filename:

SMorganMSc2018_AppendixC_Additional Petrel figures.pdf

Appendix D.

Importing the Petrel models into MODFLOW

The AV GR 1 Quaternary model and bedrock model were exported from Petrel for import into MODFLOW. Both models were exported in the format 'GSLIB', which generates an ASCII file containing the xyz and ijk coordinates, along with the property code (facies or bedrock) for each cell. Cells that do not have a defined property code were not included in the export.

There is not a direct export from Petrel to MODFLOW; therefore, the export files had to be manipulated into a format that could be brought into MODFLOW. The manipulated export files contained values to replace a generic hydraulic conductivity distribution in the .vmp file (Visual MODFLOW property) with the facies/bedrock codes generated in Petrel. The generic hydraulic conductivity distribution was created by setting up a model "shell" in MODFLOW. This shell was created using the same dimensions of the model exported from Petrel. The full model area is approximately 61.5 x 65.5 km^2. Using a uniform cell size of 200 x 200 m, the model was discretized into 308 columns and 327 rows, with 20 layers. Matlab was used to manipulate the export files into the same format as the .vmp file. The methodology below describes this process and was developed by Polina Abdrakhimova (personal communication, October 2017). Descriptions of the Matlab functions used and associated scripts are provided below.

A grid with the same dimensions, discretization, and node placement as the MODFLOW shell was created in Matlab. The DEM surface elevation raster was used as the top surface and the base of the bedrock model was used as the bottom surface. For each combination of x and y coordinates in planar view, the model top and model bottom z coordinates were determined. The thicknesses of the layers at each point were then determined using geometric progression within Matlab, using the 'fzero' function. The facies/bedrock codes were then interpolated onto the grid using nearest neighbour interpolation. These facies/bedrock codes represent hydraulic conductivity properties in the flow model in MODFLOW. Matrices of the bottom elevations for each layer and hydraulic conductivity distribution for each layer were exported in ASCII format. The ASCII files for layer bottom elevations were imported into MODFLOW, and the hydraulic

conductivity ASCII files were used to replace the original hydraulic conductivity distribution in the .vmp file for each model layer.

Matlab Functions and Scripts

Matlab functions used:

- Create.grid.m: main function which creates the grid, interpolates points, and outputs to ASCII files
- Import_SurfEl.m: reads surface elevation raster into Matlab
- Import_br.m: reads bedrock Petrel export into Matlab
- Import_Q1.m: reads Quaternary Petrel export into Matlab

Input files used:

- Surface elevation.txt: DEM surface elevation raster
- Bedrock sandstone or shale.txt: Petrel bedrock export differentiating between sandstone and shale formations
- Quaternary1: Petrel AV GR 1 Quaternary export

Associated scripts:

Create_grid.m

```
%%

nlay=20; %number of layers

xcoord=[532611:200:(532611+200*307)]+100; %x coordinates of grid
centerpoints

ycoord=flipud([6283431:-200:(6283431-326*200)])-100; %y coordinates of
grid centerpoints, shifted 200 m down from top left corner

[XX,YY]=meshgrid(xcoord,ycoord); %creates matrix of all combinations of
x and y
```

```
for i=1:nlay %creates a structure of all layers filled with not-a-
number

   Layer(i).depth=NaN(size(XX)); %bottom of layer

   Layer(i).midpoint=NaN(size(XX)); %midpoint of layer

end

%% Import surface elevation

Import_SurfEl %calls function to import surface elevation

SurfZ=griddata(SurfEl.x,SurfEl.y,SurfEl.z,XX,YY); %using linear
interpolation, interpolates DEM on a defined grid

%% Find lower layer surface elevation

Import_br %Import bedrock petrel output

x=Br_x; %redefine names of x y z and zone

y=Br_y;

z=Br_z;

Zn=Br_Zn; %hydraulic conductivity zone



Zn(x==9)=[]; %delete all points which are equal to zero hence not a
number

x(x==9)=[];

y(y==9)=[];

z(z==9)=[];



ilayer=4; %define bottom of model elevation using layer 4

xx=Br_x(Br_k==ilayer);
```

```
yy=Br_y(Br_k==ilayer);

zz=Br_z(Br_k==ilayer);

Zzn=Br_Zn(Br_k==ilayer);

Zzn(xx==9)=[];

xx(xx==9)=[];

yy(yy==9)=[];

zz(zz==9)=[];

Z_bot_lay=griddata(xx,yy,zz,XX,YY);



%% Create Z coordinates for each layer using geometric progression

b1=4; %first layer thickness in m.

for i=1:size(XX,1) %loop over all grid points

    for j=1:size(YY,2)

    S=SurfZ(i,j)-Z_bot_lay(i,j); %calculates sum of the progression -
thickness of model in current point

        if ~isnan(S) % if the model defined in this point

        q=fzero(@(x)b1*(1-x^nlay)/(1-x)-S,b1); %estimate common ratio
of geometric progression

        vect=b1*q.^([1:nlay]-1); %estimate elements of geometric
progression, hence each layer thickness

                for k=1:nlay

                    Layer(k).depth(i,j)=SurfZ(i,j)-sum(vect(1:k));
%calculates layer bottom
```

```
                    Layer(k).midpoint(i,j)=SurfZ(i,j)-sum(vect(1:k-1))-
0.5*vect(k); %calculates layer middle point

                end

        end

    end

end


%% Interpolate quaternary Petrel output on a regular grid

Import_Q1 %calls function which reads quaternary petrel output

x_all=coordQ1.x;  %redefine names of x y z and zone

y_all=coordQ1.y;

z_all=coordQ1.z;

Zone_all=Q1Zone; %hydraulic conductivity zone

Zone_all(x_all==9)=[]; %delete all points which are equal to zero hence
not a number

y_all(x_all==9)=[];

z_all(x_all==9)=[];

x_all(x_all==9)=[];

x_all(Zone_all==9)=[]; %delete all points where zone is not a number

y_all(Zone_all==9)=[];

z_all(Zone_all==9)=[];

Zone_all(Zone_all==9)=[];

Zone_all=Zone_all+1;
```

```
% Interpolate quaternary points on a regular X Y grid

x2=XX(:);

y2=YY(:);

x_all2=NaN(size(x_all));

y_all2=NaN(size(x_all));

d_all2=NaN(size(x_all));

for i=1:length(x_all)

    dist=sqrt((x_all(i)-x2).^2+(y_all(i)-y2).^2);

    [a,ind]=min(dist);

    if a<200 %if distance between current point and petrel output is
smaller than 200 m assign K value

        x_all2(i)=x2(ind);

        y_all2(i)=y2(ind);

        d_all2(i)=a;

    end

end

x_all=x_all2;

y_all=y_all2;



%%

x=Br_x;

y=Br_y;

z=Br_z;
```

```
Zn=Br_Zn;

Zn(x==9)=[]; %delete all points in Bedrock dataset where zone is not a
number

y(x==9)=[];

z(x==9)=[];

x(x==9)=[];

x(Zn==9)=[];

y(Zn==9)=[];

z(Zn==9)=[];

Zn(Zn==9)=[];



x_all=[x_all; x]; %merge quaternary and bedrock dataset

y_all=[y_all; y];

z_all=[z_all; z];

Zone_all=[Zone_all; Zn];



%% Interpolate K values of quaternary and bedrock over defined XYZ grid

count=0;

ntot=size(YY,2)*size(YY,1)*nlay;

for i=1:nlay

Layer(i).zone=NaN(size(XX)); %Create a structure for hydraulic
conductivity Zone nr

end
```

```
for i=1:size(XX,1)
    for j=1:size(YY,2)
        if ~isnan(Z_bot_lay(i,j))
                for k=1:nlay
                    count=count+1;
                    fprintf('%d of %d\r',count,ntot)
                    dist=sqrt((x_all-XX(i,j)).^2+(y_all-
YY(i,j)).^2+(z_all-Layer(k).midpoint(i,j)).^2);
                    [a,ind]=min(dist);
                    if a<200
                    Layer(k).zone(i,j)=Zone_all(ind);
                    end
                end
        end
    end
end


%% Create and save figures for each layer
for k=1:20
    figure()
    p=pcolor(XX,YY,Layer(k).zone);
    set(p,'EdgeColor','none')
    title(sprintf('Layer %d',k))
```

```
    colorbar

    caxis([1 6])

    saveas(gcf,sprintf('Layer_%d.png',k))

end

%% Output ASCII for each layer K matrix and raster for model layer
depth

for k=1:20

filename1=sprintf('New\\Model%dlayer.txt',k);

filename2=sprintf('New\\Layer%d_bottom_depth.txt',k);

Bottom=Layer(k).depth;

Bottom2=Bottom(:);

x2=XX(:);

y2=YY(:);

x2(isnan(Bottom2))=[];

y2(isnan(Bottom2))=[];

Bottom2(isnan(Bottom2))=[];

dlmwrite(filename2,[zeros(size(Bottom2)) x2 y2
Bottom2],'delimiter','\t','precision','%d %18.11f %18.11f %6.2f');

end
```

Import_SurfEl. m

```
%% Import data from text file.

filename = 'Surface elevation.txt';
```

```
delimiter = '\t';

startRow = 2;

formatSpec = '%*s%f%f%f%[^\n\r]';

fileID = fopen(filename,'r');

dataArray = textscan(fileID, formatSpec, 'Delimiter', delimiter,
'EmptyValue' ,NaN,'HeaderLines' ,startRow-1, 'ReturnOnError', false);

fclose(fileID);

SurfEl.x = dataArray{:, 1};

SurfEl.y = dataArray{:, 2};

SurfEl.z  = dataArray{:, 3};

clearvars filename delimiter startRow formatSpec fileID dataArray ans;
```

Import_br.m

```
%%

filename = 'Bedrock sandstone or shale.txt';

delimiter = '\t';

startRow = 10;

formatSpec = '%f%f%f%f%f%f%f%[^\n\r]';



fileID = fopen(filename,'r');

dataArray = textscan(fileID, formatSpec, 'Delimiter', delimiter,
'EmptyValue' ,NaN,'HeaderLines' ,startRow-1, 'ReturnOnError', false);
```

```
fclose(fileID);

Br_i = dataArray{:, 1};

Br_j = dataArray{:, 2};

Br_k = dataArray{:, 3};

Br_x = dataArray{:, 4};

Br_y = dataArray{:, 5};

Br_z = dataArray{:, 6};

Br_Zn = dataArray{:, 7};

clearvars filename delimiter startRow formatSpec fileID dataArray ans;
```

Import_Q1.m

```
%%

filename = 'Quaternary1.txt';

delimiter = ' ';

startRow = 10;

formatSpec = '%f%f%f%f%f%f%f%[^\n\r]';

fileID = fopen(filename,'r');

dataArray = textscan(fileID, formatSpec, 'Delimiter', delimiter,
'MultipleDelimsAsOne', true, 'EmptyValue' ,NaN,'HeaderLines' ,startRow-
1, 'ReturnOnError', false);

fclose(fileID);

indQ1.i  = dataArray{:, 1};
```

```
indQ1.j = dataArray{:, 2};

indQ1.k = dataArray{:, 3};

coordQ1.x= dataArray{:, 4};

coordQ1.y = dataArray{:, 5};

coordQ1.z = dataArray{:, 6};

Q1Zone= dataArray{:, 7};

clearvars filename delimiter startRow formatSpec fileID dataArray ans;
```

Appendix E.

Water Level Data

This appendix contains the water level data obtained for wells in the study area from the BC WELLS database (BC Ministry of Environment, 2017).

Table E1. Water level data and associated information from well records retrieved from the BC WELLS database (BC Ministry of Environment, 2017) for wells in the study area.

WTN or Well ID	Easting (m)	Northing (m)	Elevation (masl)	Static Water Level (mbgs)	Well Yield (US gpm)	Drilling Date (year)	Well Depth (m) or Screen Interval (mbgs)
59124	546671	6263363	698	5.5		1989	12 m
60656	550200	6263500	643	4.9	10.0	1994	11.5 m
75512	569966	6263832	686	2.4	7.0	1996	24.5 m
80279	561062	6262725	634	22.6	11.0	1999	28 m
80281	570069	6263860	695	6.7	5.0	1999	30.5 m
98361	569963	6263818	686	5.2	3.0	2008	36.5 m
102511	573190	6229161	732	1.4	300.0	2003	31 m
102658	546551	6263345	699	12.5	7.0	1989	15 - 21 mbgs
102672	559865	6261411	619	5.5		1989	12.5 m
102703	543383	6263817	676	4.7	45.0	1993	6 - 12 mbgs
102740	556466	6236530	780	12.0	1.5	1998	19.5 - 25.5 mbgs; 31.5 - 38 mbgs
102911	556486	6236530	781	22.6	3.0	1997	39.5 - 49 mbgs
104386	571851	6257017	558	6.4	10.0	1980	11 m
109909	560721	6262774	635	21.3	14.0	2014	37.5 - 41 mbgs
109942	567975	6229717	791	32.6	20.0	2014	66 m
109954	568284	6228251	769	18.3	2.5	2014	181 m
111527	554226	6248411	773	14.5	13.0	2015	65.8 - 78 mbgs
112868	578821	6230215	662	29.0	7.0	2016	84 - 90 mbgs
6a-MW	546658	6262602	667	4.7	20.0	2017	9 - 14 mbgs
10x-2	570723	6225050	697	2.0	10.0	2017	21 - 26 mbgs